UNIVERSITÉ DE SHERBROOKE
Faculté de génie
Département de génie électrique et de génie informatique

Conception et Évaluation de Nouvelles Méthodes pour Améliorer les Performances des Réseaux de Nano-Communication

Design and Evaluation of New Methods to Enhance the Performance of Nano-Communication Networks

Thèse de doctorat
Specialité: génie électrique

Oussama Abderrahmane Dambri

Sherbrooke (Québec) Canada

Décembre 2020

JURY MEMBERS

Soumaya Cherkaoui
Supervisor

Dimitrios Makrakis
Examiner

Khalid Moumanis
Examiner

Éric Plourde
Examiner

RÉSUMÉ

Le domaine des nanotechnologies a connu un développement très rapide et fascinant ces dernières années. Cette avancée rapide et impressionnante a conduit à de nouvelles applications dans les industries biomédicale et militaire, ce qui en fait un champ clé de recherche dans des domaines multidisciplinaires. Cependant, la capacité de traitement individuelle des nanodispositifs est très limitée, d'où la nécessité de concevoir des nanoréseaux qui permettent aux nanodispositifs de partager des informations et de coopérer entre eux. Il existe deux solutions pour mettre en place un système de nano-communication : soit en adaptant la communication électromagnétique classiques aux exigences de la nano échelle, soit en utilisant des nanosystèmes inspirés de la nature comme la communication moléculaire.

Dans cette thèse, nous nous intéressons à la deuxième solution, qui exploite le potentiel des nanosystèmes biologiques utilisés par la nature depuis des milliards d'années pour concevoir des nanoréseaux biocompatibles pouvant être utilisés à l'intérieur du corps humain pour des applications médicales. Néanmoins, l'utilisation de ce nouveau paradigme n'est pas sans défis. Le très faible débit réalisable et l'Interférence Entre Symboles (IES) sont les problèmes les plus influents sur la qualité de la communication moléculaire.

L'objectif principal de cette thèse est de concevoir et d'évaluer de nouvelles méthodes inspirées de la nature afin d'améliorer les performances des systèmes de nano-communication. Pour ce faire, le travail est divisé en trois parties principales.

Dans la première partie, nous améliorons les performances de la communication moléculaire en proposant une nouvelle méthode qui utilise une réaction de photolyse pour mieux atténuer l'IES. Nous proposons également une optimisation du receveur utilisé dans les systèmes MIMO en choisissant judicieusement les paramètres utilisés dans sa conception pour réduire l'influence de l'atténuation de trajet sur la qualité du système.

La deuxième partie propose un nouveau système de nano-communication filaire basé sur des polymères auto-assemblés qui construisent un nanofil électriquement conducteur pour connecter les nanodispositifs les uns aux autres. L'utilisation d'électrons comme supports d'informations augmente considérablement le débit réalisable et réduit le délai. Nous étudions le processus dynamique d'auto-assemblage du nanofil et nous proposons un receveur bio-inspiré qui détecte les électrons envoyés et les convertit en une lumière bleue.

La troisième partie applique le système de nano-communication filaire proposé pour concevoir une architecture d'un nanoréseau ad hoc filaire (Wired Ad hoc NanoNETworks) WANNET avec une couche physique, une couche de contrôle d'accès moyen (Medium Access Control) MAC et une couche d'application. Nous calculons également le débit maximum et nous évaluons les performances du système.

Mots-clés : Communication moléculaire à base de diffusion, affaiblissement sur le trajet, Interférence InterSymbole, MIMO, nano-communication à base de polymères , WANNET.

ABSTRACT

The field of nanotechnology has undergone very rapid and fascinating development in recent years. This rapid and impressive advance has led to new applications of nanotechnology in the biomedical and military industries, making it a key area of research in multidisciplinary fields. However, the individual processing capacity of nanodevices is very limited, hence the need to design nanonetworks that allow the nanodevices to share information and to cooperate with each other. There are two solutions to establish a nano-communication system: either by adapting the classical electromagnetic communication to the requirements of nano scale, or by using biological nanosystems inspired by nature such as the molecular communication proposed in the literature.

In this thesis, we are interested in the second solution, which is exploiting the potential of biological nanosystems used by nature since billions of years to design biocompatible nanonetworks that can be used inside the human body for medical applications. Nevertheless, the use of this new paradigm is not without challenges. The very low achievable throughput and the Inter-Symbol Interference (ISI) are the most influential problems on the quality of molecular communication.

The main objective of this thesis is to design and evaluate new methods inspired by nature in order to enhance the performance of nano-communication systems. To do this, the work is divided into three main parts.

In the first part, we enhance the performance of molecular communication by proposing a new method that uses a photolysis-reaction instead of using enzyme to better attenuate ISI. We also propose an optimization of the receiver used in MIMO systems by judiciously choosing the parameters used in its design to reduce the influence of path loss on the quality of the system.

The second part proposes a new wired nano-communication system based on self-assembled polymers that build an electrically conductive nanowire to connect the nanodevices to each other. The use of electrons as information carriers drastically increases the achievable throughput and reduces the delay. We study the dynamic process of self-assembly of the nanowire and we propose a bio-inspired receiver that detects the electrons sent through the conductive nanowire and converts them into a blue light.

The third part applies the proposed wired nano-communication system to design an architecture of Wired Ad hoc NanoNETworks (WANNET) with a physical layer, Medium Acess Control (MAC) layer and application layer. We also calculate the maximum throughput and we evaluate the performance of the system.

Keywords: Diffusion-based Molecular Communication, Path Loss, Inter-Symbol Interference, MIMO, Polymer-based nano-communication, WANNET.

To my parents, Lazhar and Houria for their love, support and patience

ACKNOWLEDGEMENTS

A doctoral thesis can appear to be a very arid, cold, rigid, scientific document and it effectively represents hours of hard and lonely work. Yet the doctorate itself is far from devoid of life, creativity and human interaction. It is above all a very human journey, a project full of influences and hindrances, reflections, development and links woven and transformed. Indeed, the undertaking of a doctorate is one of the most rich and vibrant times of my evolution as a student, as an adult and as a future professional.

I have a lot of gratitude and admiration to testify, first of all to my dear research director, Prof. Soumaya Cherkaoui, who is a professional model for her calm management of her time yet so loaded with important responsibilities and of course for her remarkable mastery of her role, both as an engineer and as a teacher, educator and researcher. Thank you for your availability, thank you for your openness to my character and my own touch in research, thank you for the freedom you gave me by showing me your confidence in my work. It is this confidence and this freedom that, in my opinion, spontaneously allows me to bring out the best in myself and in my work. Finally, thank you for your incredibly solid, attentive, reliable, cordial support in my final sprint over the last few weeks. You made the long journey through my doctoral years much easier.I also thank my dear supervisor of my master's degree, Prof. Nabil Benoudjit, you were more than just a teacher and supervisor, you were my mentor and more like a father to me. Thank you for the opportunity you have given me, thank you for your help and encouragement, thank you for believing in me, for accompanying me in my first research steps and for all that you have done for me.

I would like to thank my committee members Prof. Khalid Moumanis and Prof. Éric Plourde, for their valuable comments and suggestions and for agreeing to be part of the defense jury. A special thank you to Prof. Dimitrios Makrakis for agreeing to sit on this committee as an external reviewer for my thesis, thank you for your expert advice, for your enthusiasm and your always very generous help. Thank you for your confident and wise outlook on my work and my journey, for sharing some of your enormous experience with me, for your delicacy and courtesy.

Meysam and Achraf ! who witnessed and attended my early days as a new doctoral student in the laboratory, thank you very much for making my integration very easy, thank you for your wise advice and very generous help. I equally thank my lab mates Abderrahime, Amine, Afaf and Hajar who have been good colleagues and more than just friends. Thank you for the beautiful spirit of solidarity in the office, support and understanding, sensitivity to others, mutual encouragement, thank you for all the social side and humor that makes my life so much easier every day! I enjoyed all of our discussions (mostly unprofessional!) and our tea parties full of fun games. I warmly thank Azzouz for everything he has done for me, thank you for helping me; in every way that a person can be helped. Special thanks to Imen who shared with me my worst and my happiest moments, thank you for your support and for the tremendous love you are providing me even at a distance. Thank

you Okba, Hamza, Wafaa for your constant support and for all the fun that we have had in these years.

I offer my heartfelt thanks to my family for being so supportive. I would like to thank my brothers Soheib, Mossab, Zakaria, Charaf and Anes for their love and encouragement. You have always been, beyond all my expectations, a support, an appeasement, a release, an energy and a lot of comfort; thank you for your loyalty, generosity and all the good that you often reflect to me each in your own way. But above all thanks to my two sisters Khaoula and Intissar whom I adore, who never let me doubt their love, so radiant, generous, positive and confident. Thank you for your almost unshakable trust in me, thank you for your humour and your sincere encouragement.

Additionally and most importantly, my deepest and most sincere thanks go to my parents, my father Lazhar, always calm, strong, solid through the sandstorms ... the rock that supports our family, dad I am very proud to be your son, it is an immense chance to have you in my life, you are a gift and a blast for the whole family. Of all the fathers, you are the best. You have been and you will always be an example for me through your human qualities, your perseverance and perfectionism. As a testimony of brutal years of sacrifice, caring, encouragement and prayer could you find in this work the fruit of all your troubles and all your efforts. On this day, I hope to make one of your dreams come true. No dedication can express my respect, my gratitude and my deep love. May God preserve you and give you health and happiness.

To my mother Houria who raised me with love to the end of her strength, with her character, her courage, her sensitivity and her love, thank you. You are an inexhaustible source of tenderness, patience and sacrifice. Your prayer and your blessing have been of great help to me throughout my life. Whatever I may say and write, I could not express my deep affection and deep gratitude. I know that you are happy for me, proud and joyful, I have the pleasure to celebrate this accomplishment with you and to live with you all these next steps that I still cannot guess. Dear mom, I hope that this work can compensate for a tiny drop of your suffering and sacrifices for me ... May Almighty God preserve you and grant you health, long life and Happiness.

TABLE OF CONTENTS

LIST OF FIGURES

LIST OF TABLES

LIST OF ACRONYMS

Acronyms	Definition
AcCoRD	Actor-based Communication via Reaction-Diffusion
ANSI	American National Standards Institute
BASK	Bioluminescence Asynchronous Shift Keying
BER	Bit Error Rate
BISK	Bioluminescence Intensity Shift Keying
BTSK	Bioluminescence Time Shift Keying
CLT	Central Limit Theorem
CSI	Channel State Information
CSK	Concentration Shift Keying
DbMC	Diffusion-based Molecular Communication
DFE	Detection-Feedback Equalizer
DTM	Differential Transform Method
FP	Finite Pulsewidth
HRSEM	High Resolution Scanning Electron Microscopy
ILI	InterLink Interference
IM	Impulse Modulated
ISI	Inter-Symbol Interferencee
ITR	Interference-to-Total-Received molecules
MAC	Medium Access Control
MAP	Maximum A posteriori Probability
MCMC	Markov-Chain Monte-Carlo
MIMO	Multi-Input Multi-Output
MMSE	Minimum Mean- Square Error
MoSK	Molecular Shift Keying
MPE	Maximum Permissible Exposure
MUI	Multi-User Interference
OSI	Open Systems Interconnection
PAM	Pulse-Amplitude Modulated
PIC	Predicted Instant of Collision
PIT	Periodic Interference Test
PPM	Pulse Position Modulation
SER	Smooth Endoplasmic Reticulum
SISO	Single-Input Single-Output
SM	Spatial Multiplexing
RTSK	Release Time Shift Keying
THz	TeraHertz
WANNET	Wired Ad hoc NanoNETwork
ZnO	Zinc Oxide

CHAPTER 1

INTRODUCTION

The words of the great physicist and Nobel laureate Richard Feynman "*There's plenty of room at the bottom*" [Feynman, 1960], have inspired scientists to explore the nanoscale, and develop a nanotechnology that has not only made an industrial revolution, but has created a promising path to solve a lot of problems [Kostoff *et al.*, 2007]. In all areas of science and industry, nanotechnology has always a role to play and a solution to offer by using nanomachines. However, the individual processing capacity of these nanomachines is very limited, which can be compensated by using a huge number of them. The group work of these nanomachines should be synchronized to achieve a single goal, like an ant colony. To realize that two solutions have been proposed in literature, either by using the classical electromagnetic communication at nanoscale or by using molecular communication which uses molecules as carriers of information [Abbasi *et al.*, 2016].

The classical electromagnetic communication needs to be adapted to the requirements of nanoscale, since the nano size of an antenna forces it to oscillate at Terahertz frequencies. There are still problems to be solved in order to control and capture the peculiarities of Terahertz frequency such as molecular absorptions, path loss and scattering losses [Akyildiz and Jornet, 2010b]. It is also necessary to confirm the safety of using Terahertz frequencies inside the human body for medical applications.

Another promising solution to establish a nano-communication system is to imitate nature. Nature has created communicating biological nanosystems by using chemical molecules. It is the ability of these nanosystems to communicate with each other that enabled the materialization of complex biological systems, including the human brain. These nanosystems have inspired the emergence of a new paradigm that, instead of using electromagnetic waves, uses molecules to send information [Nakano *et al.*, 2012]. Molecular communication has attracted the attention of scientific researchers in the last years in all areas, especially in the medical field, where it can solve problems of diagnosis, local drug delivery and it may even help identify and treat diseases like cancer and Alzheimer's.

Considerable number of methods have been proposed in the open literature, related to molecular communication at the nanoscale, such as using nanomotors, flagellated bacteria and calcium channels in living cells. The simplest and most basic proposed method is

diffusion-based molecular communication [Pierobon and Akyildiz, 2010]. This method takes advantage of the natural diffusion of molecules due to the thermal fluctuations of the medium. The Brownian motion of molecules does not need any additional energy to transmit the information from a transmitter to a receiver [Einstein, 1905]. However, the diffusion takes a considerable amount of time to reach its destination, and is dependent on the distance between the transmitter and the receiver. In addition, molecules that fail to reach the receiver remain in the medium and interfere with new emitted ones creating Inter-Symbol Interferences (ISI), which decreases the performance of molecular communication. Most of the methods proposed in literature suffer from a very low achievable throughput and a very high delay, which increases the error probability and decreases nanosystems performance.

1.1 Objective

In this thesis, our objective is to design and evaluate new methods to enhance the performance of nano-communication networks. By increasing the achievable throughput and mitigating the ISI, we can decrease the delay and reduce the probability of error. Thus, we improve the performance of molecular systems and nano-communication networks.

To accomplish the aforementioned objective, we divide the main objective into several intermediate objectives, them presented below:

- ISI Mitigation

The first intermediate objective proposes the use of photolysis reactions with light-sensitive molecules such as Vitamin D_3 instead of using enzymes to eliminate the remaining molecules in the medium. The ability of light to be switch on/off unlike enzymes allows us to choose an optimal time to start eliminating the molecules, thus mitigating the ISI without decreasing the strength of the signal. The corresponding research questions for this intermediate objective are as follows:

When is the optimum time for light emission?

How will the photolysis reaction influence the diffusion of molecules?

Which simulator do we use to simulate the proposed system?

What criteria do we use to evaluate the performance of the proposed system?

- MIMO Receiver Optimization

The second intermediate objective proposes an optimization of the receiver's design parameters used in the Multiple-Inputs Multiple-Outputs (MIMO) technique for molecular communication. The corresponding research questions for this intermediate objective are as follows:

What parameters of the receiver design need to be optimized?

How do we formulate the optimization problems?

What algorithms do we use to solve the optimization problems?

- Polymer-based Channel for Nano-communication Networks

The third intermediate objective lays the foundation of a new method of nano-communication, which is based on self-assembled polymers. This method uses electrons to send information through self-assembled and highly conductive polymer. By applying this new method, the achievable throughput of nano-communication systems can be compared with the achievable throughput when using wired and electromagnetic communications. The corresponding research questions for this intermediate objective are as follows:

What is the architecture of wired polymer-based nano-communication?

What is the master equation for the self-assembly reaction?

Can we solve the master equation analytically and numerically?

Is the self-assembled nanowire stable enough to be used as a communication channel?

- Receiver Design for Wired Nano-communication Networks

The fourth intermediate objective is to design a receiver for wired nano-communication networks. Since electron detection at nanoscale is extremely difficult due to the quantum trade-off between information and uncertainty, the proposed bio-inspired receiver uses the electrons to trigger chemical reactions. The electrons are used to stimulate a Smooth Endoplasmic Reticulum (SER), which secretes Ca^{2+} ions inside the receiver. Then, it uses a photo-protein called *Aequorin*, which in the presence of Ca^{2+} ions, emits blue light, making electron detection much easier. The corresponding research questions for this intermediate objective are as follows:

Is the maximum throughput of the nanowire sufficient to trigger the chemical reaction?

What are the modulation techniques we can use?

How much Ca^{2+} concentration do we need to trigger the photo-reaction?

Is the radiant energy of the emitted light sufficient to be detected?

- Wired ad hoc Nanonetwork Application

The last intermediate objective is to apply an adaptation of the new proposed wired nano-communication networks in order to design Wired Ad hoc NanoNETwork (WANNET), which can be very useful in medical applications. The WANNET system can also be used to detect low concentrated molecules in real time inside the human body. The corresponding research questions for this intermediate objective are as follows:

How to design an ad hoc wired nanonetwork without any infrastructure?

What is the OSI model for WANNET systems?

How can we model the physical layer of WANNET?

1.2 Contributions and Originality

With the intention of improving the performance of nano-communication networks, this thesis proposes two approaches.The first approach is to enhance the performance of diffusion-based molecular communication by reducing the effect of path loss and by mitigating ISI. The second approach proposes a new method of nano-communication, which is based on self-assembled polymers. Our contributions in this thesis can be summarized as follows:

First:

- We propose the use of light to degrade the molecules carrying the information instead of using enzymes to better attenuate Inter-Symbol Interference without decreasing the power of the transmitted signal. Thus, we reduce the likelihood of error and we increase the transmission rate.

- We derive the lower bound expression of the expected number of molecules at the receiver after having been hit by a light beam.

- We calculate the optimal time to send the light beam so that it degrades only the molecules remaining in the medium and not the molecules carrying the information.

- We calculate the threshold that detects whether the number of received molecules represents a bit or not. We also calculate the error probability and the ITR (Interference -to-Total Received Molecules) metric to validate the proposed system.

- We propose an optimization of the receiver design parameters for molecular MIMO. These parameters are: the distance between transmitter and receiver, the diameter of the detectors constructing the receiver and the distance between them. This optimization is important for improving the performance of molecular MIMO systems.

- We derive the decision-making rule that decides whether the number of molecules absorbed by the receiver is a bit or not, by applying the maximum a posteriori probability of the Bayesian standard, and we calculate the error probability.

- We formulate two optimization problems and we propose two algorithms to solve them.

Second:

- We propose a new method of molecular communication that uses self-assembled actin to build a nanowire between transmitters and receivers. The wired nano-communication can give better results compared to other wireless molecular methods proposed in the literature so far.

- We propose two algorithms for a simulation framework that simulates the self-assembly of the proposed nanowire in a 3D environment. By using this framework, we can follow the position of the last assembled molecule in real time to study the speed of the nanowire's construction.

- We derive a master equation of the communication channel to study the dynamic process of the self-assembly, and we calculate the steady state of the self-assembly chemical reaction analytically and numerically.

- We validate the proposed analytical model with numerical and Monte-Carlo simulations and we present the simulation results in terms of the monomer's concentration changes over time.

- We approximate the derived master equation by a 1D Fokker-Planck equation and we solve this equation analytically by using a differential transform method, and numerically with Monte-Carlo simulations. We also derive the nanowire elongation rate and its diffusion coefficient expressions, and we validate them with simulations.

- We propose a bio-inspired receiver design for wired nano-communication, which uses light to detect the transmitted electrons through the nanowire and also play the role of relay for the closest gateway.

- We calculate the maximum achievable throughput of the proposed communication channel and we calculate the error probability. We also modeled the proposed receiver with an equivalent circuit and we derive the analytical expressions of the circuit's components.

- We calculate the maximum achievable throughput of the proposed communication channel and we calculate the error probability. We also modeled the proposed receiver with an equivalent circuit and we derive the analytical expressions of the circuit's components.

- We propose new modulation techniques to be used for wired nano-communication networks.

- We apply an adaptation of the proposed wired system to design a **Wired Ad hoc NanoNETwork (WANNET) with an OSI model**, which can be very beneficial to medical applications and for the detection of low concentrated molecules in real time inside the human body.

1.2.1 Originality of this Study

Molecular communication is a promising new paradigm for creating nanoscale communication networks by using biological systems. Despite the many solutions proposed in the literature to overcome the challenges of molecular communication, yet there are still problems to solve and improvements to make.

The originality of this thesis compared to other studies in literature can be summed as follows. (1) Originality in the approach: instead of mitigating Inter-Symbol Interference by using enzymes or neighboring receivers, we use light to degrade Provitamin D_3 molecules. The method was inspired by the process of building Vitamin D_3 in our skin. Inspired by muscles process we also designed a receiver that detects electrons by using SER that secretes Ca^{2+} ions inside the receiver. Then, inspired by the jellyfish *Aequorea Victoria*, we used the secreted Ca^{2+}ions to emit blue light making electron detection considerably easier and more efficient in a noisy environment. (2) Originality in the results: using light allowed to mitigate the ISI without decreasing the power of the signal, which was considered as a compromise in the literature. The results also show that the proposed wired nano-communication provides a very high achievable throughput and a very low delay compared to molecular communication systems. (3) Originality of the application: the self-assembled polymers have been studied extensively in the fields of biology and

chemistry and they have been proposed as a road for kinesin nanomotors in molecular communication systems [Farsad *et al.*, 2016]. In this thesis, they are applied to build a nanowire, which conducts electricity in a nanoscale communication system. We also propose a new application of wired nano-communication networks to design a wired ad hoc nanonetwork (WANNET), which can be very useful in medical applications and for the detection of low concentrated molecules in real time inside the human body.

It is our strong belief that this thesis would have a significant scientific and technological impact, particularly in the pharmaceutical and medical fields. The impact of wired communication based on self-assembled polymers, on nano-communication systems and their applications will be very important. With a very high achievable throughput and high flexibility to build a nano-communications network between nano-clusters, this new method can open new horizons in the fields of pharmaceutical, medical and military applications.

1.2.2 List of Papers

The research I conducted as part of my doctoral project resulted in high quality papers, which are published and submitted in highly respected conferences and journals of high caliber. The list of the papers is as follows:

Published

1. O. A. Dambri and S. Cherkaoui, "Performance Enhancement of Diffusion-Based Molecular Communication," in *IEEE Transactions on NanoBioscience*, vol. 19, no. 1, pp. 48-58, Jan. 2020. (Chapter 3)

2. O. A. Dambri and S. Cherkaoui, "Enhancing Signal Strength and ISI-Avoidance of Diffusion-based Molecular Communication," 2018 *14th International Wireless Communications and Mobile Computing Conference (IWCMC)*, Limassol, pp. 1-6, 2018.

3. O. A. Dambri, A. Abouaomar and S. Cherkaoui, "Design Optimization of a MIMO Receiver for Diffusion-based Molecular Communication," 2019 *IEEE Wireless Communications and Networking Conference (WCNC)*, Marrakesh, Morocco, pp. 1-6, 2019. (Chapter 4)

4. O. A. Dambri, S. Cherkaoui and B. Chakraborty, "Design and Evaluation of Self-Assembled Actin-Based Nano-Communication," 2019 *15th International Wireless Communications and Mobile Computing Conference (IWCMC)*, Tangier, Morocco, pp. 208-213, 2019.

5. O. A. Dambri and S. Cherkaoui, "Toward a Wired Ad Hoc Nanonetwork," ICC 2020-2020 *IEEE International Conference on Communications (ICC)*, Dublin, Ireland, pp. 1-6, 2020. (Chapter 7)
6. A. Abouaomar, S. Cherkaoui, A. Kobbane and O. A. Dambri, "A Resources Representation for Resource Allocation in Fog Computing Networks," 2019 *IEEE Global Communications Conference (GLOBECOM)*, Waikoloa, HI, USA, pp. 1-6, 2019.

   Submitted

7. O. A. Dambri and S. Cherkaoui, "A Polymer-based Channel Model for Wired Nano-Communication Networks," in *IEEE Transactions on Molecular Biological and Multi-scale Communications*, 2020. (Chapter 5)
8. O. A. Dambri and S. Cherkaoui, "Design and Evaluation of a Receiver for Wired Nano-Communication Networks," in *IEEE Transactions on Molecular Biological and Multi-scale Communications*, 2020. (Chapter 6)

1.3 Thesis Plan

The thesis consists of eight chapters. The first chapter briefly presents the context, objective, originalities and contributions of the study. It also provides a general overview of the thesis and the problems addressed in this research project. In Chapter 2, we summarize the state of the art of the technology on nano-communication networks, their advantages and disadvantages. Chapter 3 is dedicated to ISI mitigation discussed in paper 3 by using photolysis reaction instead of using enzymes. It also presents the derived analytical model and the analytical and numerical results. In Chapter 4, we discuss in paper 4 the proposed optimization of the design parameters of MIMO receivers. We also present the formulated optimization problems and the algorithms proposed to solve them. Chapter 5 presents the new proposed method of nano-communication in paper 7, which uses the self-assembly of polymers to build a conductive nanowire that links the transmitter to the receiver and uses electrons as carriers of information. It also derives the master equation of the self-assembly reaction and solves it analytically and numerically. In Chapter 6, we explain the design of the proposed receiver for wired nano-communication networks presented in paper 8 and we model it with an equivalent circuit. Chapter 7 proposes an application of the wired nano-communication system to design wired ad hoc nanonetworks presented in paper 5, which can be very useful in medical applications. Finally, chapter 8 concludes the thesis and discusses future work.

CHAPTER 2

STAT OF THE ART

2.1 Electromagnetic nano-communication

Electromagnetic communication is a paradigm that uses electromagnetic waves to send information, like the Telegraph invented by G. Marconi [Marconi, 1902]. To modulate the information, we can change the properties of the wave; its frequency, its amplitude and/or its phase [Krouk and Semenov, 2011]. It is envisioned that wireless connectivity at nanoscale materializes using frequencies located in the Terahertz (THz) band [Lawler *et al.*, 2020; Seo *et al.*, 2015], which is very challenging and requires that we come up with new technical solutions. THz is one of the least explored spectral bands [Akyildiz *et al.*, 2014], which is considered a key to overcome the never-ending wireless data traffic increase. With its huge frequency band (spanning from 0.1 THz to 100 THz), has the potential of providing extremely large communication capacity, with transmission speeds reaching up to 1 Tbps, especially when the communication distance is at the nanoscale. Reasons justifying use of the THz band for nano-communication, including those involved in the implementation of medical applications are the following:

- Suitability of use of frequencies at the THz range for wireless communication at nanoscale is natural consequence of the nano-antennas size that need to be used with nano-size devices. At such extremely small size, the resonant radiation frequencies reach tens to hundreds of THz [Yifat *et al.*, 2012]. The increase of antenna resonance frequency results in increased path loss, but at nano-distances this does not become a limiting factor.
- Continuous monitoring of the body behavior associated with certain medical applications, such as those monitoring patients suffering from Epilepsy, require broadband communication that is capable of maintaining fast data transportation in real time. The extremely high data rate the THz band can support will lead to diagnostic devices of enhanced capabilities. Moreover, using this very high data rate in medical imaging will drastically improve the resolution and the image quality, giving it more details, which offers the possibility of detecting cancers in more precocious stages [Zhao *et al.*, 2014].

- Wireless technologies above THz Band are very dangerous for the human body, because the radiation at infrared frequencies and above can easily damage human tissues. Absorption of radiation at infrared frequencies spectrum by human cells makes them vibrate. This vibration transforms kinetic energy to heat, which burns human tissue. There are additional negative implications with the use of signals at infrared frequencies. Such signals experience high diffuse reflection losses. In addition they require relatively expensive detection equipment [Federici and Moeller, 2010]. These deficiencies will limit the use of this band in biomedical applications.
- THz Band offers a secure communication link, because of its highly directional beam and its inability to travel long distances due to the high atmospheric attenuation such signals experience. Therefore, it will be very difficult for eavesdroppers to detect THz signals. Also, the extremely large bandwidth makes use of THz technology ideal for use of spread spectrum technology, which protects the signal from eavesdropping and jamming attacks [Song and Nagatsuma, 2011]. Secure communication links for medical applications are necessary, because medical information is confidential. In addition, active attacks could damage the quality of the medical application, thus placing the patient's life at risk.

However, even with all these advantages, THz communication is not applicable in the medical field yet. There are multiple challenges that need to be overcome, related to antenna, physical layer as well as the higher communication layers. The most important challenge comes from the high path loss of the THz band. Because of molecular absorption and scattering losses, especially water molecules, the absorption is very high at THz frequencies. Considering that 60% of the human body consists of water [Jéquier and Constant, 2010], it could makes the seriousness of the factors mentioned above when designing technology for medical applications evident [Smye *et al.*, 2001]. Besides, the fat contained in the human body absorbs energy, complicating further the development of effective inter and intra-body communication technology. Emission and detection of THz waves is challenging as well. The discovery of graphene was critical factor to the development of transceiver technology for operation at the THz band [Geim, 2009] and the application of the technology in the medical field. There are significant challenges concerning the communication protocols, requiring creative solutions. For example, traditional MAC protocols cannot address the peculiarities of THz band. In addition, the very limited energy of nanomachines and transmission at Terabits per second (Tbps) speeds require innovative solutions to control bit error rate.

Despite the advantages the THz band has compared to other bands when it comes to generating health risks, there is still need for the technology to be tested prior to its use in medical applications. It is possible that in order to overcome signal strength losses, the used nano-antenna will be directional. This would concentrate the power of the signal to a narrow radiation angle, producing enhanced levels of transmitted power within this angle, as compared to having omni-directional or wide angle radiation pattern. When it comes to radiation, there is always a limit, which, when crossed, it generates dangers to health. This issue needs to be studied thoroughly. The available experimental results on the subject are limited [Chopra *et al.*, 2016; Piro *et al.*, 2015; Yang *et al.*, 2015], thus more studies are required.

2.2 Molecular communication

Molecular communication is a promising new paradigm for creating biocompatible communication systems. It can be applied in environments and scenarios considered impossible before, as in acidic environments, in the oceans, and in nanoscales [Nakano *et al.*, 2012]. Inspired by nature, this system uses molecules as carriers of information instead of using electromagnetic waves. Molecular communication is applicable either at the nanoscale or at the macroscale. We can see that in the communication between the cells of the brain, or in the communication between very distant insects using pheromones. The system contains a transmitter that emits molecules, a receiver that can detect these molecules, and a communication channel. The communication channel can be an aqueous or a gaseous medium that allows molecules to propagate freely from the transmitter to the receiver. The molecules used in this communication system can be biological such as proteins, DNA, sugars, vitamins, or inorganic chemicals like nanoparticles of minerals and atoms. A propagation mechanism is needed to transport the molecules through the medium to the receiver. This mechanism can be as simple as basic diffusion, or complex as transport systems using molecular motors [Farsad *et al.*, 2016]. In this section, we discuss the types of propagation proposed in the literature, the different modulation techniques for molecular communication and the methods proposed to mitigate ISI.

2.2.1 Propagation methods

Propagation via diffusion

Diffusion is a random movement of molecules, called Brownian motion. The molecules carrying the information use the thermal fluctuations of the medium's particles to move in a random direction and arrive at the destination as shown in Figure 2.1. Therefore,

no external energy is needed for diffusion-based molecular communication systems. The diffusion dynamic can be modeled mathematically by using Fick's second law presented in equation 2.1 [Atakan, 2016; Nakano *et al.*, 2013]:

$$\frac{\partial C}{\partial t} = D\nabla^2 C \tag{2.1}$$

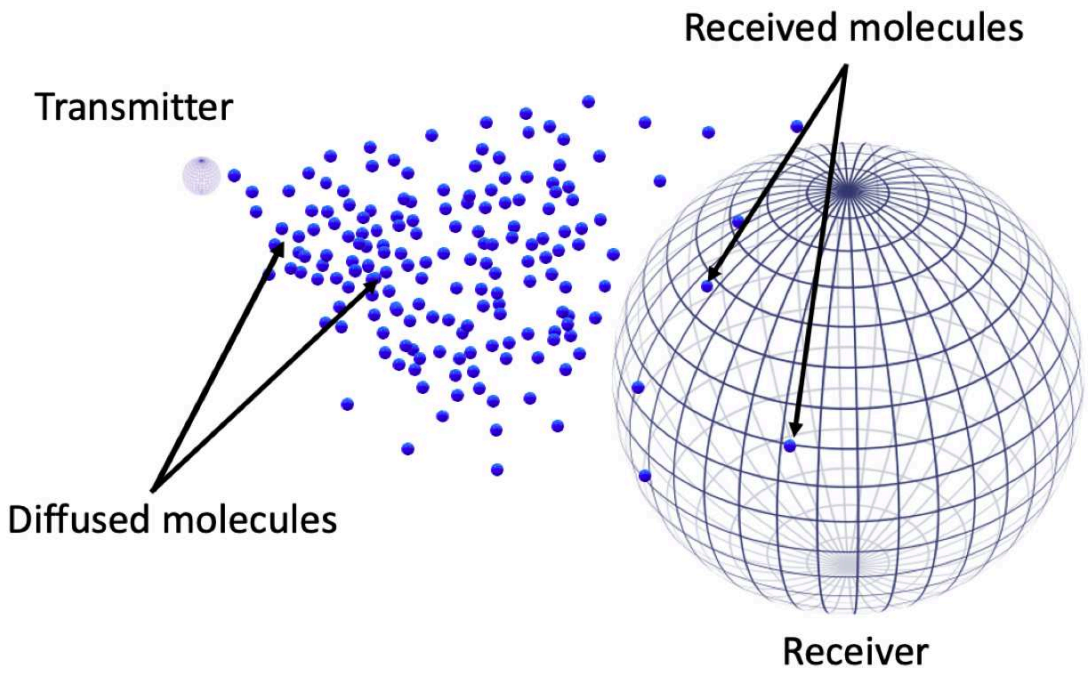

Figure 2.1 Molecular communication system based on diffusion.

where C is the concentration of molecules in the medium, t is time, and D represents the diffusion coefficient, which can be calculated with equation 2.2:

$$D = \frac{k_B T}{6\pi\eta R} \tag{2.2}$$

where k_B is the Boltzmann constant, T is the temperature in Kelvin, η is the dynamic viscosity of the fluid, R is the radius of the scattered molecules. The movement of molecules diffusing in the medium can be accelerated by using a flow that goes in the direction of the receiver. We can find that kind of accelerated diffusion in our bodies where some cells use the blood stream to target distant cells and send hormonal substances.

In nature, the cells receive the molecules carrying the information either by binding them to their membrane, absorbing them or removing them with chemical reactions after identifying them. By assuming that the molecules are removed immediately after detection, most of the receivers proposed in literature are considered as absorbing receivers and they are modeled with first hitting process in one dimensional environment as follows [Yilmaz and Chae, 2014]:

$$f_{abs}^{1D}(t) = \frac{N}{(\sqrt{4\pi D t^3})} \exp\left(\frac{-d^2}{4Dt}\right), \tag{2.3}$$

where N is the number of molecules released by the transmitter, d is the distance between transmitter and receiver and D is the diffusion coefficient. This equation can be interpreted as the impulse response of the diffusion channel in a 1-D environment with an absorbing receptor. The receiver can also be passive by just observing the molecules without interacting with them. By considering the receiver to be a 3D passive sphere, eq. 2.3 becomes [Noel *et al.*, 2014]:

$$f_{pass}^{3D}(t) = \frac{N V_{RX}}{(4\pi D t)^{3/2}} \exp\left(\frac{-d^2}{4Dt}\right), \tag{2.4}$$

where $V_{RX}$is the volume of the receiver. This equation can be interpreted as the number of the expected molecules to be observed at the receiver.

The disadvantage of this propagation method is that it is very slow, with a very low transmission rate and it is dependent on the distance between transmitter and receiver. The solution of adding a flow in the direction of the communication channel can accelerate the diffusion and decrease the dependence on the distance [Kadloor *et al.*, 2012]. Another problem is the Inter-Symbol Interference caused by the remaining molecules from a previous symbol in the medium. These remaining molecules interfere with the molecules of the next symbol. Solutions are proposed in the literature to solve the Inter-Symbol Interference problem, such as using enzymes and neighboring receivers that we will cover in the section of mitigation techniques.

Propagation via bacteria

The oldest living beings on earth are the first to adapt with the changes in nature. These flagellated bacteria have created a propagation method that directs them to nutrients and pushes them away from toxic substances [Wadhams and Armitage, 2004]. A Bacterium uses a property called chemotaxis, which allows it to move towards or in the opposite direction following a concentration gradient of a chemical substance and such behavior is

advantageous for the bacterium. Its movement consists of two phases, a swimming phase and a tumbling phase with a rotatory movement as illustrated in Figure. 2.2. Because of the random time between these two phases, the bacterium can be lost in the environment without the chemotaxis guide. Bacteria have the ability to communicate with each other by exchanging their DNA or by sending chemical substances to warn the colony of impending danger.

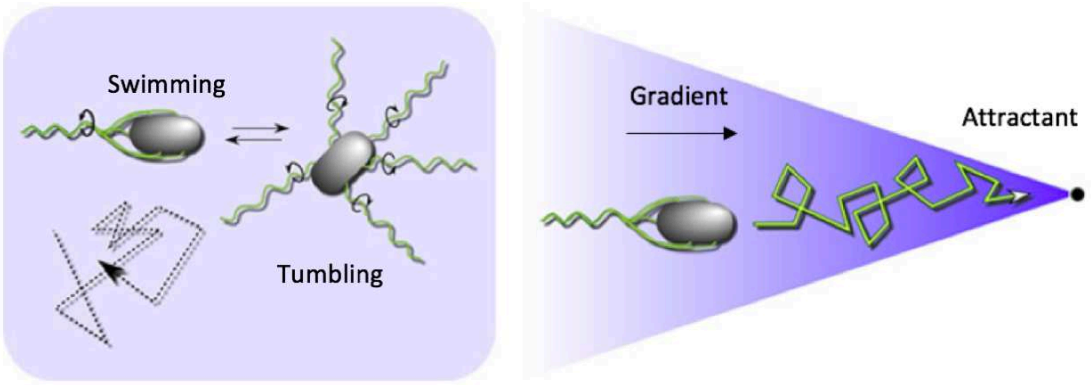

Figure 2.2 The phases of bacterial movements and the principle of chemotaxis.

In molecular communication, chemotaxis can be used to create a communication system in which bacteria represent the carriers of information. To guide the bacteria to the receiver, the latter releases attractant molecules and the bacteria follow the concentration gradient of these molecules that guide them to the destination [Cobo and Akyildiz, 2010]. The information sent will be encoded in the plasmids (cyclic DNA) inside the bacteria, and once it arrives at the receiver, they deliver the information via the bacterial genetic conjugation. [1]

A wired system is proposed in literature, which uses the self-assembly of some bacteria types and their ability to generate electricity to build a conductive wire that can be used to propagate information electrically [Meysman, 2018; Michelusi and Mitra, 2015; Michelusi *et al.*, 2014]. Several experiments revealed that cable bacteria can form a long filament that can exceed 70 mm, which at nanoscale is huge. Each cell of the bacteria constructing the cable are either donors or acceptors of electrons, where the acceptor type harvests electrons from the donors type. There are different syntrophic interactions between bacterial partners to exchange their electrons as presented in Figure. 2.3. The classical syntrophic exchanges soluble compounds by diffusion between the partners, where

1. Bacterial conjugation is a biological phenomenon that bacteria use to exchange genetic information [Gross and Caro, 1966].

each of them performs a full redox reaction. The direct interspecies electron transfer allows the partners to only perform half redox reaction and the electrons are exchanged directly between them. Finally the putative interactions between partners, which enable the bacterial cable to transfer electrons from an anodic zone to a cathodic zone. The free sulfide (H_2S) is consumed via an oxidative half reaction in the anodic zone of the cable bacterium as follows:

$$\frac{1}{2}H_2S + 2H_2O \longrightarrow \frac{1}{2}SO_4^{2-} + 4e^- + 5H^+ \tag{2.5}$$

Oppositely, in the cathodic zone if the cable bacterium, the oxygen (O_2) is consumed by the cells that perform the reductive half reaction as follows:

$$O_2 + 4e^- + 4H^+ \longrightarrow 2H_2O \tag{2.6}$$

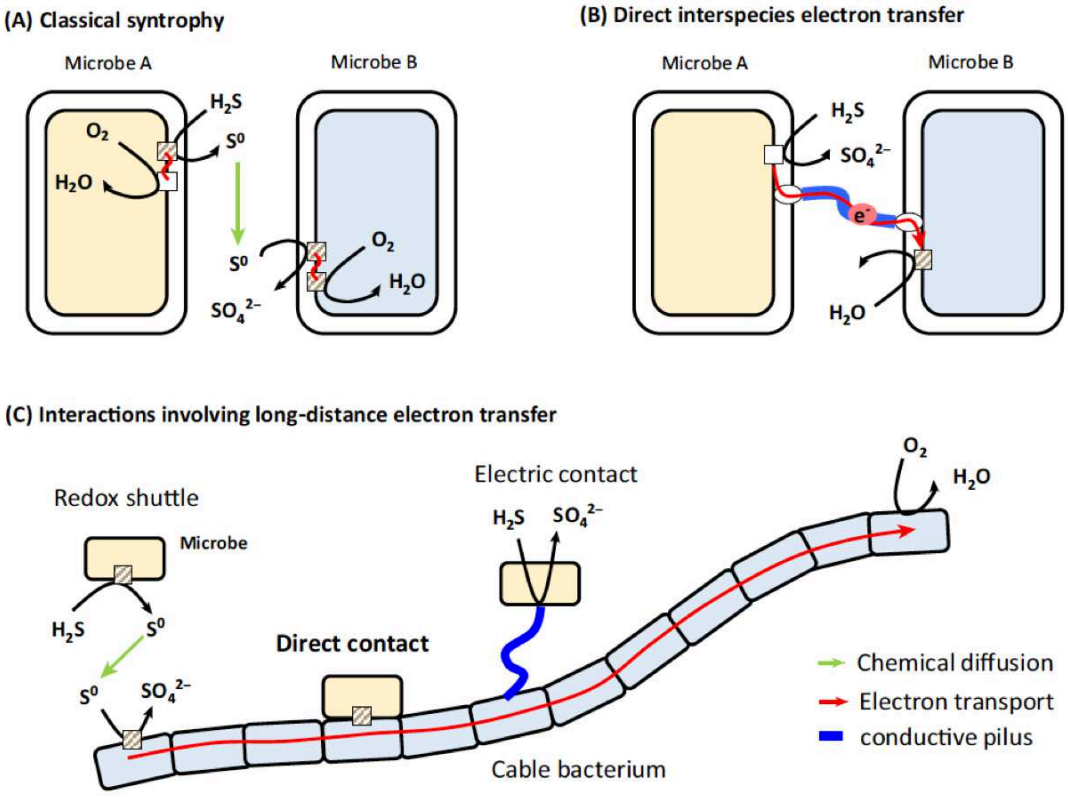

Figure 2.3 Different syntrophic interactions between bacterial partners to exchange their electrons [Meysman, 2018].

The advantage of using bacteria as a propagation method is their speed of transmission. The bacterium can swim at a speed of 25-40 μm/s, which is considerably higher compared to the speed of the random diffusion that does not exceed 2 μm/s [Zhang *et al.*, 2010]. Also, using them to build a conductive cable is very promising because it can reach very long distances. However, the achievable throughput is very low and the delay is very high. When we use their DNA to transmit information, the very limited size of the plasmids limits the quantity of information that can be sent in a symbol duration. Moreover, technically the bacterial cables do not behave as real conductive cables, because electrons are generated with chemical reactions and they take time to be transfered to the next cell which limits the throughput and increases the delay. The method that bacterial cables use to transfer electrons is closer to the proposed Ca^{2+} ions communication system [Barros, 2017] than to an actual conductive cable.

Propagation via gap junctions

Gap junctions are very small diameter channels that allow selective permeability of ions and molecules between the cytoplasm of two adjacent cells [Goldberg *et al.*, 2004]. In humans, these communicating junctions are mainly located in the central nervous system, the retina, the liver, the smooth muscles, the blood vessels and the heart. The best known and most studied is Ca^{2+} channels, which facilitate the diffusion of Ca^{2+} ions between cells.

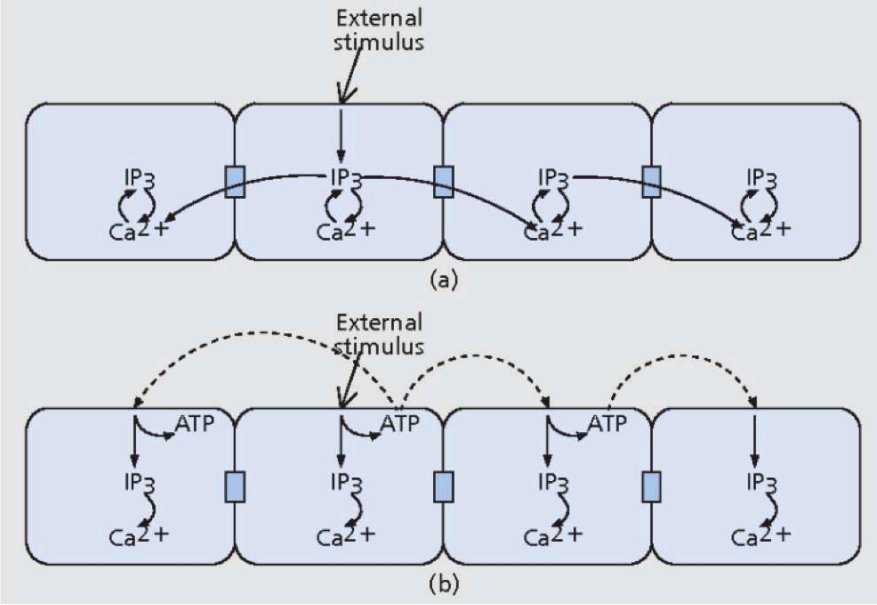

Figure 2.4 (a) Inner trajectory of Ca^{2+} ions propagation, (b) Outer trajectory.

In intercellular calcium systems, after the cell is stimulated, it generates a response to this stimulus by increasing the concentration of Ca^{2+} ions. The stronger the stimulus, the higher the concentration of the Ca^{2+} ions becomes. There are two types of trajectories for Ca^{2+} ions, inner and outer trajectories, as shown in Figure 2.4. In the case of the inner trajectory, Ca^{2+} ions pass through gap junctions to adjacent cells by using 1,4,5-triphosphate (IP3). In the case of the outer trajectory, Ca^{2+} ions cause secretion of ATP molecules to stimulate other cells, which in turn increase the concentration of Ca^{2+} ions that causes the secretion of ATP molecules. These two cases are complementary to each other, but the choice of the trajectory used in the communication has a drastic effect on the efficiency of the system. The inner trajectory is preferable in frequent and fast communications between adjacent cells, since the propagation velocity of Ca^{2+} ions can reach 23 μm/s. The outer trajectory is preferable in the communication between distant cells, which can reach 200 to 350 μm. The information sent from the stimulated cell to the target cell will be encoded in the concentration of Ca^{2+} ions [Scemes and Giaume, 2006].

Molecular communication systems based on these calcium gap junctions are proposed in the literature [Barros, 2017]. The first proposed system encodes the information in external stimulations, which trigger spikes and oscillations of Ca^{2+} concentration inside the cells [Nakano *et al.*, 2005]. Then, Ca^{2+} ions diffuse in the molecular channel using intracellular and intercellular signaling processes between adjacent cells. Finally, the nanomachines at the receiver demodulate and decode the information sent through Ca^{2+} signaling oscillations. Another work presents a new methodology for modeling Ca^{2+}-signaling-based molecular communication, which uses a linear channel model for both intracellular and intercellular Ca^{2+} signaling that accounts for Ca^{2+} wave generation for each cell and the propagation of these waves through the gap junction [Bicen *et al.*, 2016].

The advantage of using gap junctions between cells to propagate information is that it is biocompatible, which makes it one of the best choices for in-body tissue communications. Using Ca^{2+} signaling oscillations also increases the achievable throughput of molecular communication systems when they are used for short distances. However, the structure of Ca^{2+}-signaling-based systems, the encoding and decoding processes proposed in literature are impracticable at the current level of available technology. A lot of work is needed to be done in order to validate theses structures experimentally, because nature is analogue and digitalizing its data is very challenging. Moreover, high level of signal processing is inhibited because of the lack of processing power at the nanoscale. In addition, Stochastic differential equations are not enough to model Ca^{2+} signaling because of the infinite number of trips taken from cell–to-cell communications. Therefore, new approaches are

needed to design and solve this sum-over-trips problem such as mixing the network models with reaction-diffusion equations and finding the average distribution of cell-to-cell trips.

Propagation via motor proteins

The biological cell maintains its shape thanks to its cytoskeleton, which contains actin and microtubules filaments. Microtubules are made up of dimeric subunits composed of α and β-tubulin proteins, which polymerize into microtubules giving strength to the cell membrane and thus maintain its shape in the medium. It plays a major role in the separation of chromosomes during cell divisions [Moore and Endow, 1996]. The role of microtubules is also essential in the transport of vesicles inside cells, where it serves as a road between the place of the cargo to be transported and the destination [Goode *et al.*, 2000]. Kinesin is one of the most studied motor proteins in the cell. It has the ability to walk on the microtubule using the energy of ATP, and carry a cargo in one direction. As shown in Figure 2.5, kinesin contains a tail, a stalk, a neck domain and a head domain. The cargo can be attached to the tail, which is connected to the neck through the stalk. The head is the domain where kinesin binds to microtubules, while the neck gives it the flexibility needed for the act of walking. For each step, one head stays stationary while the other is detached and moves forward using the energy of adenosine triphosphate (ATP) hydrolysis. By repeating these cycles of conformational changes, the kinesin walks along the microtubule track in one direction. Therefore, kinesin acts as a locomotive inside the cell due to its ability to carry different cargoes on multiple microtubule tracks from one place to another.

Two molecular communication systems based on these motor proteins have been proposed in the literature. The first system consists of sending the information in vesicles carried by kinesin walking on a microtubule that connects the transmitter to the receiver [Enomoto *et al.*, 2011]. This is similar to the method used by living cells. The second system reverses the process. In this scenario, the carriers of the information are small microtubule filaments that move on kinesis attached to a substrate as illustrated in Figure 2.6 [Hiyama *et al.*, 2009].

The microtubule filaments carry and deliver the information using DNA bases, which covers the transmitter and the receiver. DNA is a molecule composed of two polynucleotide chains connected together with hybridization bounds, which they coil around each other to form a double helix. Each chain is made up with four types of nucleotides; adenine (A), thymine (T), guanine (G) and cytosine (C), with adenine bonding only to thymine in two hydrogen bonds, and cytosine bonding only to guanine in three hydrogen bonds, which

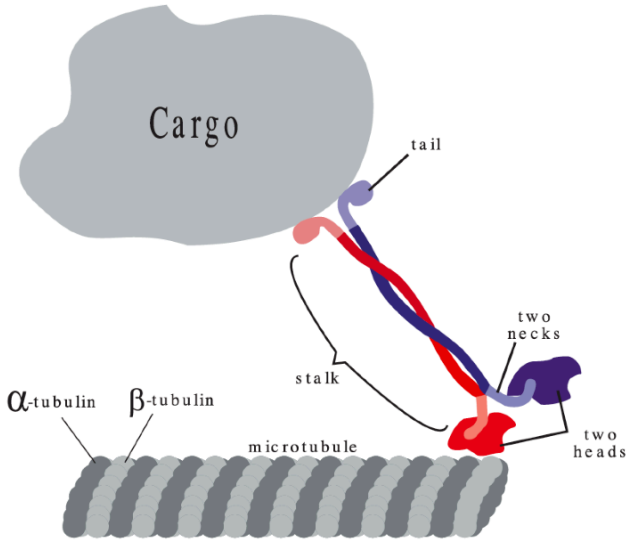

Figure 2.5 Structure of the microtubule and the kinesin motor [Farsad *et al.*, 2016].

is called complimentary base pairing. While the small microtubule filaments are covered with DNA bases, the vesicles carrying te information are covered with its complementary DNA bases. Passing the microtubule filaments closer to the transmitter forces the vesicles to bind to the complementary DNA that covers the microtubule filament and travels with it to the receiver. When the loaded microtubule filament arrives at the receiver, the vesicle binds to the complementary DNA that covers the receiver and unloads the information.

The disadvantage of this method is that it can only be used in lab-on-chip applications. Moreover, its achievable throughput is limited by the size of the vesicles and the process of propagation takes considerable amount of time, which drastically increases the delay.

2.2.2 Modulation techniques

Modulation is the process of varying the properties of the carrier signal to encode the information. In electromagnetic communication, the carrier signal is an electromagnetic wave, which is a sinusoidal signal that can be characterized by three properties namely: amplitude, frequency and phase. Several techniques have been designed for modulating the information by varying one or more properties of the sinusoidal wave. The information can be encoded by changing the peak-to-peak height of the signal's amplitude. It can also be encoded by changing the number of cycles per second (i.e. the sinusoid's frequency) or by changing the amount of shift from the origin (i.e. the sinusoid's phase) [Krouk and Semenov, 2011].

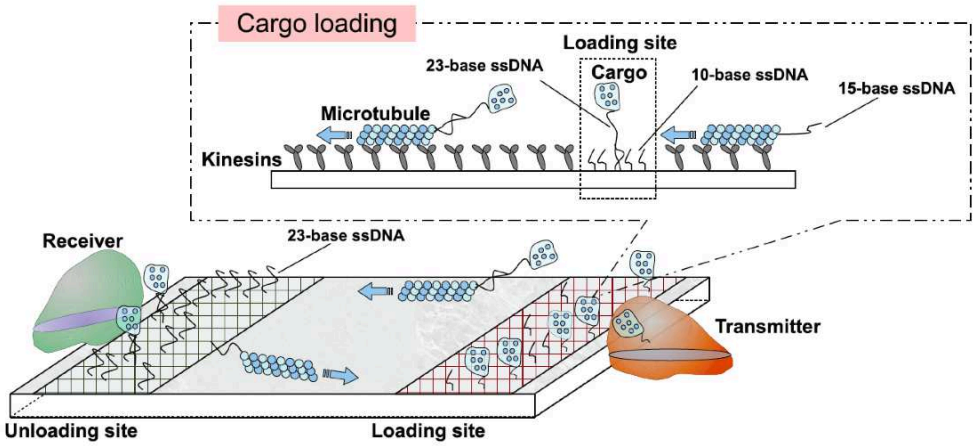

Figure 2.6 The second proposed system of motor proteins-based molecular communication [Farsad *et al.*, 2016].

In molecular communication, the carrier signal is not a wave, but diffusing molecules. Therefore, the modulation techniques used in traditional communication cannot be used in molecular communication. The techniques proposed in literature to modulate information in molecular communication are as follows:

Modulation by using the number of molecules

In this technique, the information is encoded by changing the number of molecules emitted by the transmitter. A bit "1" represents the maximum number of molecules and a bit "0" represents the minimum number of molecules. This technique is called Concentration Shift Keying (CSK) [Kuran *et al.*, 2012; Mahfuz *et al.*, 2011], which is similar to the on-off-keying of traditional communication systems. Pulse-Amplitude Modulated On-Off keying (PAM-OOK) is another modulation technique proposed in [Mahfuz, 2016], which uses Finite Pulsewidth (FP) instead of an ideal Impulse Modulation (IM) to transmit concentration-encoded symbols, and uses Strength-based method to detect the signal. While the performance of the PAM scheme is inferior compared to the performance of the IM scheme, PAM is more realistic because nanomachines cannot ideally release all the molecules as an impulse, which makes the IM scheme unfeasible. However, to have good results using this modulation technique, the pulse width should be as small as possible, which means controlling the number of released molecules and this modulation scheme does not include a mechanism for it.

Modulation by using the type of molecules

In this technique, we take advantage of the great variety of molecules in nature, and the very high selectivity of receivers to encode information in the type of molecules. A bit "1" represents a type of molecules, and a bit "0" represents another type of molecules. This technique is called Molecular Shift Keying (MoSK) [Kuran *et al.*, 2011], which is equivalent to changing the signal frequency, used in traditional communication systems. The isomer-based MoSK modulation technique is proposed in [Kim and Chae, 2013]. It uses aldohexoses isomers as messenger molecules. The study proposes three possible modulation techniques, concentration shift keying, molecule shift keying and ratio shift keying. The proposed method gives better results compared to the insulin-based technique [Kuran *et al.*, 2011], however, isomers are easily influenced by many elements present in propagation medium, which increases the error probability. Another proposed technique uses the ratio shift keying of two types of molecules to transmit a negative signal by coding the information in the difference of concentration between the two molecules [Mosayebi *et al.*, 2016]. The use of negative signals without increasing the expected number of transmitted molecules allows this technique to entirely cancel ISI, however, using two types of molecules consumes more energy and time, making the system more complex.

Modulation by using the release time of molecules

In this technique, the release of molecules is separated by a specified time interval. The information is encoded in the time between two consecutive releases. This technique is called Release Time Shift Keying (RTSK). A technique called Pulse Position Modulation (PPM) is proposed in [Garralda *et al.*, 2011], which divides the symbol interval into two equal halves. If the pulse's position is in the first half then the bit is "1", and it is a "0" if the pulse is detected in the second half of the symbol interval. This technique is similar to PPM in optical communication systems, but it can be significantly influenced by ISI.

The figure 2.7 below illustrates a comparison between the modulation techniques used in electromagnetic communication and the proposed techniques for molecular communication.

2.2.3 ISI Mitigation Techniques

The molecules carrying the information in molecular communication propagate randomly in the medium and reaches the receiver [Felicetti *et al.*, 2014]. However, some molecules from a previous transmission usually stay in the medium because of their random walk. This causes an interference with the molecules of the next transmission, which introduces

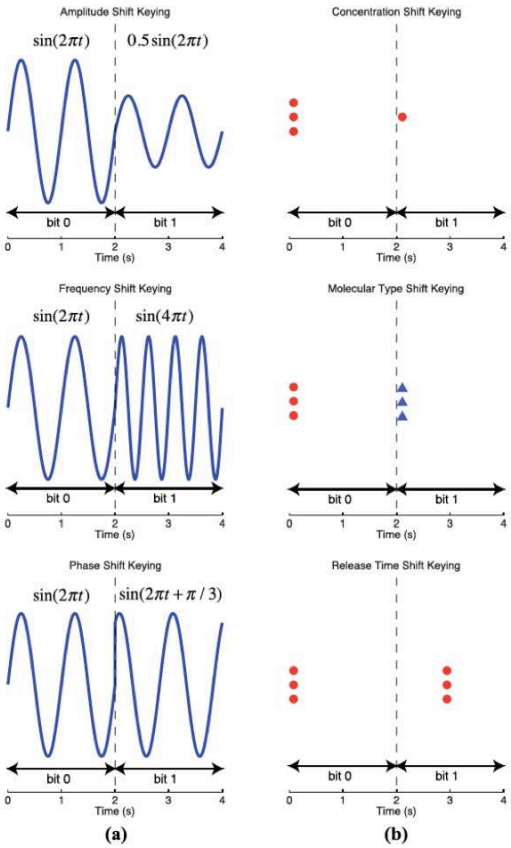

Figure 2.7 Modulation techniques(a) Electromagnetic communication (b) Molecular communication [Farsad *et al.*, 2016].

errors in the received signal and affects the reliability of the communication. To overcome this problem and mitigate the undesirable ISI, two categories of solutions have been proposed in literature; passive solutions [Akdeniz *et al.*, 2018; Arjmandi *et al.*, 2016, 2012, 2017; Chang *et al.*, 2018; Kadloor *et al.*, 2012; Kim *et al.*, 2014; Mahfuz *et al.*, 2015; Moore *et al.*, 2009; Mosayebi *et al.*, 2016; Nakano, 2017; Srinivas *et al.*, 2012; Tepekule *et al.*, 2015a,b] and active solutions [Assaf *et al.*, 2017; Dambri *et al.*, 2019; Noel *et al.*, 2014; Yilmaz *et al.*, 2016].

Passive Solutions

Passive solutions can be categorized into: a) a group that simply ignores ISI [Moore *et al.*, 2009], [Srinivas *et al.*, 2012], b) a group that uses modulation based methods [Arjmandi *et al.*, 2016, 2012, 2017; Mosayebi *et al.*, 2016; Nakano, 2017], c) a group that uses pre-equalization methods [Tepekule *et al.*, 2015a], [Tepekule *et al.*, 2015b], and d) a group

that optimizes the symbol time and the detection threshold [Akdeniz *et al.*, 2018; Chang *et al.*, 2018; Kadloor *et al.*, 2012; Kim *et al.*, 2014; Mahfuz *et al.*, 2015]. In [Arjmandi *et al.*, 2012], the authors propose a new modulation method based on hybridization between Concentration Shift Keying (CSK) and Molecular Shift Keying (MoSK). They use two types of molecules and their corresponding concentrations to encode the information and mitigate ISI. The authors in [Mosayebi *et al.*, 2016] use the same principle, but instead of using molecular concentration shift, the information is coded in the difference of concentration between the two molecules, which allows a better ISI mitigation. The work in [Arjmandi *et al.*, 2016] proposes an ion protein based modulation, which can control the rate of molecules release to avoid ISI. The modulation method proposed in [Arjmandi *et al.*, 2017] uses a short block-length constrained graph to avoid ISI in a shorter delay than in [Moore *et al.*, 2009]. However, this method can be used only in MoSK and not in CSK. Another newly proposed modulation technique uses the dynamic properties of calcium oscillation and propagation through coupled cells [Nakano, 2017]. The information is encoded in the dynamic amplitude, dynamic period or both. Nonetheless, dynamic patterns in biological cells are very complex, and their robustness against the environmental noise needs to be verified.

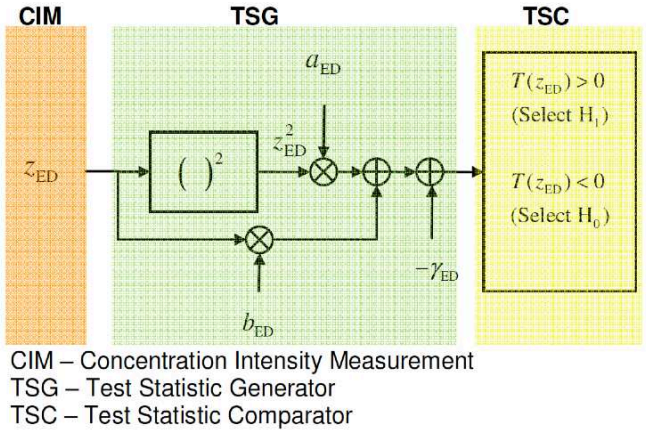

Figure 2.8 Strength-based receiver architecture to mitigate ISI [Mahfuz, 2016].

In [Tepekule *et al.*, 2015a], the authors use a pre-equalization method at the transmitter side to mitigate ISI, by means of two types of molecules; one for sending a primary signal and another for sending a secondary signal. After applying the substitution operation at the receiver, the interference can be reduced. However, the receiver needs a delay to make this substitution operation after two consecutive emissions, which may decrease the achievable throughput. The pre-equalization can also be applied at the receiver side as in [Tepekule *et al.*, 2015b], where two techniques are proposed; a linear equalization based

on Minimum Mean- Square Error (MMSE), and a complex non-linear based on Detection-Feedback Equalizer (DFE) with better performance. Another passive solution is the use of a flow to optimize the symbol time as in [Kim *et al.*, 2014] and [Kadloor *et al.*, 2012] where an optimization with drift is proposed to increase the speed of molecules and reduce ISI. In [Akdeniz *et al.*, 2018], the authors propose an optimal delay for the receiver to shift its absorption interval and mitigate ISI. Others in [Mahfuz *et al.*, 2015] propose new architectures based on molecular spike transmissions to design strength-based optimum receivers that can mitigate ISI, which is illustrated in Figure. 2.8. The previous mitigation methods are based on the case where transmitters and receivers are fixed. In [Chang *et al.*, 2018], the authors propose two adaptive signal detection schemes and an ISI mitigation method for mobile DbMC by considering the natural mobility of the bacteria *E. coli*. However, passive solutions such as those proposed in [Akdeniz *et al.*, 2018; Arjmandi *et al.*, 2016, 2012, 2017; Chang *et al.*, 2018; Kadloor *et al.*, 2012; Kim *et al.*, 2014; Mahfuz *et al.*, 2015; Mosayebi *et al.*, 2016; Nakano, 2017; Tepekule *et al.*, 2015a,b], either complicate the system or increase its delay, which results in decreasing the achievable throughput.

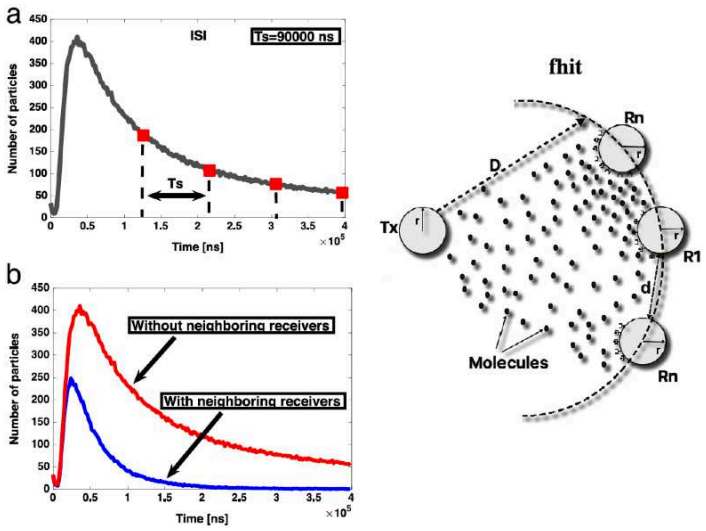

Figure 2.9 Interfering neighboring absorbing receivers and their impulse response [Assaf *et al.*, 2017].

Active Solutions

Active solutions aim to physically remove the molecules from the medium and decrease ISI without increasing the delay as nature does. In [Assaf *et al.*, 2017], the authors propose the use of neighboring receivers. The neighboring receivers compete with each other to absorb the molecules, which decreases ISI but at the same time decreases the strength of the signal as shown in Figure 2.9. The spherical receivers are located at the same distance

D from the transmitter forming an arc and conserve a distance d between them. The neighboring receivers absorb the molecules, which decreases their number in the medium, thus, the larger the number of these receivers, the better ISI is mitigated. However, the neighboring receivers also absorb the molecules carrying the information and not only the remaining ones from a previous transmission, which drastically decreases the strength of the signal. In addition, this method is used only with the scenario of fixed receivers, which limits its application.

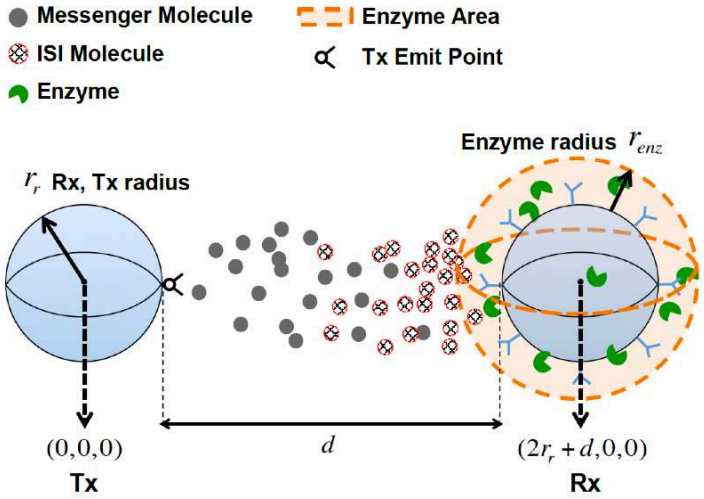

Figure 2.10 Enzyme deployment in a limited aeria around the receiver [Cho *et al.*, 2017].

Inspired by nature, another active solution [Noel *et al.*, 2014] proposes the use of diffusing enzymes in the propagation environment to catalyze the degradation of molecules already received so they will not interfere with future transmissions. Enzymes selectivity and recyclability allows transforming the shape of molecules and thus, even if they stay in the medium they become unrecognizable by the receiver, which mitigates ISI. A lower bound expression on the expected number of molecules observed at a receiver is derived in the study when enzymes are present in the propagation environement. The accurate results of this study also shows that the presence of enzymes can decrease the probability of error. Nonetheless, enzymes reduce the ISI but they also reduce the transmitted signal, which decreases the transmission rate. Moreover, the study assumes an infinite number of enzymes in the medium, which is unrealistic. Instead of using the enzymes in all communication channels, the study in [Yilmaz *et al.*, 2016] proposes the deployment of a constant and limited number of enzymes around the transmitter or around the receiver. As illustrated in Figure. 2.10, the study shows that deploying enzymes around the receiver with an optimal radius gives better results in mitigating ISI. The advantage

of this solution is that it can avoid ISI by using only a small constant quantity of enzymes and it also provides an optimal radius where we can put the enzymes around the receiver with a smaller interference-to-total-received molecules (ITR) metric. However, this method decreases the power of the signal and its application is only limited to short range communications. Moreover, putting enzymes in a fixed position in real systems is a very difficult challenge that needs to be tackled.

Nevertheless, despite their advantages, the previously discussed active solutions reduce the signal strength while mitigating ISI [Assaf *et al.*, 2017; Dambri *et al.*, 2019; Noel *et al.*, 2014; Yilmaz *et al.*, 2016]. The neighboring receivers absorb the molecules carrying the information, and the enzyme degrades not only the remaining molecules in the medium, but also the molecules carrying the information. Thus, there is a trade-off between ISI mitigation and the signal strength. Increasing the power of the signal increases ISI and mitigating ISI reduces the power of the signal.

CHAPTER 3

ISI MITIGATION

Auteurs et affiliation:

Oussama Abderrahmane Dambri: étudiant au doctorat, Département de Génie Électrique et de Génie Informatique ,Université de Sherbrooke. INTERLAB Research Laboratory.

Soumaya Cherkaoui: Professeur, Département de Génie Électrique et de Génie Informatique, Université de Sherbrooke. INTERLAB Research Laboratory.

Date de Parution: Janvier 2020

Revue: *IEEE Transactions on NanoBioscience*

Titre français: Amélioration des Performances de la Communication moléculaire Basée sur la Diffusion

Résumé français:

L'interférence inter-symboles (ISI) est l'un des défis de la communication moléculaire basée sur la diffusion bio-inspirée. La dégradation des molécules restantes d'une transmission précédente est la solution que les systèmes biologiques utilisent pour atténuer cet ISI. Alors que la plupart des travaux antérieurs ont proposé l'utilisation d'enzymes pour catalyser la dégradation des molécules, les enzymes dégradent également les molécules porteuses de l'information, ce qui diminue considérablement la force du signal. Dans cet article, nous proposons l'utilisation de réactions de photolyse, qui utilisent la lumière pour transformer instantanément les molécules émises afin qu'elles ne soient plus reconnues après leur détection. La lumière sera émise dans un temps optimal, permettant au récepteur de détecter autant de molécules que possible, ce qui augmente à la fois la force du signal et l'atténuation ISI. Une expression de limite inférieure sur l'espérance du nombre de molécules observées au niveau du récepteur est dérivée. Une expression de probabilité d'erreur sur les bits est également formulée, et les deux expressions sont validées avec des résultats de simulation, qui montrent une amélioration visible lors de l'utilisation de réactions de photolyse. Les performances de la méthode proposée sont évaluées à l'aide des molécules d'interférence au total reçu (ITR) et de la probabilité d'erreur sur les bits dérivée.

3.1 Performance Enhancement of Diffusion-Based Molecular Communication

3.2 Abstract

Inter-Symbol Interference (ISI) is one of the challenges of bio-inspired diffusion-based molecular communication. The degradation of the remaining molecules from a previous transmission is the solution that biological systems use to mitigate this ISI. While most prior work has proposed the use of enzymes to catalyze the molecules degradation, enzymes also degrade the molecules carrying the information, which drastically decreases the signal strength. In this paper, we propose the use of photolysis reactions, which use the light to instantly transform the emitted molecules so they no longer be recognized after their detection. The light will be emitted in an optimal time, allowing the receiver to detect as many information molecules as possible, which increases both the signal strength and ISI mitigation. A lower bound expression on the expectation of the observed molecules number at the receiver is derived. The bit error probability expression is also formulated, and both expressions are validated with simulation results, which show a visible enhancement when using photolysis reactions. The performance of the proposed method is evaluated using Interference-to-Total-Received molecules metric (ITR) and the derived bit error probability.

3.3 Introduction

The words of the great physicist Richard Feynman "There's Plenty of Rooms at the Bottom"[Feynman, 1960] were an inspiration for nanotechnology progress over the last century. The exponential growth in the use of nanodevices in every area in science and industry paved the way to a big interest in nanonetworks design. Nanonetworks allow the communication between nano-devices at a nanoscale level. Nanonetworks can be used in medical applications such as drug delivery and monitoring in medical field [Femminella *et al.*, 2015], [Chude-Okonkwo *et al.*, 2017]. Several research works proposed using radio frequency communications to enable nanonetworks. However, using the traditional electromagnetic field at the nano level entails using the terahertz band with all its peculiarities and challenges. Indeed, THz suffer from a high path loss, which is caused by molecular absorption [Akyildiz *et al.*, 2014; Federici and Moeller, 2010; Khan *et al.*, 2016; Song and Nagatsuma, 2011].

One of the most promising solutions to communicate at such small level is using the method which nature adopted billions of years ago; utilizing molecules as information carriers between the transmitter and the receiver. The most basic method proposed for this bio-inspired paradigm is the Diffusion-based Molecular Communication (DbMC) [Nakano *et al.*, 2012; Nakano and Suda, 2017; Pierobon and Akyildiz, 2010].

DbMC is based on the thermal fluctuations that allow molecules to move randomly in the medium using all possible degrees of freedom. This diffusive Brownian motion of molecules from the transmitter to the receiver is the wireless molecular communication used in the Biosystems, from bacterial colonies to the human brain [Meer *et al.*, 1997; Pacheco and Sperandio, 2009; Vizi *et al.*, 2004]. Instead of using electromagnetic waves, the transmitter sends molecules as carriers of the information, which propagates randomly in the medium, and reaches the receiver [Felicetti *et al.*, 2014]. However, some molecules from a previous transmission usually stay in the medium because of their random walk. This causes interference with the molecules of the next transmission, those introducing errors at the receiver and affecting the communication reliability. To overcome this problem and mitigate the undesirable Inter-Symbol Interference (ISI), two categories of solutions have been proposed in literature; passive solutions [Akdeniz *et al.*, 2018; Arjmandi *et al.*, 2016, 2012, 2017; Chang *et al.*, 2018; Kadloor *et al.*, 2012; Kim *et al.*, 2014; Mahfuz *et al.*, 2015; Moore *et al.*, 2009; Mosayebi *et al.*, 2016; Nakano, 2017; Srinivas *et al.*, 2012; Tepekule *et al.*, 2015a,b] and active solutions [Assaf *et al.*, 2017; Dambri *et al.*, 2019; Noel *et al.*, 2014; Yilmaz *et al.*, 2016].

Passive solutions can be categorized into; a) a group that simply ignores ISI [Moore *et al.*, 2009], [Srinivas *et al.*, 2012], b) a group that uses modulationbased methods [Arjmandi *et al.*, 2016, 2012, 2017; Mosayebi *et al.*, 2016; Nakano, 2017], c) a group that uses pre-equalization methods [Tepekule *et al.*, 2015a], [Tepekule *et al.*, 2015b], and d) a group that optimizes the symbol time and the detection threshold [Akdeniz *et al.*, 2018; Chang *et al.*, 2018; Kadloor *et al.*, 2012; Kim *et al.*, 2014; Mahfuz *et al.*, 2015]. In [Arjmandi *et al.*, 2012], the authors propose a new modulation method based on hybridization between Concentration Shift Keying (CSK) and Molecular Shift Keying (MoSK). They use two types of molecules and their corresponding concentrations to encode the information and mitigate ISI. The authors in [Mosayebi *et al.*, 2016] use the same principle, but instead of using molecular concentration shift, the information is coded in the difference between the two molecules concentrations, which allows a better ISI mitigation. The work in [Arjmandi *et al.*, 2016] proposes an ion protein based modulation, which can control the rate of molecules release to avoid ISI. The modulation method proposed in [Arjmandi *et al.*,

2017] uses a short block-length constrained graph to avoid ISI in a shorter delay than in [Moore *et al.*, 2009]. However, this method can be used only in MoSK and not in CSK. Another newly proposed modulation technique was found to use the dynamic properties of calcium oscillation and propagation through coupled cells [Nakano, 2017]. The information is encoded in the dynamic amplitude, dynamic period or both. Nonetheless, dynamic patterns in biological cells are very complex, and their robustness against the environment noise needs to be verified.

In [Tepekule *et al.*, 2015a], the authors use a pre-equalization method at the transmitter side to mitigate ISI, by means of two types of molecules; one for sending a primary signal and another for sending a secondary signal. After applying the substitution operation at the receiver, the interference can be reduced. However, the receiver needs a delay to make this substitution operation after two consecutive emissions, which may decrease the achievable throughput. The pre-equalization can also be applied at the receiver side as in [Tepekule *et al.*, 2015b], where two techniques 2 are proposed; a linear equalization based on Minimum Mean- Square Error (MMSE), and a complex non-linear based on Detection-Feedback Equalizer (DFE) with better performance. Another passive solution is the use of a flow to optimize the symbol time as in [Kim *et al.*, 2014] and [Kadloor *et al.*, 2012] where an optimization with drift is proposed to increase the speed of molecules and reduce ISI. In [Akdeniz *et al.*, 2018], the authors propose an optimal delay for the receiver to shift its absorption interval and mitigate ISI. Others in [Mahfuz *et al.*, 2015] propose new architectures based on molecules spike transmissions to design strength-based optimum receivers that can mitigate ISI. The previous mitigation methods are based on the case where transmitters and receivers are fixed. In [Chang *et al.*, 2018], the authors propose two adaptive signal detection schemes and an ISI mitigation method for mobile DbMC by considering the natural mobility of the bacteria *E. coli*. However, passive solutions such as those proposed in [Akdeniz *et al.*, 2018; Arjmandi *et al.*, 2016, 2012, 2017; Chang *et al.*, 2018; Kadloor *et al.*, 2012; Kim *et al.*, 2014; Mahfuz *et al.*, 2015; Mosayebi *et al.*, 2016; Nakano, 2017; Tepekule *et al.*, 2015a,b], either complicate the system or increase its delay, which results in decreasing the achievable throughput.

Active solutions aim to physically remove the molecules from the medium and decrease ISI without increasing the delay as nature does [Chude-Okonkwo *et al.*, 2019]. In [Assaf *et al.*, 2017] and [Dambri *et al.*, 2019], the authors propose the use of neighboring receivers. The neighboring receivers compete with each other to absorb the molecules, which decreases ISI but at the same time decreases the strength of the signal. Another active solution [Noel *et al.*, 2014] uses enzymes to catalyze the degradation of molecules in the medium.

Enzymes selectivity and recyclability allows transforming molecules so that they become unrecognizable by the receiver, which mitigates ISI. Instead of using the enzymes in all communication channels, the study in [Yilmaz *et al.*, 2016] proposes the deployment of a constant and limited number of enzymes around the transmitter or around the receiver. The study showes that deploying enzymes around the receiver with an optimal radius gives better results in mitigating ISI. Nevertheless, despite their advantages, the previously discussed active solutions reduce the signal strength [Assaf *et al.*, 2017; Dambri *et al.*, 2019; Noel *et al.*, 2014; Yilmaz *et al.*, 2016]. The neighboring receivers absorb the molecules carrying the information, and the enzyme degrades not only the remaining molecules in the medium, but also the molecules carrying the information.

To mitigate ISI without decreasing the signal strength or increasing the delay, we need faster reaction to catalyze the remaining molecules in the medium and a catalyzer that can be switched ON/OFF. Using light can help to satisfy these two criteria. The photolysis is a chemical process where chemical bonds are broken as the result of a light energy transfer [Speight, 2017]. Photolysis occurs with a very fast, first order degradation rate. The rate depends upon several chemical and environmental factors such as the light adsorption properties of the medium, the intensity of light radiation and the reactivity of the target chemical. The most famous photolysis reaction is the photosynthesis in plants, where light energy splits water molecules and produces oxygen. However, the most studied photolysis reaction is the one that triggers the daily vitamin D formation in human skin after sunlight exposure.

In our previous work [Dambri and Cherkaoui, 2018], we proposed the use of UV light to instantly degrade provitamin D_3 molecules into previtamin D_3. The figure 3.1 presents the proposed system model by showing molecules propagation (shown as blue circles), released from the transmitter (Tx) to the 3D spherical receiver (Rx) away with distance d. The received molecules (shown as red stars) are inside the 3D receiver Rx. At time T_{op}, the light emitters (shown as black rectangles) up and down the receiver Rx emit light waves (shown as green arrows) hitting the molecules, which they absorb the light energy and instantly transform to photolysis reaction's products (shown as yellow squares). The UV light is turned ON at an optimal time, i.e. when the maximum number of molecules is absorbed at the receiver, to degrade only the remaining molecules and mitigate ISI without decreasing the strength of the signal. This kind of photolysis reaction happens daily in human skin and it could be used safely in medical applications inside the body.

This paper is an extension of the work proposed in [Dambri and Cherkaoui, 2018], where we introduced the system concept and some preliminary simulation results. In this paper,

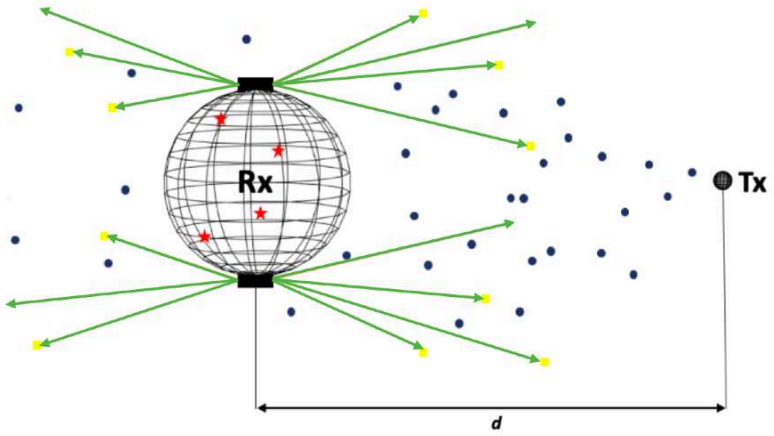

Figure 3.1 System model that uses photolysis reaction to mitigate ISI.

we propose an analytical model for analyzing diffusion-based molecular communication systems in general, when they are exposed to any light in a larger spectrum than solely UV. The main contributions of the paper are summarized as follows:

1. We present a lower bound expression on the expected number of molecules observed at a passive receiver when using a binary modulation and a light beam as a molecule catalyzer.
2. We present an analytical comparison between a scenario without reaction, a scenario with enzymatic reaction and the proposed photolysis reaction scenario.
3. We derive the expression of the optimal time to turn the light ON, giving more chance to as many molecules as possible to reach the receiver before triggering the photolysis reaction.
4. We derive the bit error probability as a function with a threshold value to evaluate the proposed analytical model and the simulation results.

The rest of the paper is organized as follows. In section 3.4, we present the proposed system model that comprises a single transmitter using binary CSK modulation, and a single receiver, which can emit a controlled flash light. In section 3.5, we present the derived lower bound expression on the expected number of molecules at the receiver when exposing the medium to light. Then a comparison between a scenario without reaction, a scenario with enzymatic reaction and the proposed photolysis reaction scenario is presented. The expression of the optimal time at which to turn the light ON and the bit error probability

as a function with a threshold are derived in the section 3.6. In section 3.7, we discuss the obtained results. And finally, conclusion and future work are described in section 3.8.

3.4 System Model

The proposed system model in this paper is similar to the system studied in [Dambri and Cherkaoui, 2018], where we consider that the DbMC process takes place inside a 3D fluidic environment. The system contains a fixed point transmitter, a spherical receiver with a radius r and a communication channel with a distance d as shown in Fig. 3.1. The modulation of the signal at the transmitter in DbMC can be done by shifting the concentration of molecules, changing their types or shifting their time of release. In this study, the signal is modulated with a binary Concentration Shift Keying (CSK). The transmitter sends an impulse of molecules to represent bit 1 and to reduce the energy consumption, it sends nothing to represent bit 0. The receiver is a 3D spherical passive observer, which can only count the number of molecules while they diffuse through it and cannot interact with them or change their behavior. If we neglect the interaction among the independent propagating molecules, and if we assume that all molecules have an identical spherical shape and the same diffusion constant D, we can deduce that their diffusion follows a continuoustime stochastic process. This Brownian motion that allows molecules to diffuse towards the receiver can be described with Fick's second law as follows:

$$\frac{\partial S}{\partial t} = D\nabla^2 S, \tag{3.1}$$

where S is the concentration of the released molecules, t is the time and D is the diffusion coefficient that can be calculated with the following equation:

$$D = \frac{k_B T}{6\pi\eta R}, \tag{3.2}$$

where R is the radius of the molecules, T is the temperature in kelvin, kB is the Boltzmann constant, and η is the viscosity of the medium ($\eta \approx 10^{-3} kg.m^{-1}s^{-1}$ at temperature $25°C$) [Noel *et al.*, 2014].

We assume the existence of a light nano-emitter that can emit a monochromatic light with a predetermined wavelength λ and in a controlled optimal time T_{op}. The light nano-emitter will wait for a maximum number of molecules to reach the receiver and then, it switches ON the light emission to degrade the remaining molecules in the medium. To implement the nano-emitter on the top and the bottom of the receiver as shown in Fig. 3.1 and use it

safely inside the human body, we can take advantage of the specific and selective receptors that we find embedded in cell membranes. We can also use the DNA hybridization to safely bind the nano-emitter with the receiver as proposed in [Farsad *et al.*, 2016]. By inserting a sequence of DNA on the surface of the receiver, and its complementary on the surface of the nano-emitter, they bind together with hydrogen bonds when they get close to each other, which binds the nano-emitter to the receiver. The implementation of the nano-emitter will be noninvasive and safe because of its small size. While the miniaturization of monochromatic light generators is reaching the millimeter level as the photochemical UV-LED proposed in [Zou *et al.*, 2018], with the fast progress of nanotechnology, reaching the micro and nano levels is just a matter of time.

The light in this proposed system is the reaction catalyzer, which instantly transform the molecules that absorb the light energy by breaking specific chemical bonds. Therefore, the transforming molecules will no longer be recognized by the receiver and they cannot cause ISI. The reaction that breaks chemical bonds by using the absorbed light energy is called a photolysis reaction.

3.4.1 Photolysis Reaction

The photodissociation famously known as the photolysis is a reaction where a chemical bond of a chemical compound is broken down by a photon [Speight, 2017]. This photon must have a sufficient energy that allows the bond to overcome its dissociation barrier. The photons in the infrared spectral range do not have enough energy for a direct photodissociation of molecules, because the photons energy is inversely proportional to its wavelength. Thus, the energy of the visible light or higher electromagnetic waves as UV light, X-rays and gamma rays are usually the ones involved in this reaction. The photolysis has been intensively studied in different domains such as in the atmosphere reactions that creates the ozone layers [Chowdhury, 1998]. It is also studied in photosynthesis as part of the light-dependent reactions [McEvoy and Brudvig, 2006], and in astrophysics, where

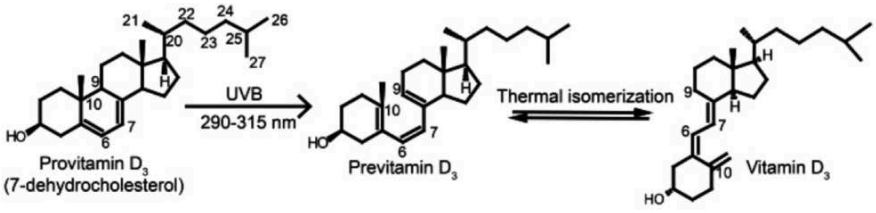

Figure 3.2 Vitamin D_3 Synthesis with a photolysis and a thermal reaction. [Jäpelt and Jakobsen, 2013]

photolysis plays an important role in interstellar clouds formation [Dishoeck *et al.*, 1988]. However, even if the wavelength, the chemical compound and its by-product change in every study, the photolysis principle stays the same. Each chemical compound needs a specific amount of energy to break a bond, and when the electromagnetic wave passes through it with the specific wavelength, it transfers the energy of the wave to the bond and breaks it. In the case of the ozone layer, the energy needed to split oxygen molecules into two individual atoms in the Mesosphere can be provided with an ultraviolet photon with a wavelength between 200 and 300 nm [Chowdhury, 1998]. The by-product of this photolysis reaction combines with an unbroken O_2 to create the ozone O_3 in the Stratosphere. On the other hand, the light-dependent reactions in the photosynthesis need the visible light, to split water molecules, especially the blue with a wavelength between 450-495 nm and the red with a wavelength between 620-750 nm [McEvoy and Brudvig, 2006]. In human body, we can find photolysis in the skin, where the provitamin D_3 transforms to previtamin D_3 when exposed to the UV photons of the sun light [MacLaughlin *et al.*, 1982]. Then, the previtamin D_3 transforms to vitamin D_3 with a thermal isomerization as in the reaction shown in Fig. 3.2 [Jäpelt and Jakobsen, 2013].

In our previous study [Dambri and Cherkaoui, 2018], we proposed the use of provitamin D_3 molecules as carriers of the information and the UV light as a catalyzer to the photolysis reaction in order to mitigate ISI. We chose 298 nm wavelength for the UV light photons because it is the wavelength where the absorption of provitamin D_3 is in its maximum as proved in the study [Kimlin, 2008]. In this paper, we generalize the use of the catalyzers wavelength from 298 nm to a spectrum range between [200-750 nm]. We can use photons with any wavelength inside that spectrum, with a condition that the chosen wavelength should be absorbed by the molecules carrying the information to dissociate them.

The choice of sensitive molecules to the chosen wavelength as information carriers can be either from already existed molecules in nature as the chromophores and provitamin D_3 or from bioengineered molecules. The chromophores are sensitive to visible light, and the provitamin D_3 is sensitive to UV light. However, molecules with a specified wavelength absorption can be engineered, as in the study [Handy *et al.*, 1992], where they proved that by doping pure vanadia, they can change their optical absorption spectra as shown in Fig. 3.3.

For medical applications, the visible light is not dangerous to be used inside the human body. However, if shorter wavelengths are chosen to be used, as we proposed in our previous study, there are some standards that should be respected to ensure the safety of its use. The UV light by itself is fairly safe, but the level of the radiation energy and

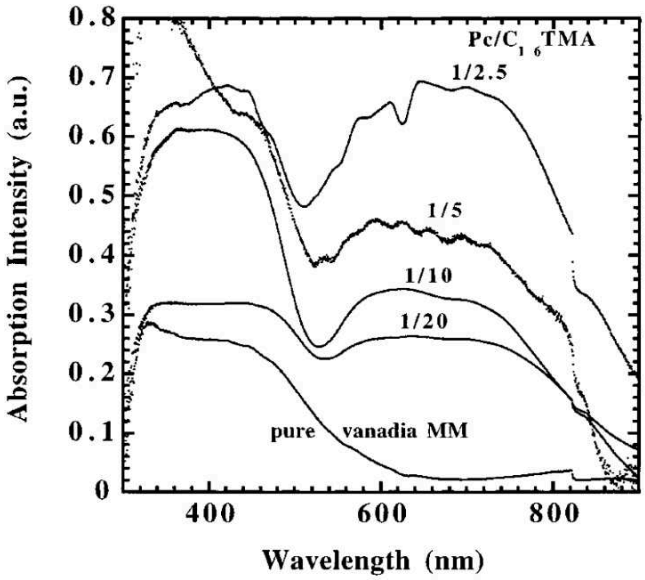

Figure 3.3 Optical absorption spectra for the pure and the doped vanadia. [Handy *et al.*, 1992]

time of exposure are what influence whether or not it is harmful. Therefore, the American National Standards Institute (ANSI) defined the standard ANSI Z-136.1 [America and N/A, 2014], which gives the Maximum Permissible Exposure limits (MPEs) for users. The minimum MPE for the UV light is 3.0 mJ/cm^2 over 8 hours. The exposure limits given by the ANSI Z-136.1 are measured under worst- case conditions at the cornea of the human eye, because it is the most sensible part of our body to light. Therefore, if the generated UV energy and the exposure time are safe for the cornea, then they are safe to be used inside the body. While the predominant cause of UV radiation injury is a thermal process [McKenzie, 1990], a safe UV generator should be designed to generate nonthermal radiation by using pulsed beam instead of continuous one. The energy will be concentrated into a very short time, and this compression delivers the beam light more rapidly, which gives more power using less energy [Sliney and Trokel, 2012]. The shorter the time of the pulse, the less energy is used, which drastically decreases the risk of tissue burn. Thus, to safely generate UV light inside the body, the generator should use picosecond pulses or less, with energy less than 3 mJ/cm^2. That can justify the chosen value of the pulse duration in our previous study [Dambri and Cherkaoui, 2018], which is 4 picosecond pulse and 2 mJ/cm^2 as incident energy [Gottfried *et al.*, 1984].

3.5 Receiver Observations

The passive receiver observes and counts the number of molecules, which diffuse through it. In order to derive the expression of the expected molecules number at the receiver, we can use the differential equation of molecules diffusion described in Fick's second law 3.1. In this section, we use this differential equation as in [Noel *et al.*, 2014] to derive the expected molecules number for three different scenarios: a) the scenario without reaction, b) the scenario with enzyme reactions and c) the scenario with photolysis. The enzyme reactions can be modeled using the Michaelis-Menten kinetics presented as follows [Ingalls, 2013]:

$$E + S \underset{k_{-1}}{\overset{k_1}{\rightleftharpoons}} M_c \xrightarrow{k_2} E + P, \tag{3.3}$$

where E is the concentration of enzymes, S is the concentration of the substrate, P is the concentration of the reaction product and M_c is the complex enzyme-substrate called Michaelis complex. The rate constants of the reaction k_n represent the speed of each reaction's step [Alberts *et al.*, 2002]. The first reaction rate constant where n=1 represents the speed at which enzymes and substrates bind together. The second reaction rate constant (n=-1) represents the speed of their unbinding, and the last one (n=2) represents the substrate degradation speed to the product. We can notice from 3.3 that enzymes are released intact after degradation and they can be reused and participate in future reactions. The photolysis reaction can be modeled as follows :

$$S + h\upsilon \xrightarrow{J} P, \tag{3.4}$$

where h is Planck's constant, and υ is the photon frequency. The reaction rate J is a very fast first order reaction decay constant, which degrades S to P by using the photon energy and we can write:

$$\frac{\partial S}{\partial t} = -JS, \tag{3.5}$$

The J coefficient is dependent on solar radiation intensity and the photo-physical properties of the substrate. We can calculate it as described in [Jacob, 2000]:

$$J = \int_{\lambda} \phi(\lambda, T)\sigma(\lambda, T)F(\theta, \lambda)d\lambda, \tag{3.6}$$

where the function ϕ is the quantum yield for the substrate as a function the wavelength λ and temperature T. The function σ is the absorption cross-section for a wavelength λ and a temperature T, which can be determined experimentally. $F(\theta, \lambda)$ is the light point irradiance (actinic flux) as a function of the wavelength λ and the light zenith angle θ.

3.5.1 Diffusion Without Degradation Reaction

The received information at the receiver is represented by the observed impulse of molecules diffused from the transmitter at a distance d. The pdf expression of the expected molecules to be located inside the spherical receiver can be derived by solving the differential equation in (1). As in [Noel *et al.*, 2014], we assume that the receiver is a point observer and that the concentration inside the receivers volume is uniform and equal to the expected concentration in the center. The solution of the differential equation can be written as:

$$S(t) = \frac{NV}{8(\pi Dt)^{3/2}} \exp(\frac{-d^2}{4Dt}), \tag{3.7}$$

where $S(t)$ is the probability density function (pdf) of the expected molecules number. N is the number of molecules released by the transmitter for one bit. V is the volume of the receiver, D is the diffusion coefficient, d is the distance between the transmitter and the receiver, t is the time when molecules are detected by the receiver. The equation 3.7 is the starting point from which we begin the build of our proposed system model, and against which we compare and evaluate the two other scenarios.

3.5.2 Diffusion With Enzyme Reaction

In nature, enzymes are used to accelerate biochemical reactions to build or to degrade molecules. In most cases, enzymes are specific to only one reaction, because of their high selectivity. In the second scenario, enzymes are added in the medium and diffuse between the transmitter and the receiver. Binding to the molecules carrying the information, the enzymes influence the diffusion of the molecules, thus, the equation 3.1 becomes [Noel *et al.*, 2014]:

$$\frac{\partial Z}{\partial t} = D\nabla^2 Z + f(Z, t), \tag{3.8}$$

where $f(.)$ is the term of the reaction in 3.3 using the chemical kinetics principles, and Z represents the different species of the reaction, molecules, enzymes, products and Michaelis complex. In this study, we are interested only in the term reaction of the molecules and

the equation 3.8 can be written as:

$$\frac{\partial Z}{\partial t} = D\nabla^2 Z - k_1 SE + k_{-1} M_c, \tag{3.9}$$

where k_1 represent the rate of the binding between the molecules S and the enzymes E, k_{-1} is the rate of Michaelis complex (M_c) degradation into enzymes and molecules.

An analytical closed-form solution for the equation 3.9 is hard to find, and by making simplified assumptions as explained in [Noel *et al.*, 2014], we can derive a lower bound expression on the expected impulse response. To simplify the solution, we need to slow down the unbinding reaction by converging the rate k_{-1} to zero, and accelerate the degradation reaction until we use all the enzymes in the medium, so that their concentration becomes constant E_{tot}. Therefore, the lower bound expression can be written as:

$$S(t) \geq \frac{NV}{8(\pi Dt)^{3/2}} \exp(-k_1 E_{tot} - \frac{-d^2}{4Dt}), \tag{3.10}$$

where E_{tot} is the total concentration of bound and free enzymes in the medium. The authors of the study in [Noel *et al.*, 2014], proved that this lower bound expression can be more accurate and improves with time, and its accuracy is dependent on the accuracy of the two assumptions made about the reaction. We can notice that the equation 3.10 can directly be compared to the equation 3.7. We see that the addition of enzymes in the medium increases the decaying exponential caused by the distance. If we increase the binding rate or the total concentration of enzymes, we can increase the decaying speed, which decreases the ISI. However, that will also decrease the strength of the useful signal, because we cannot control the time of enzyme reactions. Although, this can be possible with photolysis reactions.

3.5.3 Diffusion With Photolysis Reaction

The third scenario is similar to the second one, but instead of degrading the molecules with enzymes, we use the energy of photons. The diffusion of molecules in this case exercises two phases, a phase without light and a phase with light. The diffusion in the first phase is the same as in the first scenario (without any reaction), and it can be described with equation 3.1. The diffusion in the second phase when the light is turned ON changes, because when the photon hits the molecule, the energy that degrades it also slightly change its direction. Light influence the diffusion of molecules as enzymes do in the second scenario, and the

second phase can be described with the equation 3.8. Therefore, the differential equation in this scenario is the sum of (3.1) and (3.8), and it can be written as:

$$\frac{\partial S}{\partial t} = \begin{cases} D\nabla^2 S, & \text{if } t < T_{op}, \\ D\nabla^2 S + f(S,t), & \text{if } t \geq T_{op}. \end{cases} \tag{3.11}$$

where S is the concentration of the released molecules, T_{op} is the optimal time to turn the light ON, which will be derived in the next section. $f(S,t)$ is the term of the reaction in (3.4), and by using (3.5) we can write (3.11) as:

$$\frac{\partial S}{\partial t} = \begin{cases} D\nabla^2 S, & \text{if } t < T_{op}, \\ S(D\nabla^2 - J), & \text{if } t \geq T_{op}. \end{cases} \tag{3.12}$$

where J is the reaction rate coefficient.

The assumptions made to simplify the solution of the equation (3.9) in the case of enzymes do not exist in the case of photolysis. However, we assume that the intensity of light is uniformed around the receiver with a radius $r = d$ so that the degradation of molecules will be homogeneous, which is not the case in the real system. Under the boundary conditions of the third scenario, the solution of the equation (3.12) gives a lower bound expression on the expected number of molecules at the receiver. Then, the expected impulse response of the photolysis scenario can be written as:

$$\begin{cases} \frac{\partial S}{\partial t} = \frac{NV}{8(\pi Dt)^{3/2}} \exp(\frac{-d^2}{4Dt}), & \text{if } t < T_{op}, \\ \frac{\partial S}{\partial t} \geq \frac{NV}{8(\pi Dt)^{3/2}} \exp(-Jt - \frac{-d^2}{4Dt}), & \text{if } t \geq T_{op}. \end{cases} \tag{3.13}$$

The equation 3.13 shows that the emitting light acts as an additional decaying exponential, which helps accelerating the process of ISI mitigation. Before emitting the light, the molecules diffuse in the medium without being degraded, which gives time to a maximum number of molecules to be observed by the receiver, so that the strength of the useful signal is maintained. After emitting the light at the optimal time, the additional decaying exponential degrades the remaining molecules, which mitigates the ISI. Increasing the coefficient J will result in a faster decaying, which can be done by increasing the light intensity, increasing the energy of the photons or using a wavelength for which the absorption of molecules is at its maximum. The time of light emission is important, as shown in our previous study [Dambri and Cherkaoui, 2018]. In the next section, we present the

derived expression of light emissions optimal time T_{op}, and the expression of the bit error probability.

3.6 Performance Evaluation

In order to evaluate the performance of the proposed system and compare it with the other two scenarios, we simulate each scenario using AcCoRD simulator [Noel *et al.*, 2017]. We also use the Interference-to-Total-Received molecules metric (ITR) and the derived bit error probability. The Actor-based Communication via Reaction-Diffusion (AcCoRD) contains a microscopic and mesoscopic hybrid algorithm, which increases its computational efficiency and its simulation accuracy.

3.6.1 Light Emission's Optimal Time

The time of light emission at the receiver is crucial for the quality of the received signal. If the light is emitted too early, the strength of the signal will be decreased, and if it is emitted too late, the ISI mitigation will be decreased. Therefore, in order to have an optimal impulse response at the receiver, an expression of the optimal time for light emission must be derived. First, we simulate the proposed system with different light emission times, and with a fixed distance between the transmitter and the receiver (5 μm). The results of the simulation showed that the optimal time to emit the light is when the expected number of molecules at the receiver is in its maximum. The optimal time in the simulation result is $t = 0.04s$ as shown in Fig. 3.4. Since this maximum only occurs in the first phase of our proposed system, which means when the model follows the first case of this study, the expression of the optimal time should be derived from (3.7). A simple calculation of the equations derivative with respect to t is needed to find the time of its peak and thus, the expression of the optimal time to emit light can be written as follows:

$$T_{op} = \frac{d^2}{6D}, \tag{3.14}$$

The optimal time is proportional to the distance between the transmitter and the receiver, which implies that the proposed system would favorably use a fixed transmitter and a fixed receiver. However, if the distance d of the system is variable, the receiver should have a mechanism that allows it to know the position of the transmitter before emitting the light. The variable distance of the system is an interesting problem, which we will leave for future work.

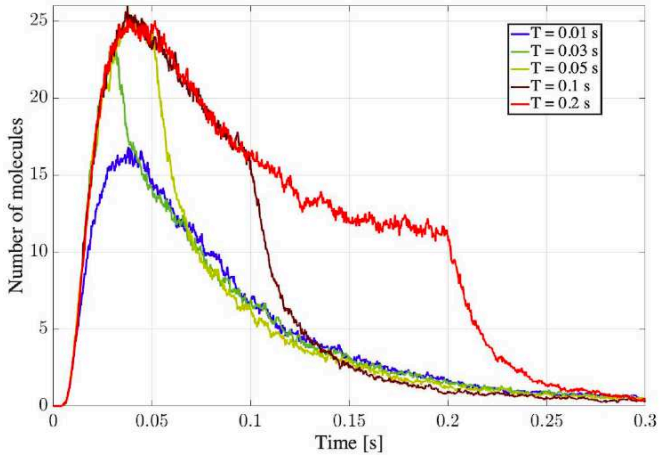

Figure 3.4 Effect of the light emission's time variation on the impulse response.

3.6.2 Interference-to-Total-Received molecules (ITR)

We use the ITR in this study to evaluate the performance of the proposed system model, because this metric clearly highlights the enhancement of the signal strength and the ISI mitigation at the same time. The ITR metric analysis provides an in-depth understanding of the difference between the three studied scenarios and it can be defined as [Yilmaz *et al.*, 2016]:

$$ITR(t_s, t_{end}) = \frac{F(t_{end}) - F(t_s)}{F(t_{end})}. \tag{3.15}$$

where $F(t_{end})$ is the total expected number of molecules at the receiver, and $F(t_s)$ is the expected number of molecules at symbol period t_s, which we take it in this study as in [Dambri and Cherkaoui, 2018] ($t_s = 0.1$s).

The ITR calculates the normalized difference between the total expected molecules and the molecules observed before the symbol period. This difference represents the ISI problem. If the calculated difference is small, that means the received signal is strong, and the system is better at ISI mitigation. Therefore, in our study, the smaller the ITR, the better the performance of the system.

3.6.3 Bit Error Probability

In this study, we modulated the signal with a binary shift in the number of molecules. We assume that the receiver contains a simple detector, which compares the received molecules number with a decision threshold value ζ. The threshold can determine whether the sent

bit is 0 or 1 and thus, we define the error in our study as the decided bit value that is not equal to the actual bit value sent from the transmitter. In this paper, we considered only the case of transmitting one bit, because the purpose of the study is to prove that the proposed system can mitigate ISI without decreasing the strength of the signal, and one bit is sufficient to do it. The case of bits sequence will be considered in future work. Let's consider β be the information bit sent by the transmitter, which it can be either 0 or 1. The *a priori* probabilities of the bit are P_0 and P_1=1-P_0, which are the probabilities of β to be 0 or 1 respectively. Let's consider $\hat{\beta}$ the received bit at the receiver at time T_{op}, $\hat{\beta}$ should be equal to β otherwise, there will be an error. The detection scheme can be written as follows:

$$\hat{\beta} = \begin{cases} 1, & \text{if } S(T_{op}) \geq \zeta, \\ 0, & \text{if } S(T_{op}) < \zeta. \end{cases} \tag{3.16}$$

Threshold ζ is chosen empirically by trying several values and then choosing the one with the smallest probability of error. Since we're considering the case of only one bit, P_0 is not the best option to study the error probability, because there would be no molecules to be observed at the receiver, so instead, we study the probability P_1. The probability of β =1 is the probability of $S(T_{op})$ to be bigger or equal to the threshold value which can be written as $P_r(S(T_{op}) \geq \zeta)$. If we assume that each molecule is independent of all the other ones, and if we put N=1, we can use the lower bound expression on the expected molecules number in equation (3.13) as the probability density function of a single molecules location at any time. As we mentioned before, we assume that the receiver is a point observer and the concentration of the molecules within its volume is uniform. In order to lighten the writing of the equation (3.13), we note the first phase of the equation as W_R. Thus, the lower bound expression on the probability $P_S(t)$ that one molecule shortly exposed to the light is observed at the receiver can be written as:

$$P_S(t) = \begin{cases} W_R, & \text{if } t < T_{op}, \\ W_R \exp(-Jt), & \text{if } t \geq T_{op}. \end{cases} \tag{3.17}$$

The equation (3.17) can be met with equality if we assume that the light intensity is uniform and the molecules degradation is homogenous. So the probability that all molecules shortly exposed to the light are observed at the receiver is N times the probability of one molecule. The molecules have two possibilities in the medium, whether they pass through

the receiver and being observed or they miss the receiver without being observed. Thus, the probability $P_r(S(t) \geq \zeta)$ follows a binomial distribution [Wilkinson, 2011] and can be written as:

$$P_r(S(t) \geq \zeta) = \sum_{q=\zeta}^{N} \binom{N}{q} P_S(t)^q (1 - P_S(t))^{N-q}, \tag{3.18}$$

By substituting (3.17) in the binomial equation (3.18), we write:

$$P_r(S(t) \geq \zeta) = \begin{cases} \sum_{q=\zeta}^{N} \binom{N}{q} W_R^q (1 - W_R)^{N-q}, t < T_{op}, \\ \sum_{q=\zeta}^{N} \binom{N}{q} (W_R \exp(-Jt))^q \\ \quad (1 - (W_R \exp(-Jt)))^{N-q}, t \geq T_{op}. \end{cases} \tag{3.19}$$

As we mentioned above, the error probability in this study is higher if $P_r(S(t) < \zeta))$ when the sent bit is 1 or if $P_r(S(t) \geq \zeta)$ when the sent bit is 0. In our case of a single bit transmission, the error probability is:

$$P_e = P_1(P_r(S(t) < \zeta)), \tag{3.20}$$

where P_1 is the *a priori* probability of the bit to be 1, and we put it as P_1=0.5. (20) can also be written as:

$$P_e = P_1(1 - P_r(S(t) \geq \zeta)), \tag{3.21}$$

However, the equation in (3.19) can give exact results only for one molecule probability, and the results become very difficult to evaluate for greater values of N, as in molecular communication case. Poisson distribution is a special case of the binomial, where the number of trails is large (which is the total number of molecules in our case) and the probability of success in each trial is small (the probability of one molecule to be observed). So, we can approximate the binomial distribution in equation (3.19) for larger values of N and small values of $P_S(t)$ to a Poisson distribution with mean and variance $S(t) = NP_S(t)$. Therefore, the probability $P_r(S(t) \geq \zeta)$ can be written as [Noel *et al.*, 2014]:

$$P_r(S(t) \geq \zeta)|_{Poiss} = 1 - \exp(-S(t)) \sum_{q=0}^{\zeta-1} \frac{S(t)^q}{q!}, \tag{3.22}$$

By substituting (3.17) in the Poisson equation (3.22), we write:

$$P_r(S(t) \geq \zeta)|_{Poiss} = \begin{cases} 1 - \exp(-W_R) \sum_{q=0}^{\zeta-1} \frac{W_R^q}{q!}, t < T_{op}, \\ 1 - \exp(-(W_R \exp(-Jt)) \\ \quad \sum_{q=0}^{\zeta-1} \frac{(W_R \exp(-Jt)^q}{q!}, \ \ t \geq T_{op}. \end{cases} \tag{3.23}$$

However, the factorial in the Poisson distribution increases the computational burden. By using the Central Limit Theorem (CLT) [Wilkinson, 2011], it is generally considered appropriate to approximate the Poisson by a Gaussian distribution when the mean of the Poisson is bigger than 20. Despite the fact that Poisson gives more accurate approximation, in this study, we consider the Gaussian distribution because of its computational efficiency, by assuming that $P_S(t)$ is not close to zero or one. The study in [Noel *et al.*, 2014] proved that Gaussian approximation gives an acceptable loss in accuracy, and we validated this result in this study as we will see in the next section. The mean and variance of the approximated Gaussian are $S(t)$ and $S(t)(1 - PS(t))$ respectively, and we write:

$$P_r(S(t) = \zeta)|_{Gauss} = \frac{\exp\left(\frac{(\zeta - S(t))^2}{2[S(t)(1-P_S(t))]}\right)}{\sqrt{2\pi S(t)(1 - P_S(t))}}, \tag{3.24}$$

The integral solution of this equation cannot be expressed in terms of elementary functions. However, by using the error function, it can be approximated as [Oldham *et al.*, 2008]:

$$P_r(S(t) \geq \zeta)|_{Gauss} = \frac{1}{2}\left[1 + \text{erf}\left(\frac{\zeta - S(t)}{\sqrt{2S(t)(1 - P_S(t))}}\right)\right], \tag{3.25}$$

By substituting (3.17) in the error function (3.25), and putting the variances $W_R(1 - \frac{W_R}{N})$ and $(W_R \exp(-Jt)(1 - \frac{W_R}{N} \exp(-Jt))$ as ρ_1 and ρ_2 respectively, we write:

$$P_r(S(t) \geq \zeta) = \begin{cases} \frac{1}{2}\left[1 + \text{erf}\left(\frac{\zeta - W_R}{\sqrt{2\rho_1}}\right)\right], & t < T_{op}, \\ \frac{1}{2}\left[1 + \text{erf}\left(\frac{\zeta - (W_R \exp(-Jt))}{\sqrt{2\rho_2}}\right)\right], & t \geq T_{op}. \end{cases} \tag{3.26}$$

To evaluate the error probability P_e of the proposed system, we can calculate the value $P_r(S(t) \geq \zeta)$ in equation (3.21) by using either the equation (3.19), (3.23) or (3.26). In this study, we favored the computational efficiency over the accuracy by using the equation (3.26) in the bit error probability calculation.

3.7 Numerical and Simulation Results

The environment parameters for each simulated scenario in this study are chosen so that the simulation gives clear results without increasing the calculation burden. The distance between the transmitter and the receiver is chosen to be between 5 and 10 μm as in [Chude-Okonkwo *et al.*, 2017] because in that range, the simulation gives clear results with the used number of molecules N =10,000. After 10 μm , the impulse response drastically decreases so that the graph becomes hard to read. For the receiver radius, we used an algorithm similar to the one used in our recent work [Dambri *et al.*, 2019] to find the optimal radius for our proposed system (5 μm). As for the diffusion coefficient, its value depends on the viscosity of the medium. The diffusion coefficient of molecules in a biological medium is usually in the order of $10^{-11} m^2 s^{-1}$ [Wakeham *et al.*, 1976], other works in the literature use $10^{-9} m^2 s^{-1}$ as in [Chang *et al.*, 2018]. In our study we used the average between the two values, and we also decreased the reaction rates to simulate the worst case in the last two scenarios, as shown in table 1.

In order to simulate the photolysis reaction, we use fast virtual enzymes in the medium to play the role of the light degradation. The choice of virtual enzymes to simulate the first order degradation rate of the photolysis is a normalization attempt to facilitate the comparison between our proposed method that uses light and the method that uses enzymes. In this study, we simulate the worst case in the three scenarios to use them as upper bound results. The worst case in the photolysis reaction is when the viscosity of the medium is high, and light intensity is reduced in far distances from the receiver. To take into account this light intensity reduction in our simulation, we add virtual spheres with increasing diameters around the receiver, and we fill each sphere with fast virtual enzymes. The concentration of the enzymes is degraded with the increase in the spheres diameter to capture the influence of light intensity reduction on the proposed system.

The simulation results presented in this paper are the average of the received molecules number in each iteration, with a maximum number mean of 24.78 $\pm$ 0.49 and 19 as a standard deviation. The confidence interval of the results is 99% with a margin error of 0.49. The sample mean is between [24.29-25.27].

3.7.1 Impulse Response

The impulse responses at the receiver for the three studied scenarios are presented in Fig. 3.5. We can notice that in the first scenario (without reaction), the ISI is very high, presented with a heavy tail, which is drastically decreased in the second scenario with the enzyme presence. However, the enzyme also decreases the amplitude of the signal

Table 3.1 System Parameters Used for Simulation.

Parameters	Scenario 1	Scenario 2	Scenario 3
Released molecules	10,000	10,000	10,000
Diffusion coefficient (m2/s)	10-10	10-10	10-10
Simulation repetition	100	100	100
Simulation time (s)	0.5	0.5	0.5
Distance (μm)	5	5	$5 \sim 10$
Receiver radius (μm)	5	5	5
Number of enzymes	-	12980	12980
Binding rate (ns^{-1})	-	5	10
Unbinding rate (s^{-1})	-	1	10
Degradation rate (s^{-1})	-	1	10
Symbol period t_s (s)	0.1	0.1	0.1
Simulation time step Δt (μs)	0.2	0.2	0.2

with 36%, which is considered in the literature as a trade-off, a strong signal creates more ISI, and mitigating ISI weaken the signal. Nonetheless, in the case of the photolysis, a clear comparison between the three scenarios shows that the proposed system mitigates ISI faster, without decreasing the strength of the signal, because of the switching ability of the light. The ISI in the first scenario is in its worst case because the simulated environment is bounded, and the receiver is close to the reflected molecules in its boundaries, which increases the ISI possibility.

The Fig. 3.5 also shows a comparison between the simulation results and the lower bound expressions discussed in section 3.5. We can notice that the analytical results are accurate for the amplitude of the signal, but not accurate for ISI mitigation, due to the fact that the simulations represent the worst case and the lower bound expressions represent the best case for the ISI. The actual response at the receiver will be between the analytical and the simulation results. It is clear though that ISI mitigation of the worst case in our proposed system is comparable to the best case of the enzymes and without decreasing the signal strength.

The Fig. 3.6 shows the influence of the distance on the impulse response of the system. The distance is inversely proportional to the expected number of molecules as shown in the equation 3.13 of the proposed system model. We can notice that the analytical results accurately predict the maximum number of molecules for distances between 5 and 10 μm.

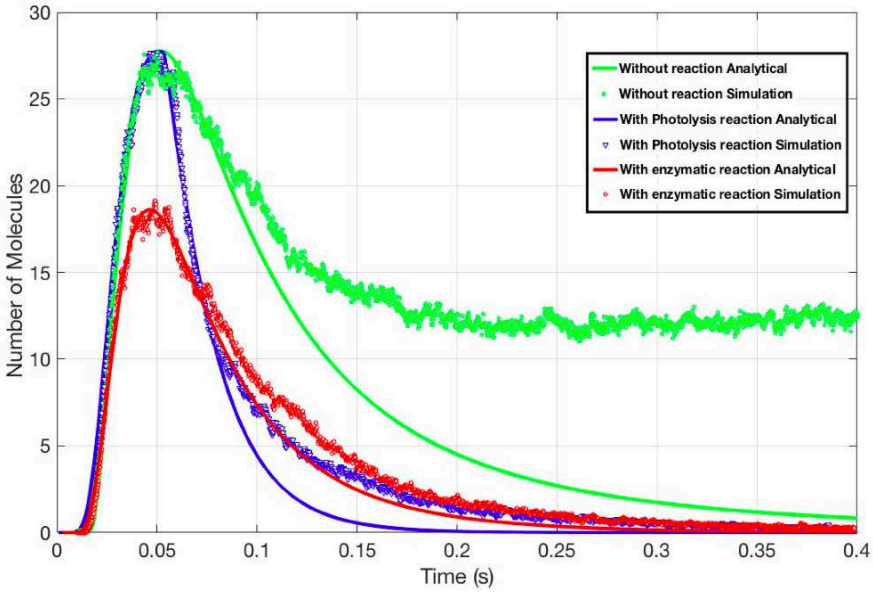

Figure 3.5 Analytical and simulation results of the impulse response for the three studied scenarios.

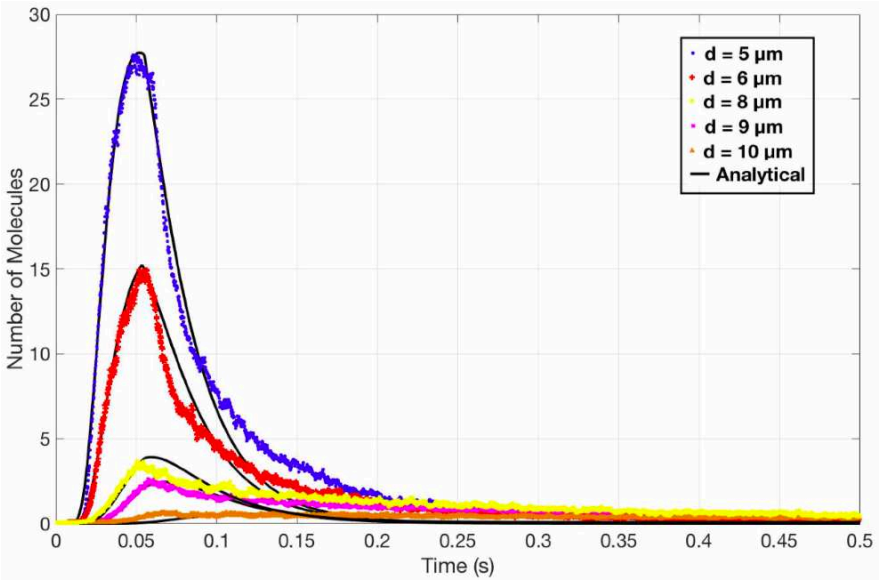

Figure 3.6 Distance influence on the impulse response of the proposed system.

3.7.2 ITR Evaluation

The ITR defined in (3.15) is a good metric to evaluate the performance of the proposed system, because it clearly highlights the enhancement in the signal strength and ISI mitigation at the same time. In this study, the smaller the ITR, the better the performance of the system as explained in the previous section.

The Fig. 3.7 shows the ITR values of the three studied scenarios and as expected, the photolysis of our proposed system has the smallest ITR value. We can see that the first scenario where there is no degradation reaction has better ITR value than the scenario of enzymes. The bigger value of ITR in the presence of enzymes can be explained by the decrease in the signal strength, which drastically increases the ITR. The evaluation of the three studied scenarios using ITR validates the numerical and the simulation results, and proves that the performance of the proposed system is better in mitigating ISI, without decreasing the useful signal.

3.7.3 Bit Error Probability Evaluation

In the previous section, we derived the Poisson and Gaussian expressions to approximate the probability of molecules number observed at the receiver. Fig. 3.8 shows that Poisson approximation follows the simulation more accurately than Gaussian, which has some loss in accuracy as proved in [Noel *et al.*, 2014]. However, the Gaussian has more computational efficiency and its accuracy loss is not very large, and it still can be used to predict the probability of error. We can also notice that the photolysis scenario has a little bit less probability of errors compared to the enzyme scenario for a threshold value between 3.5 and 5. Nonetheless, if we increase the threshold value $\zeta \geq 5$, we can note a considerable difference between the proposed system using photolysis and the enzyme system in terms of error probability. In Fig. 3.9, we can clearly see that the performance of the proposed scenario is better than the other two scenarios. With a threshold value ζ=7, the proposed system can have less than 10^{-3} probability to make errors. For small threshold values, enzymes and photolysis have similar performance, which is logical because the maximum number of molecules expected at the receiver is bigger than the threshold value. The considerable difference between the two systems for higher threshold values can be explained with the significant decrease in the signal strength when using enzymes (36% loss). When the threshold value becomes bigger than the maximum number of molecules, the receiver has more probability to make errors, and thus, the bigger the amplitude of the signal, the better its performance. The scenario that uses no reaction has the worst error probability with 10^{-1} , because of the heavy tail that causes the ISI.

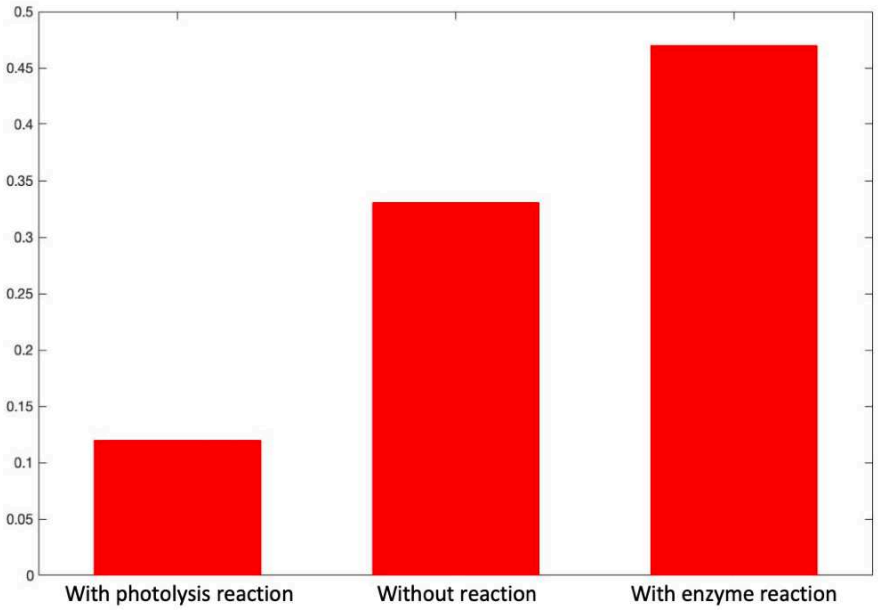

Figure 3.7 ITR values of the three studied scenarios, 1) without reaction, 2) with enzymes, 3) with photolysis.

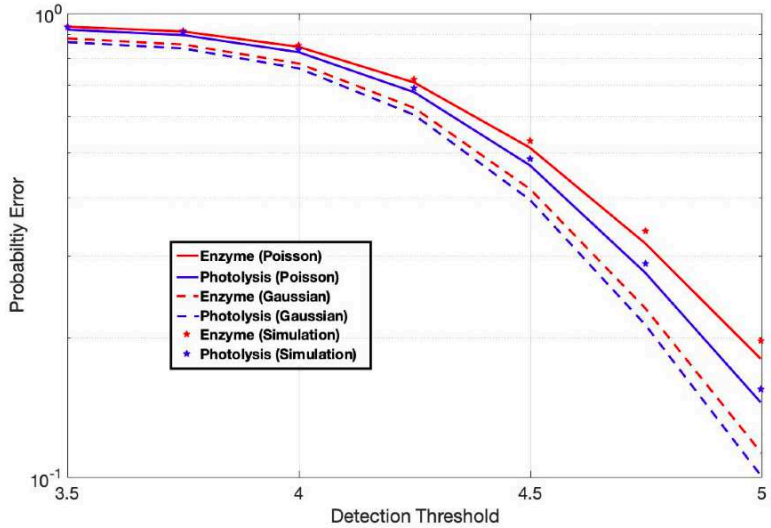

Figure 3.8 Accuracy of Poisson and Gaussian approximations for the enzyme and the photolysis reactions.

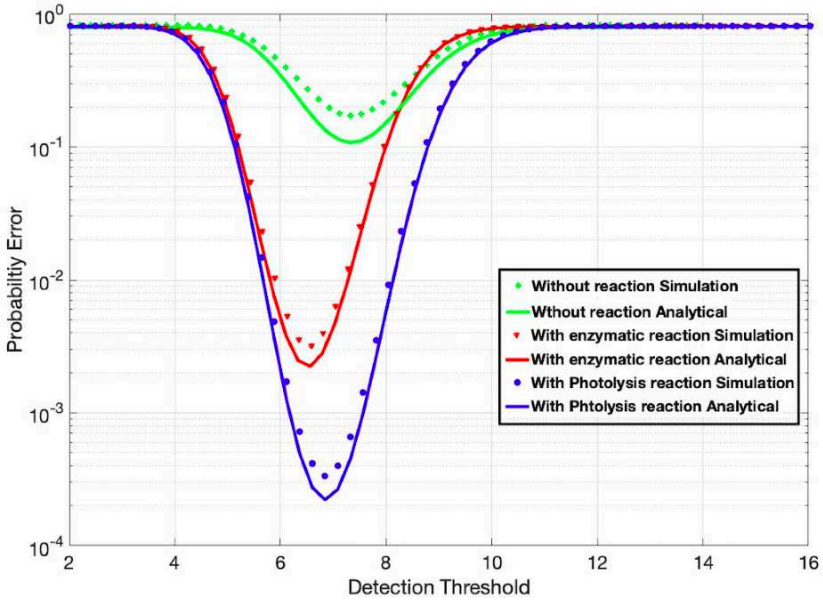

Figure 3.9 Bit error probability of the three studied scenarios as a function with the detection threshold.

We can also notice in Fig. 3.9 that the analytical values of the error probability, for the three studied scenarios, are smaller than the simulation values. As explained in the previous section, the analytical expressions are lower bounds on the systems actual response, and the simulations are used as upper bounds. Therefore, the actual value of the error probability is expected to be between the analytical and the simulation results, and again, the worst case of our proposed system outperforms the best case of the two others. We can conclude that using photolysis reactions can mitigate ISI faster, without decreasing the useful signal, which clearly enhance the performance of molecular communication.

3.8 Conclusion

Diffusion-based molecular communication is one of the most promising bio-inspired paradigms for the communication at nano scale. A lot of work was proposed in literature to mitigate one of its challenges, which is ISI. In this paper, we extended our proposed system in [Dambri and Cherkaoui, 2018], which uses photolysis reaction instead of enzymes to degrade the remaining molecules in the medium. Unlike the enzymes, the switching ability of light allows the receiver to mitigate ISI faster without decreasing the strength of the signal. We presented a comparison study between three scenarios, a system without reaction, with enzymes and with photolysis. We then derived a lower bound expression on the expected number of molecules to be observed at the receiver, while shortly exposed

to light. We also derived the bit error probability and used it alone with interference-to-total received molecules metric to evaluate the performance of the proposed system. The analytical results validated with simulation showed a visible enhancement when using photolysis reaction, which improves the performance of the diffusion-based molecular communication.

Our future work will take into account considering the variable distance problem discussed in the section 3.6, the case of bits sequence and the case of absorbing and reflective receiver. We will also consider an experimental study at the macro scale using UV light to degrade molecules, and then we will provide a comparison study between analytical, simulation and experimental results.

CHAPTER 4

MIMO RECEIVER OPTIMIZATION

Auteurs et affiliation:

Oussama Abderrahmane Dambri: étudiant au doctorat, Département de Génie Électrique et de Génie Informatique ,Université de Sherbrooke. INTERLAB Research Laboratory.

Amine Abouaomar: étudiant au doctorat, Département de Génie Électrique et de Génie Informatique ,Université de Sherbrooke. INTERLAB Research Laboratory.

Soumaya Cherkaoui: Professeur, Département de Génie Électrique et de Génie Informatique, Université de Sherbrooke. INTERLAB Research Laboratory.

Date de Parution: April 2019

Revue: *IEEE Wireless Communications and Networking Conference (WCNC)*

Titre français: Optimisation de la Conception d'un Receveur MIMO pour la Communication Moléculaire Basée sur la Diffusion

Résumé français:

La perte de chemin est un défi majeur dans les communications moléculaires. Lorsque les molécules transportent des informations, le nombre de molécules pouvant être reçues est inversement proportionnel à la distance carrée entre l'émetteur et le receveur, ce qui a un impact considérable sur la force du signal reçu. L'utilisation d'une technique MIMO peut améliorer les performances des communications moléculaires. Dans cet article, nous avons étudié le receveur utilisé dans les communications moléculaires MIMO. Nous nous sommes concentrés sur trois paramètres importants pour la conception du receveur. Pour optimiser la conception d'un receveur MIMO, nous avons utilisé le simulateur AcCoRD pour obtenir des simulations stochastiques 3D pour chaque scénario. Nous avons évalué les résultats de la simulation en étudiant la probabilité d'erreur et le nombre de molécules représentant la force du signal. Nous avons ensuite proposé deux problèmes d'optimisation visant à optimiser le choix des paramètres du receveur, et deux algorithmes pour résoudre les problèmes. L'étude montre qu'un choix judicieux de la combinaison de trois paramètres peut optimiser la conception du receveur MIMO, ce qui peut réduire la probabilité d'erreur et améliorer les performances de la communication moléculaire.

4.1 Design Optimization of a MIMO Receiver for Diffusion-based Molecular Communication

4.2 Abstract

Path loss is a main challenge in Molecular Communications. When molecules carry information based only on a natural diffusion, the number of molecules that can be received is inversely proportional to the square distance between the transmitter and the receiver, thus hugely impacting the received signal strength. The use of a Multi-Input Multi-Output (MIMO) technique can improve the performance of molecular communications by increasing the data rate. In this paper, we studied the receiver used in molecular MIMO communications. We focused on three important parameters for the receiver design, which are the channel distance, the distance between the detectors constructing the receiver and the detectors' diameter. To optimize the design of a 3×3 MIMO receiver, we used AcCoRD simulator to obtain 3D stochastic simulations for each scenario. We evaluated the simulation results by studying the error probability and the number of molecules representing the signal strength. We then proposed two optimization problems that aim at optimizing the receiver parameters choice, and two algorithms to solve the problems. The study shows that a judicious choice of the three parameters combination can optimize MIMO's receiver design, which can decrease the error probability and improve the performance of Molecular Communication.

4.3 Introduction

Nanotechnology is being extensively used today in the medical, industrial and military fields. In particular, nanomachines are able to achieve very simple tasks at the nanoscale for different purposes. However, many of the most promising nano-applications that are yet to come, involve nanomachines communicating with each other. Indeed, communication can allow these nanomachines to share information and cooperate to drastically expand their capabilities.

Nanonetworking is the paradigm that deals with communicating systems at the nanoscale level. Nanonetworking presents several engineering challenges. For example, designing a traditional electromagnetic communication system at such small level implies using nano antenna which generate waves at Terahertz frequency with all its peculiarities [Akyildiz *et al.*, 2014; Federici and Moeller, 2010; Khan *et al.*, 2016; Song and Nagatsuma, 2011]. To circumvent such challenges, researchers have been studying the use of molecules as

carriers of the information between nano transmitters and receivers. Indeed, nature has been using molecules to transmit information for billions of years. Bio-inspired Molecular Communication (MC) is one of the most promising solution for nano-communication systems [Farsad *et al.*, 2016].

The most basic method proposed to exchange information using the bio-inspired MC is the diffusion-based MC [Pierobon and Akyildiz, 2010]. This method is based on the natural diffusion process of molecules with a Brownian motion to reach the receiver. The information to be transmitted can be coded by using the number of molecules (concentration), the type of molecules (isomers), the concentration ratio, or the frequency shift [Arjmandi *et al.*, 2016; Kim and Chae, 2013]. It is a simple communication process with some obvious shortcoming. Some molecules can fail to reach the receiver, stay in the medium and interfere with the newly released molecules, thus creating an Inter-Symbol Interference (ISI) [Pierobon and Akyildiz, 2012]. Moreover, the slow propagation of molecules and the inversely proportional relationship between the diffusion and the communication channel distance causes a considerable path loss and drastically decreases the diffusion-based MC data rate [Nakano *et al.*, 2012].

The use of a Multi-Input Multi-Output (MIMO) technique is a good solution to increase the data rate and enhance MC performance. In [Meng *et al.*, 2012], the authors investigated various scenarios of MIMO transmission techniques by using and adapting the same concepts used in the traditional electromagnetic communication (e.g. like diversity and Spatial Multiplexing (SM)), and applied them for the Diffusion-based MC. The study proved that with a well-known Channel State Information (CSI) and with a proper allocation of the molecules among the transmission nodes, MIMO techniques can optimize the throughput of the system. The authors also suggested the use of a dynamic switch between the diversity mode and SM mode to have better results. However, this study did not take into account the ISI and the reception noise, by assuming them to be negligible, while focusing only on the Multi-User Interference (MUI). The authors of [Koo *et al.*, 2016], on the other hand, proposed a 2x2 Molecular MIMO system model which included ISI and InterLink Interference (ILI) using 3D particle-based simulators. The study proposed four detection algorithms specific to the molecular MIMO, by using the simulation results and the derived ISI and ILI models. To demonstrate that the proposed model is practicable at the macroscale level, the authors also presented a tabletop test bed with its measurement results. The study showed that the data rate is increased by 1.7 times compared to the Single-Input Single-Output (SISO) Systems. However, neither study took into account the

distance between, and the diameter of, the detectors at the receiver, which can influence the performance of the MIMO receiver.

In this paper, we study the design parameters of the receiver used in the molecular MIMO in order to optimize its performance. Using AcCoRD simulator [Noel *et al.*, 2017], we designed a (3×3) system, a transmitter with 3 emitters and a receiver with 3 passive detectors. In this study, we focused on 3 important design parameters, which are: the distance between the transmitter and the receiver, the distance between the detectors at the receiver and the diameter of the detectors. We allocated 3 bit sequences of molecules for each emitter, the receiver sums the signals detected by each detector and calculate the average. The 3D stochastic simulation results of each simulation scenario is an average impulse response calculated by the receiver, which varies with the parameters changes. We used the resulting statistical data from the simulations to calculate the detection threshold by applying the Maximum A posteriori Probability (MAP) criterion of the standard Bayesian detection framework. To evaluate the optimization of the receiver for each scenario, we used the function of error probability with the number of transmitted molecules as an input. We also proposed two optimization problems, to optimize the choice of the 3 design parameters, and two algorithms to solve the problems. A judicious choice of the 3 parameters combination can help to optimize the performance of the MIMO receiver for molecular communication as summarized in the optimization problem.

The rest of the paper is organized as follows. In section II, we introduce the proposed system comprising a (3×3) MIMO design using molecules as carriers of the information with binary Concentration Shift Keying (CSK) modulation. In section III, we discuss the results of the study and evaluate the performance of the receiver design, in terms of error probability, for each scenario. In section IV, we present the optimization problems and the algorithms to solve them. Finally, we conclude the paper in section V.

4.4 System Model

The system studied in this paper is a 3D fluidic environment with 3 emitters TX1, TX2 and TX3 at the transmitter, and 3 detectors RX1, RX2 and RX3 at the receiver as shown in Fig. 4.1. The transmitter releases molecules as carriers of the information. We assume that the effect of collisions between the released molecules is negligible; they diffuse in the medium with a random motion until they reach at least one detector at the receiver.

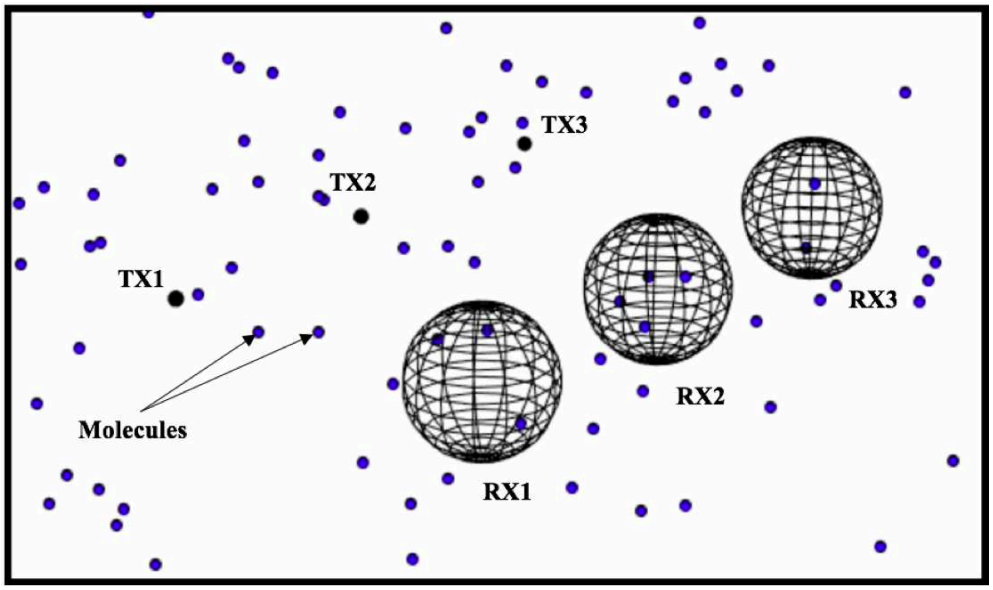

Figure 4.1 System model of Molecular MIMO

4.4.1 Diffusion

We model the information with a binary Concentration Shift Keying (CSK). We allocate a quantity Q of molecules in each emitter, and we divide the information that we want to send into 3 bit sequences. Because Channel State Information (CSI) is not available, we assume a uniform molecule allocation for each emitter as in [Meng *et al.*, 2012]:

$$Q_n = \frac{1}{N} Q \tag{4.1}$$

where N is the number of emitters at the transmitter. The Diffusion of the molecules in the medium follows a continuous-time stochastic process. This arbitrary motion can be described mathematically with Fick's second law:

$$\frac{\partial C}{\partial t} = D\nabla^2 C \tag{4.2}$$

where D is the Diffusion coefficient of the released molecules.

We assume that all molecules have the same radius and all of them diffuse independently with the same coefficient D.

This constant diffusion coefficient D can be calculated an in Eq. 4.3:

$$D = \frac{k_B T}{6\pi\eta R} \tag{4.3}$$

where R is the radius of the molecules, T is the temperature in kelvin, k_B the Boltzmann constant, and η is the viscosity of the medium.

4.4.2 MIMO Receiver

The MIMO receiver is constructed of 3 spherical passive detectors, which can count the received molecules number. The amplitude of the signal at the receiver is the sum of the received molecules number of each bit sequence at each detector divided by the number of detectors over a symbol interval. The amplitude is demodulated and interpreted as "1" if the amplitude overtops the decision threshold, otherwise, it is interpreted as "0". The counted number of molecules at a distance d from the transmitter is the impulse response received at each spherical detector, which can be calculated with Eq.4.4 [Noel *et al.*, 2016]:

$$f(t) = \frac{QV_R}{(4\pi Dt)^{3/2}} \exp^{\frac{-d^2}{4Dt}} \tag{4.4}$$

where f(t) is a probability density function with respect to the distance d at a given time t for each detector. Q is the number of molecules released for one bit by each emitter, D is the diffusion coefficient, d is the distance between the transmitter and the receiver, t is the time when molecules are detected by the receiver and V_R is the volume of the detectors which is defined in Eq.4.5:

$$V_R = \frac{4\pi}{3}(r^3) \tag{4.5}$$

where r is the radius of the detector.

To find the time when the peak concentration is expected in each detector, it is trivial to calculate the derivative of (4.4) with respect to t. The solution of this derivative gives t_{max} as in Eq. 4.6:

$$t_{max} = \frac{d^2}{6D} \tag{4.6}$$

The maximum number of molecules expected to be received at each detector at time t_{max} is inversely proportional to the square distance between the transmitter and the receiver. The peak of the impulse response is also independent of the diffusion coefficient as shown in the expression Eq. 4.7 resulting from the substitution of t_{max} of Eq. 4.6 in Eq. 4.4:

$$h = \left(\frac{3QV_R}{2\pi e}\right)^{\frac{3}{2}} \frac{1}{d^3} \tag{4.7}$$

h is the expected number of molecules received at time t_{max}.

The closed expression in eq. 4.4 is valid only for SISO systems. In this study we use 3D stochastic simulations to generate statistical data which help us to study molecular MIMO systems. The study in [Koo *et al.*, 2016] showed that the application of the Spatial Multiplexing mode from the traditional electromagnetic communication for n×n MIMO systems allows us to write a discrete final received number of molecules as [Koo *et al.*, 2016]:

$$\begin{aligned} Y_{RX_n}[b] = h_{nn}[1].x_n[b] + I_n[b] + \sum_{k=2}^{b-1}(h_{nn}[k].x_n[b-k]) \\ +h_{nm}[1].x_m[b] + \sum_{k=2}^{b-1}(h_{nm}[k].x_m[b-k]) \end{aligned} \tag{4.8}$$

where h_{nn} is the number of molecules received from a corresponding emitter, h_{nm} is the number of molecules received from other emitters, b is the symbol time slot, $I_n[b]$ is the noise generated from MUI, $x_n[b]$ is the binary information received from a corresponding emitter, and $x_m[b]$ is the binary information received from other emitters. Note that $x_i[b]$ could be 0 or 1. We assume that there is a sufficient number of interfering molecules so that the noise follows a Gaussian distribution $\mathcal{N}(\mu_{I_n}, \sigma^2_{I_n})$ according to the Central Limit Theorem. The sum expressions represent the ISI caused by the remaining molecules from previous symbols sent by a corresponding emitter and other emitters. To capture the effect of MUI on each detector, we first simulate the response of a single detector RX1 from its corresponding emitter TX1, and from the other emitters TX2, TX3 using one type of molecules. We use the system described above with fixed receiver design parameters, distance of channel $d = 5\mu m$, radius of the detectors $r = 3\mu m$ and distance between the detectors $S = 7\mu m$. The result in Fig. 4.2 shows that the effect of MUI on the detector RX1 is small with the chosen parameters. However, with another combination of design parameters as the results will show in the next section, the effect of MUI can be important and can influence the performance of the system. We can write (eq.4.8) in a matrix form for the 3×3 MIMO system as:

$$\begin{bmatrix} Y_{RX_1[b]} \\ Y_{RX_2[b]} \\ Y_{RX_3[b]} \end{bmatrix} = \begin{bmatrix} h_{11} & h_{12} & h_{13} \\ h_{21} & h_{22} & h_{23} \\ h_{31} & h_{32} & h_{33} \end{bmatrix} \begin{bmatrix} x_1[b] \\ x_2[b] \\ x_3[b] \end{bmatrix} + \begin{bmatrix} \chi_1 + I_1[b] \\ \chi_2 + I_2[b] \\ \chi_3 + I_3[b] \end{bmatrix} \tag{4.9}$$

where χ_n represents the sum of the ISI and MUI noise in Eq. 4.8.

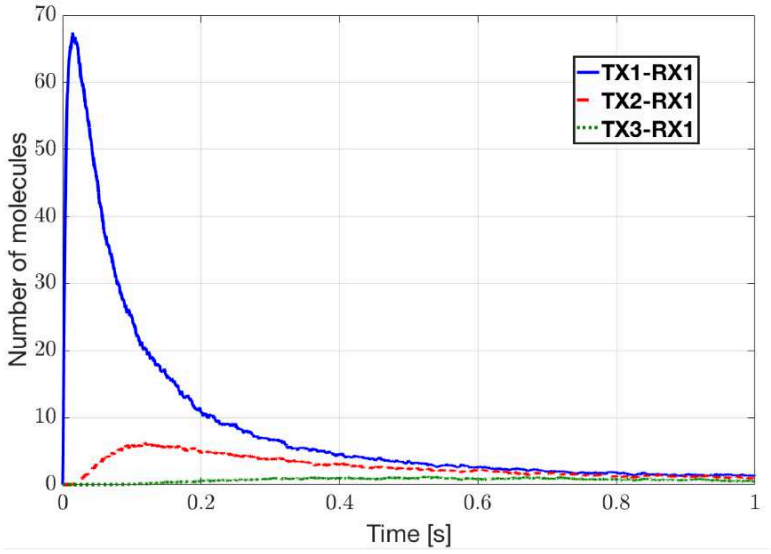

Figure 4.2 Multi-User Interference (MUI) at the detector RX1of the proposed MIMO system when using one type of molecules

We can also write the matrix in Eq. 4.10 in a short form as:

$$Y = Hx + I \tag{4.10}$$

where H represents the number of molecules received at each detector from its corresponding emitter h_{nn} and from the other emitters h_{nm}, x represents the binary information, and I represent the noise of the system, which represents the ISI and MUI.

4.4.3 Decision Rule and Error Probability

The optimization of the receiver for molecular MIMO requires the minimization of the average probability error, and in order to do that, we need to maximize the probability of a correct decision. We applied the Maximum A posteriori Probability (MAP) criterion as a decision rule, as in [Proakis and Salehi, 2007]:

$$Y \underset{0}{\overset{1}{\gtrless}} \frac{\sigma^2}{2(\mu_1 - \mu 0)} \ln\left(\frac{1-p}{p}\right) \equiv \xi \tag{4.11}$$

where ξ is the decision threshold, and means μ_1 , μ_0 and variance $\sigma^2_{I_n}$ are calculated as in Eq. 4.13, where μ_{I_n} and $\sigma^2_{I_n}$ are the mean and the variance of a normal distribution, and

p is the *a priori* probability.

$$\begin{aligned}\mu_0 &= \mu_{I_n} + \sum_{k=2}^{b-1} p(h_{nn}[k]) + p(h_{nm}[k]) \\ \mu_1 &= \mu_0 + h_{nn}[1] \\ \sigma^2 &= \sigma_{I_n}^2 + \sum_{k=2}^{b-1} p(1-p)(h_{nn}[k])^2 + p(1-p)(h_{nm}[k])^2\end{aligned} \tag{4.12}$$

The average error probability is calculated as in Eq. 4.14:

$$P_e = pP_{Md} + (1-p)P_{Fa} \tag{4.13}$$

where P_{Md} is the probability of Mis-detection, and P_{Fa} is the probability of False alarm, which can both be calculated as in Eq. 4.15, where Q is the number of the released molecules for each emitter and ξ is the decision threshold.

$$\begin{aligned}P_{Md} &= Q\left(\frac{\mu_1 - \xi}{\sigma}\right) \\ P_{Fa} &= Q\left(\frac{\xi - \mu_1}{\sigma}\right)\end{aligned} \tag{4.14}$$

4.5 Evaluation and Simulation Results

To evaluate the optimization of the proposed MIMO receiver for molecular communication, we change the parameters of the receiver design and we simulate each scenario using AcCoRD simulator [Noel *et al.*, 2017]. Actor-based Communication via Reaction-Diffusion (AcCoRD) is a new sandbox designed by Noel et al. to solve reaction-diffusion for molecular communication studies. The sandbox allows us to simulate 3D model systems for MC and evaluate their performance with more accuracy, because of its microscopic and mesoscopic hybrid algorithm.

In this section, we present the simulation results of the system described above and the error probability of each scenario. We used $Q = 1500$ molecules for each molecule release; $Q = 500$ molecules for each emitter. The diffusion coefficient D was calculated from Eq. 4.3, and we took the *a priori* probability $p = 1/2$. We took the same value for $\eta = 10^{-3}\ kg.m^{-1}s^{-1}$ of Eq. 4.3, as the one described in[Noel *et al.*, 2014]. We assumed that the mean and variance of the normal noise are identical for all detectors as in [Meng *et al.*, 2012], with a coefficient of variation 0.3 such that $\sigma_{I_n} = 0.3\mu_{I_n}$, and the mean

$\mu_{I_n} = 2 \times 10^{16}\ molecules.cm^{-3}$. The parameters that we changed in the simulations are the Diameter of the detectors $(1, 2, 3, 4\mu m)$, the distance between the transmitter and the receiver $(5, 7, 9, 11\mu m)$ and the distance between the detectors $(4, 7, 10, 15\mu m)$.

4.5.1 Diameter of the Detectors

The MIMO receiver in our study uses three detectors, and the choice of the detectors diameter has proven to be very important for the system performance as shown in Fig. 4.3. We can see that when the diameter is $1\mu m$, the maximum number of molecules is 3, and the more the diameter is increased, the more the signal strength increases, from 3 to 81 molecules. With only $3\mu m$ increase in the diameter, the strength of the signal was increased 26 times. This is is due to the fact that a bigger diameter of the detectors allows the MIMO receiver to detect a bigger number of molecules. We can also observe that the time to reach the maximum number of molecules is unchanged with the change of the diameter, and that is explained in Eq. 4.6. The time t_{max} is only dependent on the distance of the channel d and the constant diffusion coefficient D.

However, increasing the diameter has a disadvantage too. The bigger the diameter, the more the probability to get a mis-detection or false alarm, which increases error probability. We can see in Fig. 4.4 that when the diameter is $4\mu m$, the error probability is 0.3, and the smaller the diameter, the smaller the error probability, until it reaches 10^{-4} with $1\mu m$ diameter when releasing 400 molecules. This can be explained by the fact the small volume of the detector makes it hard to detect molecules which decreases the probability to make errors and, in turn, decreases the ISI. The tradeoff between the strength of the signal and the error probability will be presented as an optimization problem in the next section.

4.5.2 Distance Between the Transmiter and the Receiver

One of the main reasons of the path loss in molecular communication is the distance d between the transmitter and the receiver. The Eq. 4.7 shows that the distance d adversally affects the maximum number of molecules received at each detector at time t_{max}. This is indeed confirmed by the simulations results shown in Fig. 4.5. We can see that the number of the received molecules dropped from 45 molecules to 6 molecules with just $6\mu m$ increase in the channel distance. We can also observe that t_{max} is changing with distance too, because molecules need more time to reach a far receiver, which is clear in the Eq. 4.6.

Decreasing the distance increases the signal strength, but also decreases the error probability. As we can see in Fig. 4.6, small distances show less probability for the receiver to

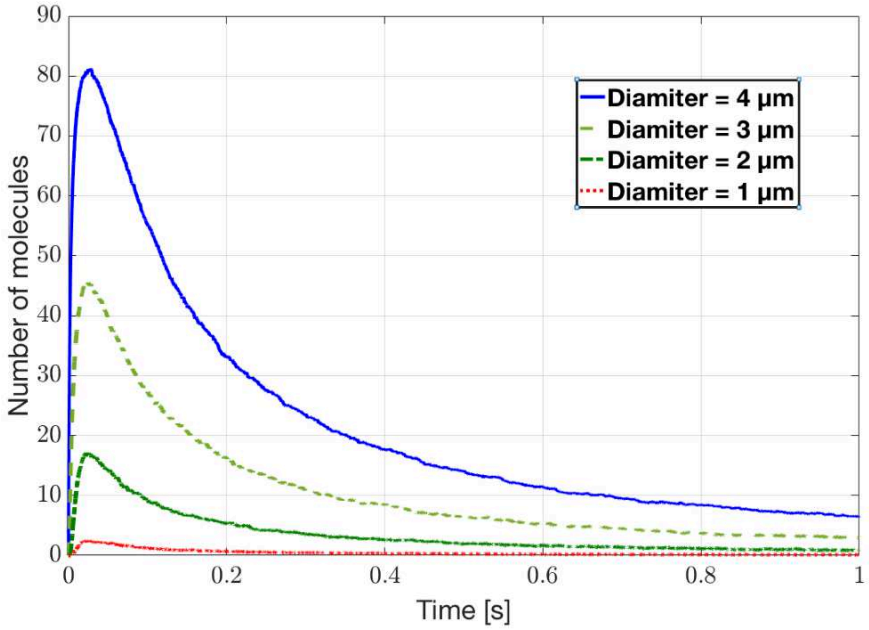

Figure 4.3 Impulse response of the MIMO receiver for different detector diameters

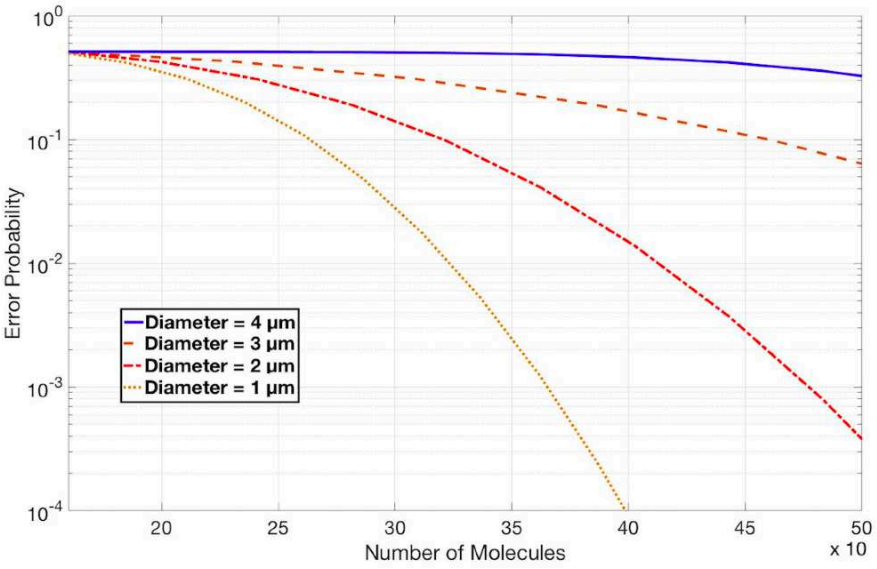

Figure 4.4 The error probability as a function with the released number of molecules for different diameters

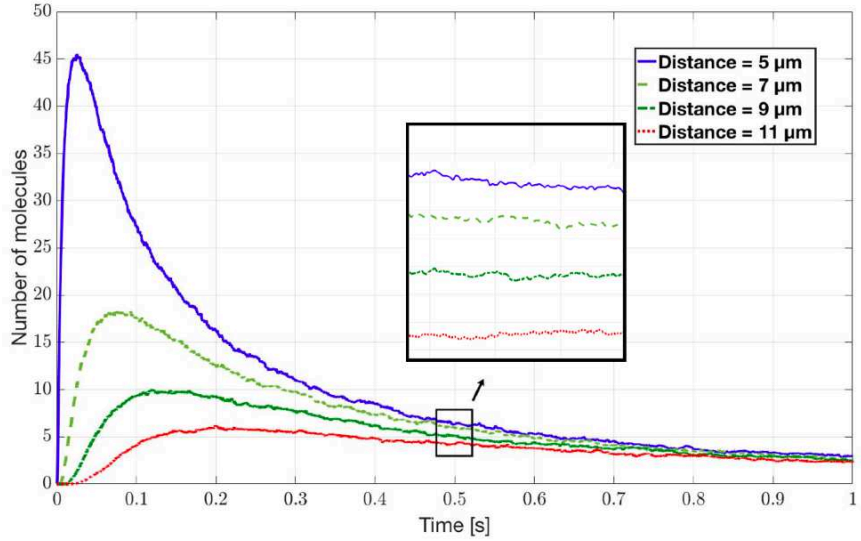

Figure 4.5 Impulse response of the MIMO receiver for different channel distances

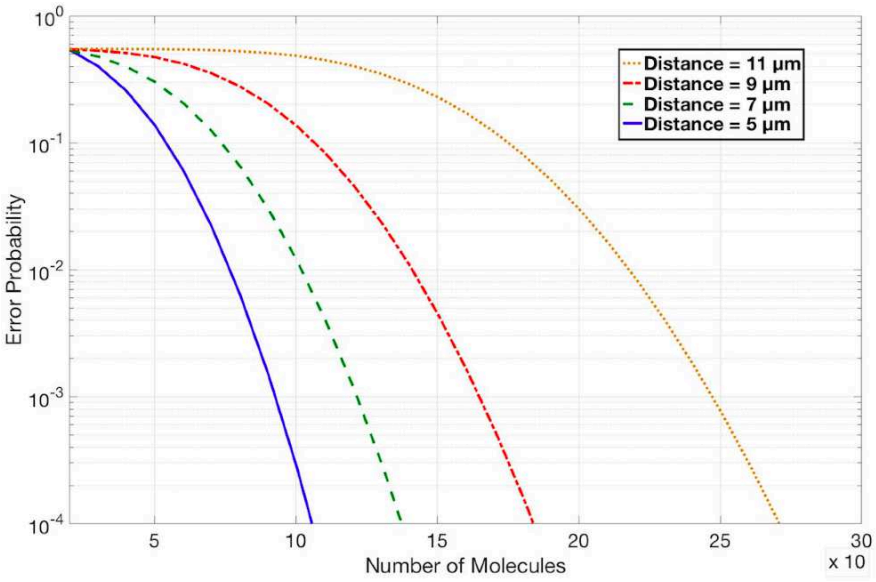

Figure 4.6 The error probability as a function with the released number of molecules for different channel distances

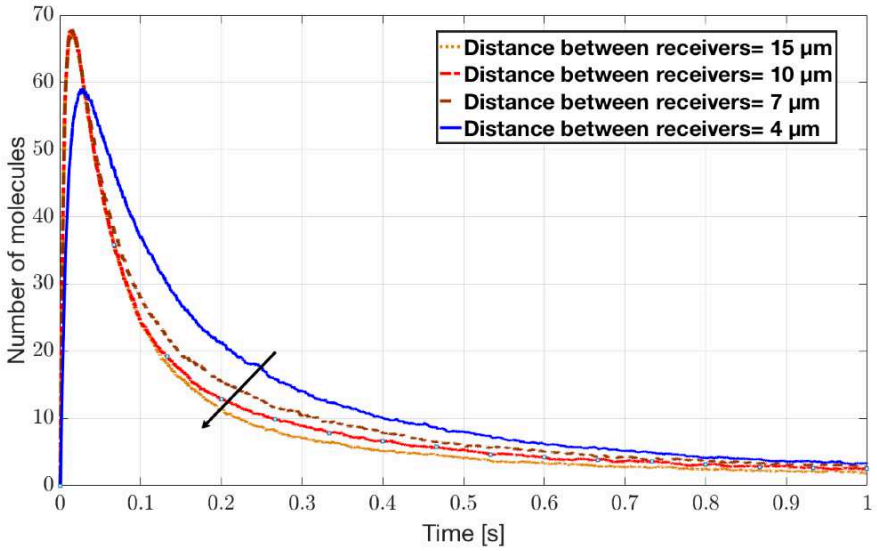

Figure 4.7 Impulse response of the MIMO receiver for different distances between detectors

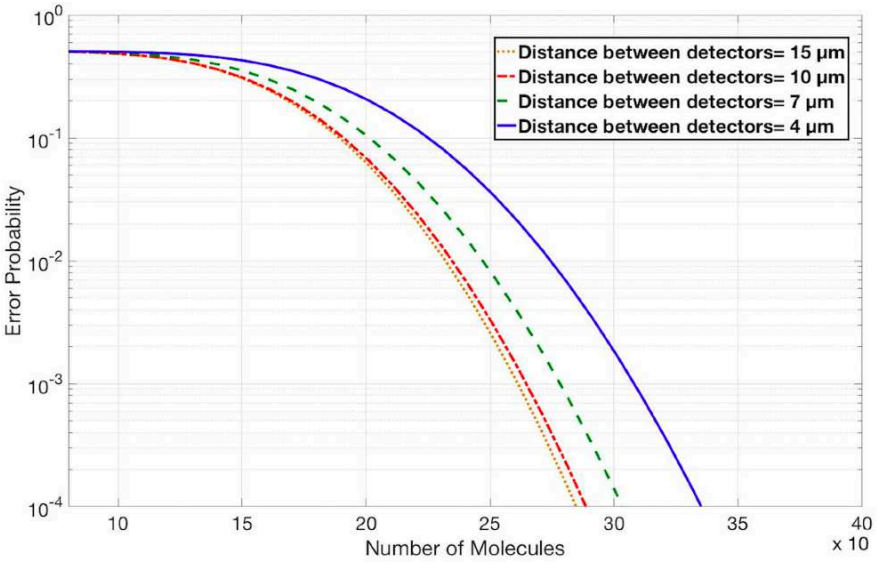

Figure 4.8 The error probability as a function with the released number of molecules for different distances between detectors

make mistakes. The results also show that we can conserve the same error probability in bigger distances by increasing the number of allocated molecules for each emitter.

4.5.3 Distance Between the Detectors

Path loss is not the only challenge that needs to be overcome so as to enhance the link quality, ISI caused by the remaining molecules in the medium also decreases the data rate. In [Assaf *et al.*, 2017], the authors studied the influence of neighboring receivers upon ISI, and they concluded that an optimal distance between these receivers can mitigate ISI by decreasing the width of the impulse response. Also, they found out that an optimal number of the neighboring receivers can increase the achievable throughput and decrease the error probability. However, the study in [Assaf *et al.*, 2017] assumed that all neighboring receivers should have the same distance from the transmitter (arc) in a Single-Input Multiple-Output (SIMO) system. In our study, the number of the neighboring detectors is 2. Fig. 4.7 shows the impulse response of the proposed MIMO system with different distances between the detectors. We can see that the more we increase the distance between the detectors, the more the width of the impulse response decreases. We notice that the amplitude of the impulse with a $4\mu m$ distance between detectors is smaller than the amplitude with the other distances. The explanation of this small decrease in the amplitude is that the closer the detectors to each other, the less space they cover of the channel. Therefore, the detectors miss some molecules and the amplitude is decreased. The missed molecules can remain in the medium and also cause more ISI. Bigger distances between the detectors allow the receiver to cover bigger spaces to receive more molecules, and thus decrease ISI, as illustrated in Fig 4.7 using an arrow.

The mitigation of ISI automatically decreases the probability of error, which is clear in Fig. 4.8. We see that bigger distances between the detectors give a smaller error probability with around 300 allocated molecules. The optimization of this parameter leads to a steady state in the maximum number of molecules, and decreases the errors, which can increase the achievable throughput of the molecular MIMO system.

4.6 Optimization Problems

In this section, we formulate our two optimization problems, and we propose two algorithms to solve them.

4.6.1 Problems Formulation

In Fig 4.3 and 4.5, we notice that the receiver response improves when we increase the diameter of the detectors and minimize the distance between the transmitter and the receiver. However, in Fig 4.4, we can see that by increasing the diameter, the error probability increases as well. Therefore, to find the optimal parameters, our objective is to maximize h in eq. 4.7, with a maximum probability error as a constraint. The first optimization problem is formulated as follows:

$$\max_{r\in\mathbb{R}_*^+} h(r) = \left(\frac{2Qr^3}{e}\right)^{\frac{3}{2}} \frac{1}{d^3} \; s.t : S = \frac{|L-(2nr)|}{n-1} \geq \alpha \tag{4.15}$$

where $h(r)$ is obtained by the substitution of V_R eq. 4.5 in eq. 4.7. L is length of the receiver, n is the number of the detectors at the receiver, r is the radius of the detectors, α is the minimum allowable distance between the detectors. The second derivative of the objective function is positive in the studied interval, so the above optimization problem (4.15) is convex. By maximizing the diameter, the distance d will be minimized automatically in order to have a maximum $h(r)$. The maximization of the diameter is constrained with a predetermined P_{max}, and with a required minimum distance α between the detectors.

In Fig 4.7, we also notice that by increasing the distance S between the detectors, the receiver response improves in terms of ISI mitigation, as illustrated in Fig 4.7 using an arrow. To find the optimal distance between the detectors, our objective is to maximize S equation defined in (4.15), with a maximum receiver length as a constraint. The second optimization problem is formulated as follows:

$$\max_{S\in\mathbb{R}_*^+} g(S) = n2\hat{r} + (n-1)S \; s.t : g(S) \leq L \; and \; P_e \leq P_{max} \tag{4.16}$$

where S is the distance between the detectors, $\hat{r}$ is the optimal detector radius solution of the first optimization problem (4.15) and L is the maximum length of the receiver. The objective function is linear, so the above optimization problem (4.16) is also convex. The maximization of the distance between the detectors is constrained with the receiver length L and P_{max}.

4.6.2 Proposed Algorithms

In this paper we propose two algorithms in order to solve the two optimization problems. The first algorithm is dedicated to solve the problem of the detectors diameter $\hat{r}$ maximization. Initially, the algorithm takes the initial parameters consisting of the diameters

Algorithm 1 Optimal detectors' diameter

Inputs: $\langle r_{init}, d_{init}, L, \alpha, Q, P_{max}, n \rangle$
Outputs: $\langle \hat{r}, \hat{d} \rangle$
$r_{new} \leftarrow r_{init}$
$er \leftarrow 0$
$S \leftarrow 0$
$d_{tmp} \leftarrow d_{init}$
while $(S < \alpha)$
$r_{new} \leftarrow r_{new} + 1$
$d_{tmp} \leftarrow d_{init} - r_{new} - r_{init}$
calculate er by using Eq. 4.13
if $(er \geq P_{max})$
$S = abs(L - (2nr_{new}))/(n-1)$
else
$\hat{r} \leftarrow r_{new}$
$\hat{d} \leftarrow d_{tmp}$
return $\langle \hat{r}, \hat{d} \rangle$

r_{init}, the distance between the transmitter and the receiver d_{init}. The parameters Q, P_{max}, n and α are used to calculate S and the error probability er. At each iteration we increase simultaneously the diameter by $1\mu m$ of the detectors and measure the error probability er. The algorithm stops when an optimal value of the detector diameter is reached.

Moreover, the objective of the second algorithm is maximizing the distance between the detectors $\hat{S}$. As input, it takes the optimal parameters obtained from the algorithm 1. For each iteration, it increases the distance between the detectors with the constraint of the receiver length L. For simplification r refers to the diameter of the detector. At each iteration we increase the distance between detectors by $4\mu m$, and check for the error probability. The algorithm stops when the error probability is lower than the tolerated value P_{max} or when the length of the detector is reached. The results of the proposed algorithms simulations give the same results found by using the simulator.

4.7 Conclusion

The bio-inspired paradigm of diffusion-based MC is one of the most promising solutions for the nano-communication. Path loss and ISI are the main challenges that need to be tackled in order to enhance the link quality and increase the achievable throughput. In this paper, we studied the optimization of a MIMO receiver design by focusing on three important parameters: the channel distance, the distance between the detectors constructing the

Algorithm 2 Optimal distance between detectors

Inputs: $\langle \hat{r}, S_{init}, \mathrm{L}, P_{max}, n \rangle$
Outputs:$\langle \hat{S} \rangle$
$S_{new} \leftarrow S_{init}$
$er \leftarrow 0$
$d_{tmp} \leftarrow d_{init}$
while $(g(S) \leq \mathrm{L})$
$S_{new} \leftarrow S_{new} + 4$
calculate er by using Eq. 4.13
if$(er \geq P_{max})$
$g = (2n\hat{r}) + (n-1)S_{new}$
else
$\hat{S} \leftarrow S_{new}$
return$\langle \hat{S} \rangle$

receiver and the diameter of the detectors. A 3×3 MIMO system was simulated using AcCoRD simulator. In the simulations, we evaluated the function of the error probability with the number of the allocated molecules in each emitter as an input. We also formulated two optimization problems and proposed two algorithms to solve them. The study showed that a judicious choice of the optimized three parameters combination can optimize the MIMO receiver response by decreasing the error probability and increasing the achievable throughput. The use of a MIMO technique with an optimized receiver can enhance the link quality of molecular communication and increase its data rate.

CHAPTER 5

POLYMER-BASED WIRED NANO-COMMUNICATION

Auteurs et affiliation:

Oussama Abderrahmane Dambri: étudiant au doctorat, Département de Génie Électrique et de Génie Informatique ,Université de Sherbrooke. INTERLAB Research Laboratory.

Soumaya Cherkaoui: Professeur, Département de Génie Électrique et de Génie Informatique, Université de Sherbrooke. INTERLAB Research Laboratory.

Date de Parution: en cours de révision

Revue: *IEEE Transactions on Molecular Biological and Multi-scale Communications*

Titre français: Un modèle de canal à base de polymère pour des Réseaux de nano-communication filaires

Résumé français:

Dans cet article, nous proposons un nouveau système de bout en bout pour les réseaux de nano-communication filaires utilisant un polymère auto-assemblé. L'auto-assemblage d'un polymère crée un canal entre l'émetteur et le receveur sous la forme d'un nanofil conducteur qui utilise des électrons comme porteurs d'informations. Nous dérivons le modèle analytique du canal et son équation maitresse pour étudier le processus dynamique de l'auto-assemblage du polymère. Nous validons le modèle analytique avec des simulations numériques et Monte-Carlo. Ensuite, nous approchons l'équation maitresse par une équation de Fokker-Planck unidimensionnelle et nous résolvons cette équation analytiquement et numériquement. Nous formulons les expressions du taux d'allongement du polymère, de son coefficient de diffusion et du nullcline pour étudier la distribution et la stabilité du nanofil auto-assemblé. Cette étude montre des résultats prometteurs pour la réalisation de nanoréseaux câblés stables à base de polymères qui sont capables d'atteindre un débit très élevé.

5.1 A Polymer-based Channel Model for Wired Nano-Communication Networks

5.2 Abstract

In this paper, we propose a new end-to-end system for wired nano-communication networks using a self-assembled polymer. The self-assembly of a polymer creates a channel between transmitter and receiver in the form of a conductive nanowire that uses electrons as carriers of information. We derive the channel's analytical model and its master equation to study the dynamic process of the polymer self-assembly. We validate the analytical model with numerical and Monte-Carlo simulations. Then, we approximate the master equation by a one-dimensional Fokker-Planck equation and we solve this equation analytically and numerically. We formulate the expressions of the polymer elongation rate, its diffusion coefficient and the nullcline to study the distribution and the stability of the self-assembled nanowire. This study shows promising results for realizing stable polymer-based wired nanonetworks that can achieve high throughput.

5.3 Introduction

Nanomachines are used in pharmaceutical and medical applications such as monitoring, drug delivery and real time chemical reactions detection. However, the capabilities of nanomachines are still very limited. This has prompted an interest in the design of nanonetworks that allow nanomachines to share information and to cooperate with each other [Akyildiz and Jornet, 2010b]. Nanonetworks call for a new networking paradigm that adapts traditional communication models to the nanoscale systems requirements. Two kinds of solutions are proposed in literature to create nanonetworks: first, using electromagnetic waves in the Terahertz (THz) band, or second, using bio-inspired molecular communications.

Using the THz band for electromagnetic nanonetworking is necessary given the nanoscale of the antennas[Akyildiz and Jornet, 2010a]. Communications in the THz frequency band suffer from scattering losses, molecular absorption and path loss [Alsheikh *et al.*, 2016; D'Oro *et al.*, 2015; Guo *et al.*, 2016; Han and Akyildiz, 2017; Han *et al.*, 2017; He *et al.*, 2017; Hosseininejad *et al.*, 2017; Jadidi *et al.*, 2015; Jianling *et al.*, 2016; Kim and Zajić, 2016; Kokkoniemi *et al.*, 2015; Nafari *et al.*, 2017; Piro *et al.*, 2016; Wang *et al.*, 2017; Yao and Jornet, 2016; Zakrajsek *et al.*, 2017; Zarrabi *et al.*, 2017; Zhang *et al.*, 2016]. Molecular communication is a promising bio-inspired solution to enable nanonetworks. Instead of

using electromagnetic waves, molecules are used as wireless carriers of information between the transmitter and the receiver [Pierobon and Akyildiz, 2010]. However, the achievable throughput with molecular communications is still very low and the delay is very high, despite the efforts reported in the literature to enhance both of them and to decrease the inter-symbol interference [Ahmadzadeh *et al.*, 2017; Akdeniz *et al.*, 2018; Ardeshiri *et al.*, 2017; Arjmandi *et al.*, 2016; Assaf *et al.*, 2017; Barros, 2017; Bicen *et al.*, 2016; Chahibi *et al.*, 2016; Chang *et al.*, 2018; Cho *et al.*, 2017; Dambri *et al.*, 2019; Dambri and Cherkaoui, 2018, 2019; Damrath *et al.*, 2017; Deng *et al.*, 2016; Einolghozati *et al.*, 2016; Enomoto *et al.*, 2011; Farsad *et al.*, 2016; Kim *et al.*, 2014; Mosayebi *et al.*, 2016; Nakano and Suda, 2017; Noel *et al.*, 2014; Tavakkoli *et al.*, 2017a,b; Tepekule *et al.*, 2015a,b; Unluturk and Akyildiz, 2017].

In our previous work [Dambri *et al.*, 2019], we proposed the use electrons as carriers of information in a wired system at the nanoscale. Using electrons as information carriers is not new, a cable of assembled bacteria is proposed in literature, which uses the ability of bacteria to generate and transfer electrons[Meysman, 2018; Michelusi and Mitra, 2015; Michelusi *et al.*, 2014]. However, the bacterial cables are closer to the proposed Ca^{2+} ions communication system [Barros, 2017] than to an actual conductive cable. The proposed system in this paper is based on a polymer called "actin" [Lodish *et al.*, 2000], which self-assembles to construct a filament that plays the role of a conductive nanowire. Actin is a bi-globular protein with self-assembly capabilities, that is naturally used by biological systems such as the human body for cell skeletal maintenance, cell movement, cell division [Alberts *et al.*, 2002]. The direction of self-assembled actin filaments is random, however, experimental studies proved that we can guide actin filaments to a desired direction by using electric [Arsenault *et al.*, 2007; Kaur *et al.*, 2012; Patolsky *et al.*, 2004] or magnetic fields [Kaur *et al.*, 2010]. The polymer-based system was shown to enable wired nano-communication networks that are capable of very high throughput while presenting biocompatibility advantages [Dambri *et al.*, 2019]. In fact, the achievable throughput was demonstrated to reach mega bits per second [Dambri and Cherkaoui, 2020b], which is several orders of magnitude bigger than the throughput reported in the literature for other molecular communication systems [Arjmandi *et al.*, 2016; Farsad *et al.*, 2016; Kim *et al.*, 2014; Noel *et al.*, 2014]. Other communication systems proposed in literature can also acheive high throughputs such as redox reactions [Liu *et al.*, 2017] and FRET methods [Kuscu and Akan, 2014]. However, their delay is very high because the transmission of information is random.

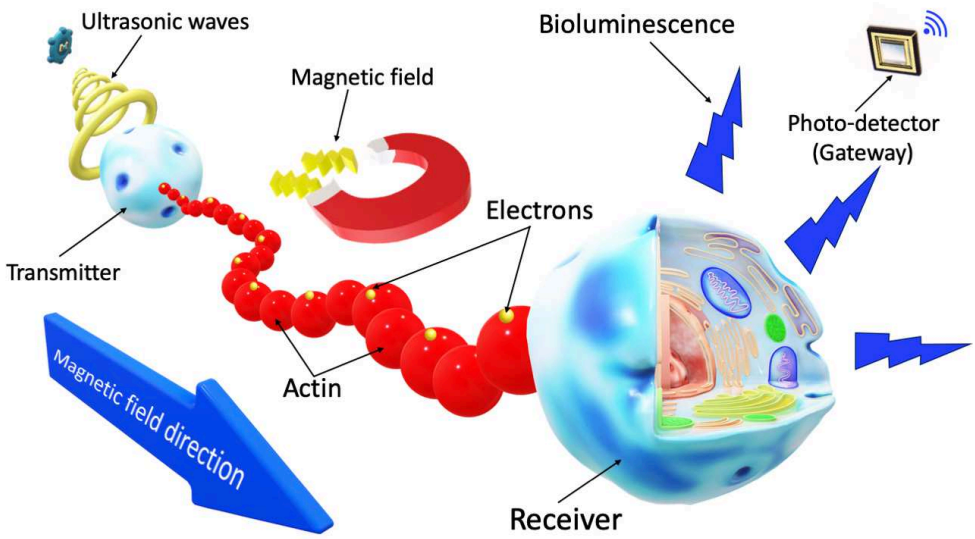

Figure 5.1 System design of a polymer-based wired nano-communication system.

The design of the end-to-end wired polymer-based system is shown in Fig. 5.1, where the transmitter contains a ZnO matrix to transform ultrasonic waves into electricity. The electrons are then sent through a self-assembled actin filament, which is guided by a magnetic field towards the receiver's direction. Finally, the receiver plays the role of a relay by absorbing the electrons and emitting bioluminescent light, which will be detected by a photo-sensor (gateway). The intensity of the light emitted by the receiver is dependent on the transmitted electrons' intensity. This property can be used as a modulation technique.

This paper is an extension of the work proposed in [Dambri *et al.*, 2019], where we introduced the system concept and some preliminary simulation results. In this paper, we propose an analytical model to study the dynamic process of the polymer self-assembly, its elongation rate and its diffusion. We also validate the model with numerical and Monte-Carlo simulations. The main contributions of the paper are summarized as follows:

1. We derive a master equation of the communication channel to study the dynamic process of the polymer self-assembly, and we calculate the steady state of the self-assembly chemical reaction analytically and numerically.
2. We validate the proposed analytical model with numerical and Monte-Carlo simulations and we present the simulation results in terms of the monomers' concentration changes over time.

3. We approximate the derived master equation by a 1D Fokker-Planck equation and we solve this equation analytically by using a differential transform method, and numerically with Monte-Carlo simulations.
4. We derive the nanowire elongation rate and its diffusion coefficient expressions, and validate them with numerical simulations.
5. We derive a nullcline expression to study the stability of the constructed self-assembled nanowire, and we provide an analysis using a phase plane graph.

The rest of the paper is organized as follows. In section II, we summarize the state-of-the-art of the works proposed in the literature for electromagnetic and molecular communications, their advantages and disadvantages. In section III, we present an in-depth description of the proposed end-to-end wired polymer-based system design including a detailed view on the transmitter and the receiver. We then put the spotlight on the communication channel and study the dynamic assembly and distribution of the nanowire. In section IV, we derive the master equation of the nanowire self-assembly, and we calculate the steady state of the chemical reaction. We also derive the nullcline expression to study the stability of the self-assembled nanowire. Then, we approximate the derived master equation by a 1D Fokker-Planck equation. We solve the equation analytically by using a differential transform method and numerically with Monte-Carlo simulations. In section V, we discuss the obtained results of the analytical, numerical and Monte Carlo simulations. Finally, we present the conclusion in section VI.

5.4 State-Of-The-Art

The work on THz nanonetworks in literature can be categorized into three classes; a) Medium Access Control (MAC) protocol enhancement [Alsheikh *et al.*, 2016; D'Oro *et al.*, 2015; Han *et al.*, 2017; Jianling *et al.*, 2016; Yao and Jornet, 2016], b) antenna enhancement designs[Hosseininejad *et al.*, 2017; Jadidi *et al.*, 2015; Wang *et al.*, 2017; Zakrajsek *et al.*, 2017; Zarrabi *et al.*, 2017; Zhang *et al.*, 2016] and c) channel modeling methods [Guo *et al.*, 2016; Han and Akyildiz, 2017; He *et al.*, 2017; Kim and Zajić, 2016; Kokkoniemi *et al.*, 2015; Nafari *et al.*, 2017; Piro *et al.*, 2016]. In the first class, the researchers aim to enhance MAC protocols by designing energy-efficient nanonetworks [Alsheikh *et al.*, 2016; D'Oro *et al.*, 2015] with high throughput and low delay [Han *et al.*, 2017; Jianling *et al.*, 2016; Yao and Jornet, 2016]. To enhance THz antennas, researchers use plasmonic waves [Hosseininejad *et al.*, 2017; Jadidi *et al.*, 2015; Zhang *et al.*, 2016] and take advantage of the black phosphorus and graphene's physical properties [Wang *et al.*, 2017; Zakrajsek *et al.*, 2017; Zarrabi *et al.*, 2017] to overcome transceivers' design problems. The last

class studies the propagation of THz waves in different media, using 2D [Kim and Zajić, 2016; Kokkoniemi *et al.*, 2015] and 3D models [Han and Akyildiz, 2017; He *et al.*, 2017], by considering molecular absorption [Nafari *et al.*, 2017; Piro *et al.*, 2016] and scattering losses [Guo *et al.*, 2016]. However, the molecular absorption of THz waves is very high, which drastically increases its path loss. The scattering and path losses are the main challenges that need to be tackled in order to capture and address the peculiarities of the THz band at nanoscale. Nanonetworks could be used to expand the capabilities of single nano-machines inside the human body for medical applications. However, using THz waves for such applications could be dangerous, because the vibration of water molecules increases when they absorb electromagnetic waves in such high frequency bands. The vibration raises the heat in the medium and can cause tissues' burn [Chopra *et al.*, 2016]. Further studies are needed to investigate and ensure the safety of using THz nanonetworks inside the human body.

Molecular communication is a promising bio-inspired solution to design nanonetwork systems. Instead of using electromagnetic waves, molecules are used as wireless carriers of information between the transmitter and the receiver[Farsad *et al.*, 2016]. From bacterial colonies to the human brain, molecular communication has been adopted by nature billions of years ago, and has demonstrated its efficiency at the nanoscale. This explains the interest of the research community in designing nanonetwork biosystems based on molecular communications for medical applications inside the human body. However, molecular communications have many challenges, the most important of which are its limited throughput, its high delay and the presence of InterSymbol Interference (ISI). After a previous transmission, some molecules remain in the medium because of their random walk, caused by thermal fluctuations at nanoscale. The molecules remaining in the medium interfere with the newly transmitted molecules, thus introducing errors at the receiver and affecting the reliability of communications.

The most studied methods proposed for molecular communication are based on the principle of molecular diffusion, where molecules move randomly, because of the thermal fluctuations of the medium, until they reach the receiver. The work on molecular communication in the literature can be categorized into five classes; a) modulation techniques [Arjmandi *et al.*, 2016; Farsad *et al.*, 2016; Mosayebi *et al.*, 2016; Nakano and Suda, 2017], b) channel modeling studies [Ahmadzadeh *et al.*, 2017; Bicen *et al.*, 2016; Chahibi *et al.*, 2016; Damrath *et al.*, 2017; Deng *et al.*, 2016], c) relay assistance methods [Ardeshiri *et al.*, 2017; Tavakkoli *et al.*, 2017a,b], d) ISI avoidance [Akdeniz *et al.*, 2018; Assaf *et al.*, 2017; Chang *et al.*, 2018; Cho *et al.*, 2017; Dambri *et al.*, 2019; Dambri and Cherkaoui, 2018, 2019; Kim

et al., 2014; Noel *et al.*, 2014; Tepekule *et al.*, 2015a,b] and e) end-to-end communication system designs [Barros, 2017; Einolghozati *et al.*, 2016; Enomoto *et al.*, 2011; Unluturk and Akyildiz, 2017]. In the first class of works, the researchers propose adaptations of some of the techniques classically used with electromagnetic wave communications, to the new paradigm of molecular communications. These include aspects of modulation techniques, which encode the information in the molecules' concentration (equivalent to doing so in electromagnetic signal's amplitude), type (equivalent to doing so in electromagnetic signal's frequency), and release time (equivalent to doing so in electromagnetic signal's phase). [Farsad *et al.*, 2016]. Other researchers propose new ideas such as using ion protein channels to control molecules release [Arjmandi *et al.*, 2016], a ratio shift between two types of molecules [Mosayebi *et al.*, 2016] or the dynamic properties of propagation patterns in molecules' concentration [Nakano and Suda, 2017]. In the second class of works, the researchers modeled molecular communication channels to study the dynamic distribution of information in the medium [Chahibi *et al.*, 2016; Deng *et al.*, 2016]. They use discrete-time channels [Damrath *et al.*, 2017], or continuous stochastic models for constant [Bicen *et al.*, 2016] and mobile transmitters and receivers [Ahmadzadeh *et al.*, 2017]. To minimize error probabilities and optimize molecular communication performance, the works in the third class propose using a relay-assisted diffusion between transmitters and receivers [Ardeshiri *et al.*, 2017; Tavakkoli *et al.*, 2017a,b]. Avoiding ISI is a main challenge of molecular communication. In the fourth class of works, two types of solutions are proposed to avoid ISI: passive and active solutions. Passive solutions use pre-equalization methods [Tepekule *et al.*, 2015a,b], or optimize symbol times and detection thresholds [Akdeniz *et al.*, 2018; Chang *et al.*, 2018; Kim *et al.*, 2014]. Active solutions propose removing the molecules physically from the medium to avoid ISI, by using neighboring receivers [Assaf *et al.*, 2017; Dambri *et al.*, 2019], enzymes [Cho *et al.*, 2017; Noel *et al.*, 2014] or photolysis reactions [Dambri and Cherkaoui, 2018, 2019]. In the last class of works, inspired by nature, the researchers propose more complex biosystem nanonetworks such as bacteria colonies [Einolghozati *et al.*, 2016], plant pheromones [Unluturk and Akyildiz, 2017], Ca^{2+} signaling in the cells [Barros, 2017; Bicen *et al.*, 2016] and using molecular motors[Chahibi *et al.*, 2016; Enomoto *et al.*, 2011]. The last system uses microtubule polymers as a road for kinesin motors to walk on, and transport a cargo of information from the transmitter to the receiver. Despite the efforts reported in the literature to enhance molecular communication performance, the achievable throughput remains very low (tens of bits per second), with very high delay (minutes, hours). In the present work, we use a polymer of the kinesin motor reported in [Enomoto *et al.*, 2011] as an electric nanowire in-

stead of a road, and we show that we can design nanonetworks using this kind of nanowire which can achieve high throughput (Mbits per second).

Another way to create assembled nanowires is to use bacteria as reported in[Meysman, 2018; Michelusi and Mitra, 2015; Michelusi *et al.*, 2014], which have the ability to create bacterial cables that can generate and transfer electrons. However, bacteria do not transfer electrons instantly as real cables do, but receive them and use chemical reactions to generate other electrons and then transfer them to another bacteria. This discontinuity in electrons transmission can explain the very low acheivable rate of bacterial cables [Michelusi and Mitra, 2015].

5.5 System Design

The design of a flexible wired nano-communication network is a new promising solution to be used in pharmaceutical and medical applications that can provide a very high throughput. The proposed polymer-based nano-communication system has the potential to be implemented noninvasively inside the human body due to its tiny size. The fact that electrons generation can be controllable from the outside with ultrasonic waves, the proposed system can be used to noninvasively stimulate a specific part in the human brain and can also be used to treat epileptic diseases. The proposed end-to-end system contains a transmitter with a ZnO matrix, a receiver with photo-proteins and a photo-sensor as the gateway. The monomers diffuse randomly in the medium and their self-assembly constructs a nanowire, which links the transmitter to the receiver.

5.5.1 Transmitter

The innovative approach proposed in [Wang, 2010] that converts mechanical energy into electricity at nanoscale by using piezoelectric Zinc Oxide (ZnO) nanowire matrix is used in our transmitter to generate electrons. The piezoelectric potential is created by the polarization of the ions in some solid materials such as crystals and ceramics, or biological matter as DNA and some proteins, when subjected to strain. The authors of [Wang, 2010] used the unique coupling of semiconducting and piezoelectric dual ZnO properties and a Schottky barrier between the metal tip and the nanowire to create a DC nano-generator. The transmitter in the proposed system uses this DC nano-generator to convert mechanical vibration into electricity. The mechanical vibration is generated with ultrasonic waves. Pulses of ultrasonic waves are converted into pulses of electrons at the transmitter, which sends them through the assembled nanowire. To modulate the information at the transmitter, we can use the amplitude and the frequency of the ultrasonic waves.

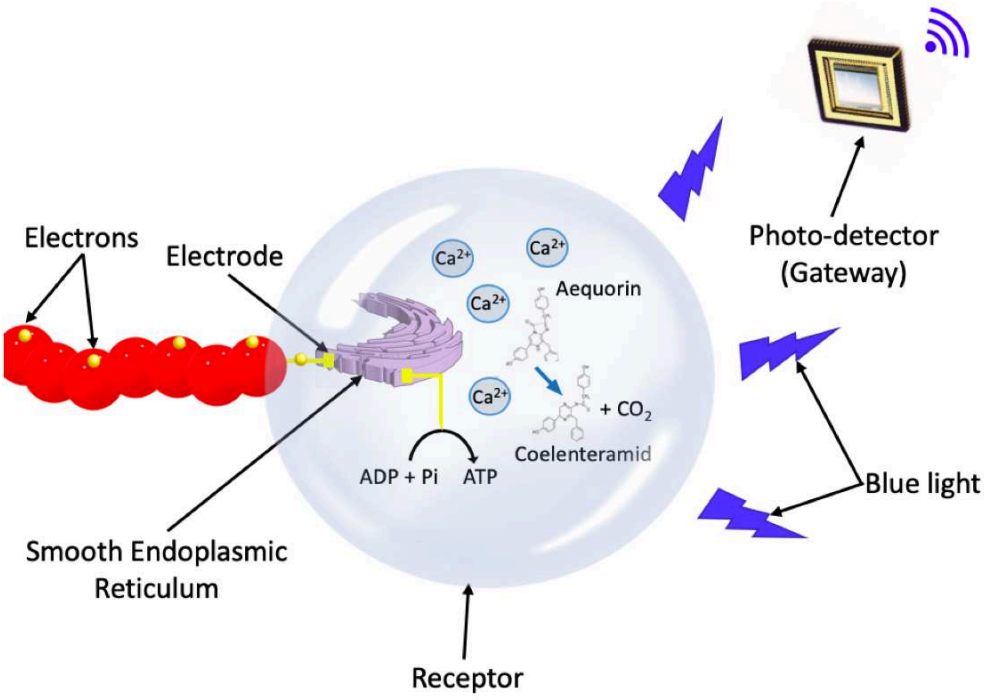

Figure 5.2 Receiver design that uses electrons to generate bioluminescent blue light.

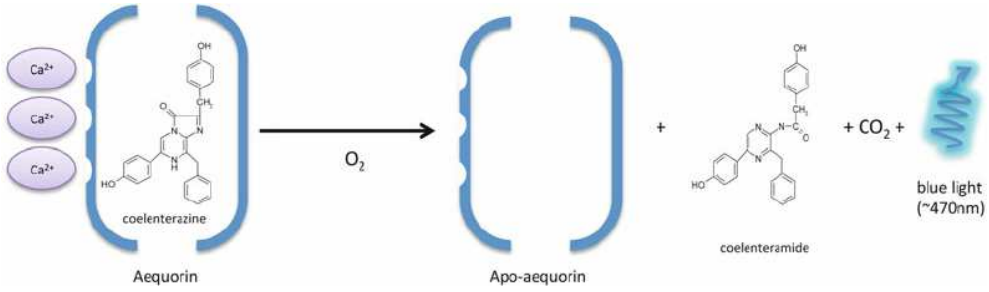

Figure 5.3 Bioluminescent reaction that uses Aequorin, which in the presence of Ca^{2+} ions, generates blue light [Badr, 2014].

5.5.2 Receiver

The electrons sent through the assembled nanowire will be absorbed by the receiver. However, it is extremely difficult for a user to extract the sent information from the received electrons at nanoscale because of the quantum trade-off between information and uncertainty. Therefore, our proposed receiver is designed to use the received electrons to provoke chemical reactions that generate bioluminescent light, which makes the extraction of information easier. Bioluminescence is a chemical emission of light by living organisms using light-emitting molecules (photo-proteins) and enzymes. Bioluminescence is a promising solution to make the shift from nanoscale to the micro and macro scales in our proposed receiver, as shown in Fig. 5.2. There are several photo-proteins in biological systems, the most studied and most famous being *Luciferin* with its enzyme *Luciferase*. *Luciferin* can be found in fireflies and deep-sea fishes. The oxidation of *Luciferin* is catalyzed by *Luciferase*, and the resulting excited intermediate state emits light upon decaying to its ground state [Aaron and Aaron, 2019]. In our proposed system, we use another photo-protein called *Aequorin* which is constructed by the jellyfish *Aequorea Victoria* that can be found in North America and the Pacific Ocean [Shimomura, 1995]. In the presence of Ca^{2+}, the *Aequorin* oxidation reaction described in Fig. 5.3 is activated, which generates blue light with 470 nm wavelength [Badr, 2014].

The proposed receiver contains high concentrations of *Aequorin*, and a Smooth Endoplasmic Reticulum (SER), which functions as a Ca^{2+} ions storage in living cells [Koch, 1990]. To avoid the absorption of electrons by the receiver's surface, it can be constructed with a hybrid phospholipid/alkanethiol bilayers membrane proposed in [Plant *et al.*, 1994], because of its insulating nature, in order to minimize the loss of electrons at the receiver. The nucleation of monomers that trigger the formation of the actin self-assembly can be tethered at the bio-engineered membrane of the receiver by using a polyethylene glycol (PEG) on one end and an electrode on the other end [Hoiles *et al.*, 2018]. The insertion of the monomer can be spontaneous, electrochemical or with a proteoliposome insertion as explained in [Hoiles *et al.*, 2018] with details. When the assembled nanowire reaches the receiver, it binds to one of the monomers already anchored to the receiver's membrane with electrodes, which creates a passage of electrons through the insulating membrane. The absorbed electrons excite the SER, as shown in Fig. 5.2, which causes the secretion of Ca^{2+} ions. The *Aequorin* inside the receiver activates in the presence of Ca^{2+} ions and emits blue light, which is detected by a photo-sensor, which is acting as gateway. When the emission of electrons ceases, the secretion of Ca^{2+} ions stops, and SER absorbs all Ca^{2+} ions inside the receiver as a sponge. Without Ca^{2+} ions, *Aequorin* becomes inactivated

and stops emitting blue light. The intensity of the blue light emission from the receiver depends on the emitted electrons intensity (at the transmitter), which itself depends on the emitted ultrasonic waves intensity (from outside the body).

Several challenges need to be tackled in our proposed receiver design. First, we need to calculate the number of electrons needed to excite the SER. Then, we determine the relation between the number of the absorbed electrons and the concentration of Ca^{2+} ions secreted by the SER. Finally, we need to establish a relation between the bioluminescent light intensity detected by the photo-sensor and the intensity of the current sent from the transmitter. An experimental study is envisioned to be proposed in our future work.

5.5.3 Channel

The cytoskeleton is an essential complex of interlinking filaments for the living cells shape, movements and division [Alberts *et al.*, 2002]. Three types of filaments construct the cytoskeleton complex, depending on the assembled protein that constructs them. Microfilaments are constructed with assembled actin, microtubules are constructed with assembled tubulin and the intermediate filaments are constructed with keratin, vimentin, lamin or desmin. The choice of actin as our polymer in this study to construct the proposed nanowire is due to the fact that microfilaments constructed by actin are more flexible and easily controllable compared to microtubules and intermediate filaments. Actin is one of the most studied and most abundant proteins, comprising 10% of muscle cells total proteins and around 5% in the other cells [Lodish *et al.*, 2000], which makes it an ideal candidate to construct our proposed nanowire. Actin filaments have a high electrical conductivity, as proven in the experimental studies in [Patolsky *et al.*, 2004] and [Hunley *et al.*, 2018]. The authors in [Patolsky *et al.*, 2004] proposed a metallic actin-based nanowire, where they labelled globular actin (G-actin) with gold nanoparticles to increase the electrical conductivity of actin filaments (F-actin). The study showed that the electrical conductivity of a metallic actin-based nanowire can reach 25 μA for 0.8 mV potential, which is very high at nanoscale. Fig. 5.4 shows a High Resolution Scanning Electron Microscopy (HRSEM) image of the studied metallic nanowire between two electrodes [Patolsky *et al.*, 2004]. The authors in [Hunley *et al.*, 2018] and [Tuszyński *et al.*, 2004] studied the electrical impulses and ionic waves propagating along actin filaments in both intracellular and *in vitro* conditions. The results of the studies revealed the existence of electrical signal impulses and ionic waves propagating through intracellular actin filaments in the form of solitons at a speed reaching 0.03 m/s. However, the polymerization process of G-actin monomers to form F-actin filament is random, because of the thermal fluctuations in the medium. One

of the main challenges to construct a nanowire in a randomly diffusive medium is to guide its assembly to a desired direction.

To guide the direction of actin filaments assembly, two solutions are proposed in the literature, either by using electric [Arsenault *et al.*, 2007; Kaur *et al.*, 2012; Patolsky *et al.*, 2004] or magnetic field [Kaur *et al.*, 2010]. The experimental study in [Arsenault *et al.*, 2007] has shown that by applying an electric field to the actin filaments, they align themselves parallel to the field lines. The study proved that as the electric field intensity increases, the variance in actin displacement decreases, which affects the filament's behavior and causes its alignment. The authors in [Kaur *et al.*, 2012] also used AC electric field to guide the direction of actin assembly. The same authors proposed in [Kaur *et al.*, 2010] a new idea to align assembled actin filaments by using a magnet bar with a low-intensity magnetic field (22 mT). The study has shown that the majority of F-actin got permanently aligned towards the magnetic lines. The authors concluded that a magnetic field can be safely used to permanently orient and guide the alignment of F-actin towards a desired direction. Because using AC electric field inside the human body is dangerous, our proposed system shown in Fig. 5.1 is designed to guide the actin assembly direction by using a magnetic field. The path of the transmitted electrons through the proposed nanowire is circular because of the helicoidal shape of actin filaments.

In the next section, we will derive an analytical model to study the dynamic process of the actin nanowire self-assembly. We also calculate the steady state of the chemical reaction, and we derive a nullcline expression to study the nanowire stability.

5.6 Channel Model

Actin proteins exist under two forms, monomeric (G-actin), and filamentous (F-actin). The self-assembly of actin monomers creates actin filaments, and this polymerization re-

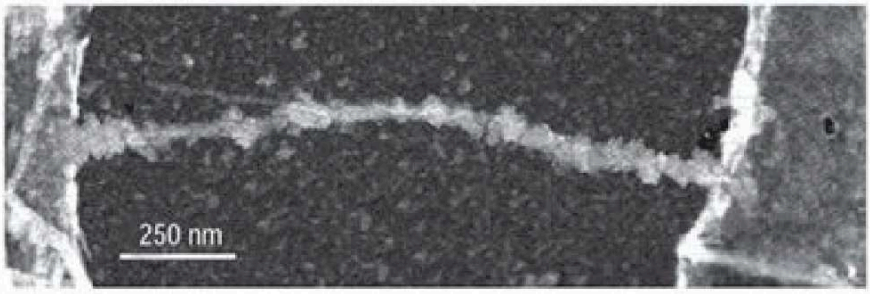

Figure 5.4 High Resolution Scanning Electron Microscopy (HRSEM) image of a metallic actin-based nanowire between two electrodes [Patolsky *et al.*, 2004].

action involves three steps: nucleation, elongation and steady state [Pollard and Mooseker, 1981]. The first step consists in the construction of an actin nucleation core, which is a three-actin monomers protein. This nucleation core is energetically unfavorable, unless it binds with another actin monomer, which leads to an energetically favorable elongation reaction [Liu *et al.*, 2013]. The second step is where the polymerization and depolymerization change the rate of actin filaments elongation. The polymerization and depolymerization take place on both sides of actin filaments as shown in Fig. 5.5, but with different rates. The faster side is called the pointed end, and the slower side is called the barbed end. The final step occurs when the addition and dissociation of actin monomers to the filament sides are balanced and a steady state is reached.

5.6.1 Chemical Reaction

In this paper, the studied polymerization of the actin nanowire does not consider the nucleation step because we assume that nucleation cores are already anchored at the transmitter's surface, as shown in Fig. 5.5. When an actin monomer binds with one of the anchored nucleation cores, the elongation of the nanowire is triggered, thus, the studied reaction in this paper starts directly with the elongation step. To simplify the complex polymerization reaction of the actin nanowire, we consider fixed reaction rates. We also consider a nanowire N_i consisting of i actin monomers. When a monomer N_1 binds with the complex N_i, it becomes N_{i+1}, and a monomer dissociation gives N_{i-1}. Knowing that a nucleation core contains 3 monomers, the nanowire polymerization in this study starts with N_4. The pointed end is written as [Pollard and Mooseker, 1981]:

$$N_i + N_1 \underset{k^p_{-1}}{\overset{k^p_1}{\rightleftharpoons}} N_{i+1}, \tag{5.1}$$

and for the barbed end:

$$N_i + N_1 \underset{k^b_{-1}}{\overset{k^b_1}{\rightleftharpoons}} N_{i+1}, \tag{5.2}$$

where k^p_1 and k^p_{-1} are the polymerization and depolymerization rates for the pointed end, k^b_1 and k^b_{-1} are the rates of the barbed end. N_1 is the actin monomer and N_i is the actin nanowire, where $i \in \mathbb{N}^*$ and $4 \leq i \leq l$. l is the maximum number of actin monomers in the constructed actin nanowire.

However, the anchored nucleation core at the transmitter's surface fixes the barbed end of the actin nanowire as shown in Fig. 5.5, and there will be no addition nor dissociation from that side. Therefore, this study uses only the reaction in 5.1, and to simplify the notations, we write k_+ and k_- instead of k^p_1 and k^p_{-1} respectively. The equation 5.1 is

described by a differential equation as follows:

$$\frac{d}{dt}n(t) = -2k_+N_i^2 + k_-, \tag{5.3}$$

and the elongation of the actin nanowire is described as:

$$\frac{d}{dt}a(t) = -k_- + 2k_+N_i^2, \tag{5.4}$$

where $\frac{d}{dt}n(t)$ is the change of the monomers concentration in the medium with time. $\frac{d}{dt}a(t)$ is the change of the actin nanowire elongation with time. The stoichiometric factor 2 appears because each reaction event consumes two molecules and the square appears because it is a bimolecular reaction with one single type of molecules $N_i \times N_i$. The unit of the nanowire's elongation is μm.

5.6.2 Markov Process Model

The proposed nanowire channel is nucleation-limited because every G-actin monomer is unpopulated at most times, which makes their binding random. Thus, the actin polymerization must be treated as a stochastic system [Betz *et al.*, 2009]. If the conditional probability distribution of a stochastic process's future states depends only upon the present state and not on the events that preceded it, the process is called a Markov process. Our proposed channel is formulated as a Markov chain, which is a type of Markov process that has either discrete state space or discrete time index set [Wilkinson, 2011]. Before deriving the chemical master equation of the proposed channel from the Markov process model, we need first to determine the reaction propensities. A reaction propensity tells us how likely a reaction is to occur per unit time [Ingalls, 2013]. If we assume that the reaction events are independent and that at most one reaction event between two actin monomers can occur at a time, then, the propensity of this bimolecular polymerization reaction is[Ingalls, 2013]:

$$n = k_+N_ie^M, \tag{5.5}$$

where N_i is the number of actin monomers in the medium, which we will write it as N in next equations for simplification. M is the intensity of the magnetic field. The propensity of the depolymerization reaction is k_-e^{-M}. The magnetic field increases the polymerization and decreases the depolymerization, which increases the stability of the nanowire as we will see in the next subsection. The reaction stoichiometries s_i are [1] or [−1], which means that only one monomer is added or dissociated at a time. The polymerization that leads to the nanowire elongation is a Markov chain that changes the system, at each reaction, from

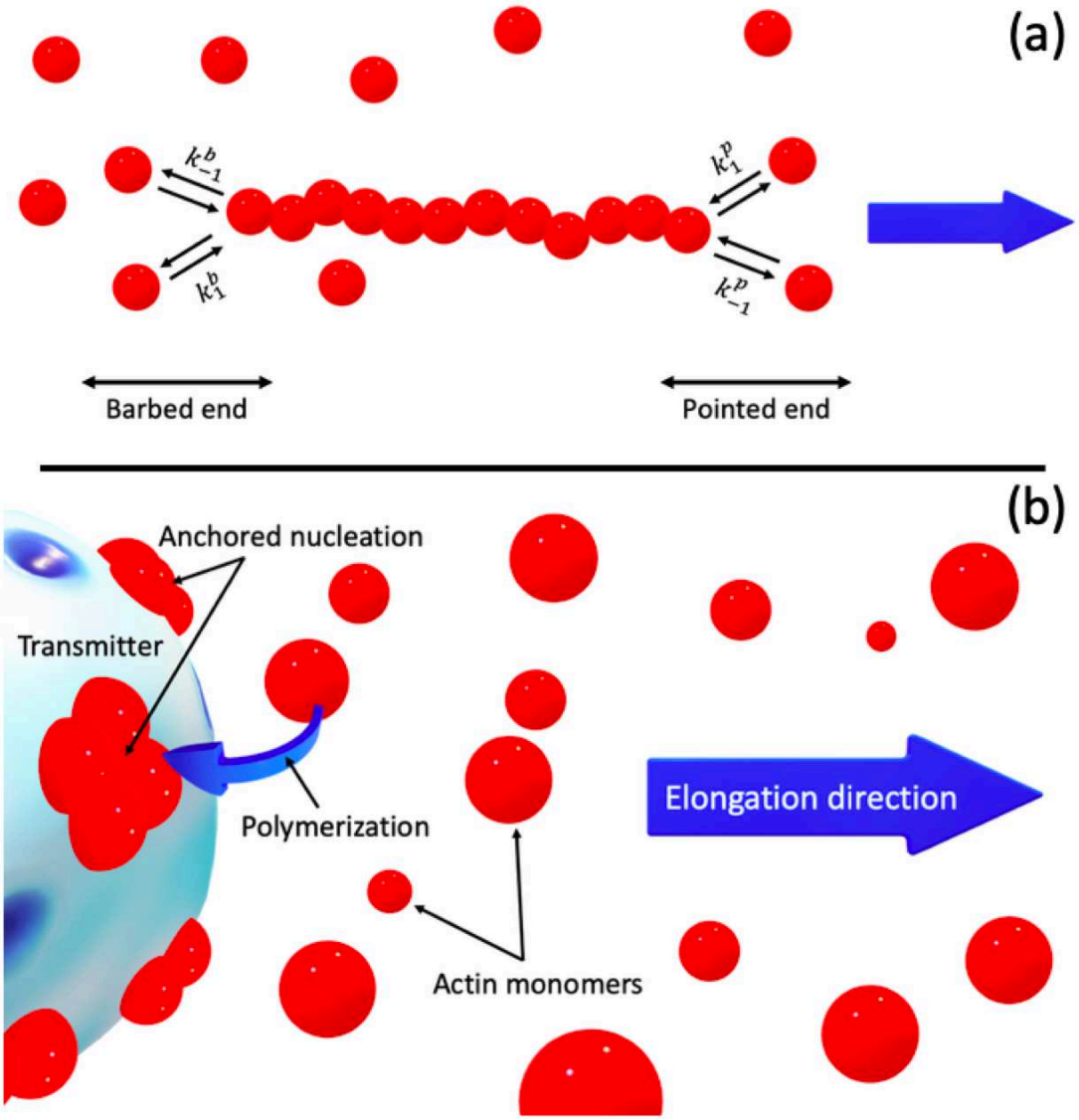

Figure 5.5 Polymerization and depolymerization of actin nanowire. (a) The fast pointed end and the slow barbed end of the actin self-assembly. (b) The nucleation already anchored in all the surface of the transmitter to quickly activate the actin elongation.

state N to state $N+1$. In our stochastic model, we assume a small-time increment, dt and we assume that, at each time interval $[t,\, t+dt]$, the probability that a reaction occurs is the product of the interval length and the reaction propensity $n_i(N(t))dt$ [Ingalls, 2013]. Thus, the probability that no reaction occurs in the time interval is $1-\sum_i^l n_i(N(t))dt$, where i represents all the occurring reactions in the channel.

Let's consider $P(N,t)$ be the probability that the channel is in state N at time t, and is dependent on the initial conditions. If we know the distribution of $P(N,t)$ at time t, we can express the distribution at an incremented time $t+dt$ as follows:

$$P(N,t+dt) = P(N,t)\left(1-\sum_i^l n_i(N)dt\right) + \sum_i^l P(N-s_i,t)n_i(N-s_i)dt, \tag{5.6}$$

where s_i represents the reaction stoichiometries. The first half of the equation represents the probability of no reactions occurring. The second half represents the probability of the reactions firing, while in a state $(N-s_i)$. By substituting the reaction propensities in the equation 5.6 we write:

$$P(N,t+dt) = P(N,t)(1-(k_+N(N-1)/2)dt) + P(N-1,t) (k_+(N-1)(N-2)/2)dt + P(N+1,t)k_-dt, \tag{5.7}$$

This equation is called the probability balance, and we can use it to derive our chemical master equation by substituting $P(N,t)$ from each side of equation 5.7, which gives:

$$P(N,t+dt) - P(N,t) = -P(N,t)(k_+N(N-1)/2)dt + P(N-1,t) (k_+(N-1)(N-2)/2)dt + P(N+1,t)k_-dt, \tag{5.8}$$

This chemical master equation can be written as a differential equation:

$$\frac{d}{dt}P(N,t) = -P(N,t)(k_+N(N-1)/2)dt + P(N-1,t) (k_+(N-1)(N-2)/2)dt + P(N+1,t)k_-dt \tag{5.9}$$

Our derived chemical master equation can also be written as an iterative probability differential equation by putting $P(N,t)$ as $P_i(t)$ and we write:

$$\frac{d}{dt}P(N,t) = -(k_+M + k_-)P_i(t) + k_+MP_{i-1}(t) + k_-P_{i+1}, \tag{5.10}$$

where $M{=}N(N-1)/2$. The master equation in 5.10 is a finite system of differential equations that describe the time-varying of the proposed actin nanowire probability distribution, and it can be written in a general form as:

$$\frac{d}{dt}P_i(t) = \sum_i^l \Big(W_{i,i+1}P_{i+1}(t) + W_{i+1,i}P_i(t) \Big), \tag{5.11}$$

where $W_(i,i+1)$ and $W_(i+1,i)$ are the transition probabilities. The exact solution of the master equations for bimolecular reactions are complex and hardly obtained. Several works have been proposed to find the solution of some bimolecular reactions' master equation [Laurenzi, 2000; Lee and Kim, 2012]. Other works use the Gillespie algorithms to run stochastic Monte-Carlo simulations [Gillespie, 1992; Ingalls, 2013; Wilkinson, 2011]. The disadvantage of this method is that it needs a lot of trajectories in order to estimate accurately the master equation's solution [Székely and Burrage, 2014]. The approximation of the master equation by a 1D Fokker-Planck equation is considerably more efficient computationally and gives an accurate solution. In the last subsection, we will approximate the derived master equation by a 1D Fokker-Planck equation, and we solve it analytically and numerically.

5.6.3 Reaction Steady State

The actin self-assembly reaches a steady state when the addition and dissociation of actin monomers is balanced, which means that the change rate of actin concentration is zero and we can write:

$$-2k_+N_{ss}^2 + k_- = 0, \tag{5.12}$$

where N_{ss} is the actin monomers steady state concentration, which is equal to an equilibrium constant $K = \sqrt{k_-/2k_+}$ (critical concentration) for polymerization [Pollard and Mooseker, 1981]. We expect the solution of the differential equation in 5.3 to approach the steady state value exponentially, and we can derive an explicit description of the time-varying concentration as:

$$n(t) = (N_0 - K)e^{-2k_+t} + K, \tag{5.13}$$

where N_0 is the initial concentration of actin monomers, and K is the equilibrium constant. The solution indicates that when $t \to \infty$ the concentration of actin monomers decays exponentially until it reaches the critical concentration of polymerization K. Phase plane analysis is another approach to study the steady state of a dynamic system. Instead of plotting the concentration of actin monomers as functions of time, the phase plane plots the decaying concentration of actin monomers in the medium $n(t)$ against the concentration of actin monomers constructing the nanowire $a(t)$, which can be written as :

$$g(n_i, a_i) = -2k_+ n_i^2 + k_- a_i, \tag{5.14}$$

Phase plane analysis shows the trajectories that the concentrations take starting from initial conditions and converging to the steady state. The total points (n_i, a_i) where the trajectories of the phase plane change their direction constitutes the channel's null-clines. The determination of these nullclines analytically is not always possible, because the function $g(n_i, a_i)$ is usually nonlinear and so may not be solvable except via numerical simulations. However, it is possible to determine the analytical expression of the null-cline in our proposed linear system by putting $g(n_i, a_i)= 0$ and simply write the nullcline expression as:

$$n_i = K\sqrt{a_i}, \tag{5.15}$$

We notice that the nullcline expression of our proposed channel depends on the ratio $k_-/2k_+$. When $k_+ > k_-$, the actin nanowire elongates with polymerization, and when $k_+ < k_-$, the actin nanowire dissociates with depolymerization.

5.6.4 Channel's Stability

The dynamic process of the biological systems do not often diverge or follow a chaotic behavior. The biochemical systems either converge to a steady state, or converge to a sustained periodic oscillation [Ingalls, 2013]. The proposed actin nanowire self-assembly also converges to a steady state, and to see if that steady state is stable of unstable, we need to calculate the eigenvalues of the channel's Jacobian matrix. The stability of the channel depends on the eignevalues signs. If all eigenvalues are negative, then the steady state of the system is stable. If one of the system's eigenvalues is positive, then the system is unstable. The differential equations described in 5.3 and 5.4 can be written as a square

Jacobian matrix as follows:

$$J = \begin{bmatrix} -4k_+N(t) & 0 \\ 4k_+N(t) & 0 \end{bmatrix} \tag{5.16}$$

The eignevalues of this Jacobian matrix represent the roots of the quadratic equation:

$$\lambda^2 + 4k_+N(t)\lambda = 0, \tag{5.17}$$

which gives a zero eigenvalue $\lambda_1 = 0$ and a negative eigenvalue $\lambda_2 = -4k_+N(t)$. The case where one of the eigenvalues is zero happens only if the system has more than one equilibrium point as confirmed in the nullcline expression (5.14). In this case, we can say that the system is stable, but not asymptotically stable, where the stability is determined by the nonlinear terms of the system's equations [Roussel, 2019]. The stability of the actin nanowire is experimentally proven, where it is used by the cell to divide and move. If the actin nanowire was not stable, living cells would never divide, which is the tool used by living creatures to develop [Alberts *et al.*, 2002]. Therefore, we also present the stability of the proposed nanowire empirically by observing the results of our 3D stochastic simulations, and comparing them with experimental studies in the literature. The non-linearity of the proposed channel is influenced by the enzyme concentrations, the assembled nanowire length and the magnetic field that guides the direction of the nanowire self-assembly, and we write:

$$Stability = \frac{M \times E}{L} \tag{5.18}$$

where M is the intensity of the magnetic field, E is the enzyme concentration, and L is the length of the nanowire. Fig. 5.6 shows the influence of the enzyme concentration and the length on the nanowire stability with three different magnetic field intensity values. The more the intensity of the magnetic field, the less fluctuations in the medium, and the more stable is the proposed nanowire.

5.6.5 Fokker-Planck Equation

The one-dimensional Fokker-Planck equation emerges in the biological, chemical and physical sciences as an excellent approximation to the master equations, because of its elegant mathematical properties [Kampen, 2007]. The 1D Fokker-Planck in its general form can be written as [Kampen, 2007]:

$$\frac{\partial u(x,t)}{\partial t} = \Big[-\frac{\partial}{\partial x}A(x,t) + \frac{\partial^2}{\partial x^2}B(x,t) \Big] u, \tag{5.19}$$

where $u(x,t)$ is an unknown function that can represent the probability density in our study. $B(x,t) > 0$ is the diffusion coefficient, and $A(x,t)$ is the drift coefficient, with the following initial condition $u(x,0) = f(x)$, $x \in \mathbb{R}$. To derive the Fokker-Planck equation, we need to discretize the chemical master equation into small jumps. The transition probabilities W in eq. 5.11 change from a state N to a state $N+1$ with a small size jump, and we write [Kampen, 2007]:

$$W(N|N+1) = W(N+1;\delta), \qquad \delta = (N+1) - N, \tag{5.20}$$

where δ represents the distance between two neighboring actin monomers. By replacing the probability $P_i(t)$ with a probability density $p(x_i,t)$, the master equation, then, is written as [Kampen, 2007]:

$$\frac{\partial p(x_i,t)}{\partial t} = \int W(x_i - \delta;\delta)p(x_i - \delta, t)d\delta - p(x_i,t)\int W(x_i;-\delta)d\delta, \tag{5.21}$$

where $x_i = i \times \delta$ is the position of the i^{th} monomer in the actin filament, by assuming that only small jumps occur, we calculate the integral by means of a Tylor expansion up to second order and we write:

$$\frac{\partial p(x,t)}{\partial t} \approx -(k_+N - k_-)\delta\frac{\partial p(x,t)}{\partial x} + \frac{k_+N + k_-}{2}\delta^2\frac{\partial^2 p(x,t)}{\partial x^2}. \tag{5.22}$$

Eq. 5.22 is a special case of the Fokker-Planck equation known as the backward Kolmogorov equation. By comparison with eq. 5.19, we extract the elongation rate coefficient of the actin nanowire $E = (k_+N_0 - k_-)\delta$, and its distribution coefficient $D = \frac{k_+N+k_-}{2}\delta^2$. We note that the variance of the nanowire length is time-dependent; $\sigma^2 = 2Dt$. We use two methods to solve the eq. 5.22: numerically with simulations, and analytically by using the Differential Transform Method (DTM) as in [Hesam *et al.*, 2012]. DTM constructs analytical solutions in the form of polynomials based on the Tylor series expansion. The advantage of this method is that it calculates solutions by means of an iterative procedure, which reduces the computational burden. The differential transform of a function $f(x,y)$, is [Hesam *et al.*, 2012]:

$$F(k,h) = \frac{1}{k!h!}\left[\frac{\partial^{(k+h)}f(x,y)}{\partial x^k \partial y^h}\right]_{(x=x_0,y=y_0)}, \tag{5.23}$$

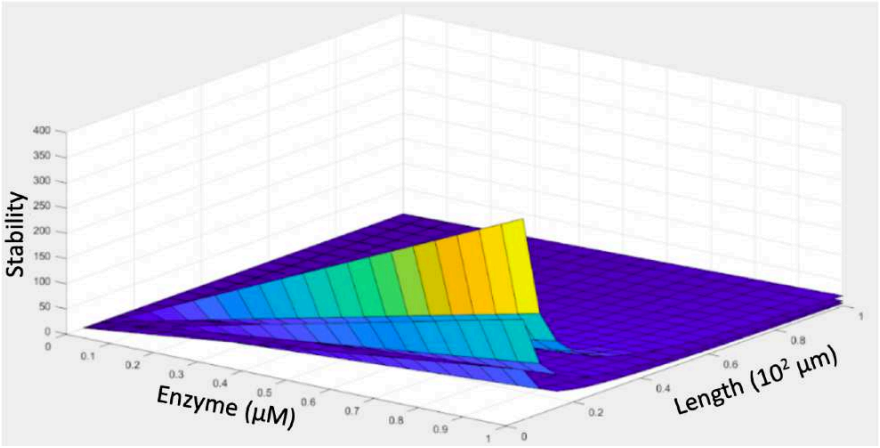

Figure 5.6 Enzyme and length effects on the nanowire stability using three intensity values of the magnetic field [Dambri *et al.*, 2019].

The inverse differential transform function of $F(k,h)$ for finite series is expressed as follows [Hesam *et al.*, 2012]:

$$f(x,y) = \sum_{k}^{n} \sum_{h}^{m} W(k,h) x^k y^h, \tag{5.24}$$

We use the fundamental mathematical operations performed by the equations 5.23 and 5.24, which are presented in Table. 1 in [Hesam *et al.*, 2012]. We determined an exact analytical solution of eq. 5.22, which satisfy the boundary conditions of the channel, where x_0 is the surface of the transmitter, $x = l$ is the surface of the receiver and we write the probability distribution of the actin nanowire as:

$$p(x,t) = \frac{1}{\sqrt{\pi D t}} \exp\left(\frac{(x - x_0 - E)^2}{2Dt}\right). \tag{5.25}$$

where x is the position of monomers along the actin nanowire, E is the elongation rate coefficient and D is the distribution coefficient. We assumed that the initial concentration of the actin monomers N_0 is constant and that their initial distribution $p(x_0, 0)$ is a Gaussian distribution, because of the random movements of actin monomers in the medium. We validated the analytical solution by using PDEPE function in MATLAB to calculate the Fokker-Planck equation numerically.

5.7 Numerical Results

Depending on the phosphorylation state of actin monomers, two types are distinguished; ATP-actin and ADP-actin, and each one of them has different reaction rates. Polymerization and depolymerization rates can also be influenced by other parameters namely; the medium viscosity and enzyme concentration, which explains the diversity of the rates values in the literature. In this study, we ignored the phosphorylation state of actin monomers, and we calculated the average of the reaction rates in the literature for the two monomer types using the viscosity of the human blood. The polymerization and depolymerization rates used in this study are approximated to $k_+ \approx 0.979\ \mu\ \mathrm{M}^{-1}\mathrm{s}^{-1}$ and $k_- \approx 0.166\ \mathrm{s}^{-1}$ respectively. The initial concentration of actin monomers in our simulations is $N_0 = 1000$, and their initial distribution is a Gaussian because of their random movement in the medium. By assuming that the diameter of the transmitter and the receiver is 1 μm and the distance between the surface of the transmitter and the surface of the receiver is 10 μm, we take the boundary conditions as $x_0 = 1\ \mu$m and $x_l = 10\ \mu$m. The diameter of each actin monomer is approximately 5.5 nm [Tuszyński *et al.*, 2004], thus, we take the distance between two neighboring actin monomers as the sum of their diameters namely; $\delta = 11$ nm.

5.7.1 Channel's Dynamics

The actin self-assembly chain reactions are very complex and to study their dynamics, we need to approximate the discrete changes in molecules' number with continuous change in their concentration as shown in Fig. 5.7. The figure compares the analytical, numerical and Monte-Carlo simulation results of the system's differential equations described in eq. 5.3 and 5.4, which represent the change in the actin monomer concentration while the actin nanowire elongates in the medium. We notice that the analytical solution calculated using eq. 5.13 matches the numerical results and Monte-Carlo simulations. The steady states of the actin nanowire polymerization and actin monomer concentration are calculated from eq. 5.12. Fig. 5.7 exhibits the dynamic behavior of the actin monomers in the medium and predicts the time needed for the nanowire to reach its steady state with the chosen initial conditions. Using the results of the derived model helps the user to determine the optimal distance channel for the nano-communication system.

Fig. 5.8 shows the probability density function p(x,t) of the actin nanowire distribution. The numerical evaluation of the Fokker-Planck equation described in 5.22 and shown in Fig. 5.8 is simulated with MATLAB by using the derived coefficients of the diffusion and the elongation rate. We observe that the actin nanowire starts propagating from a position

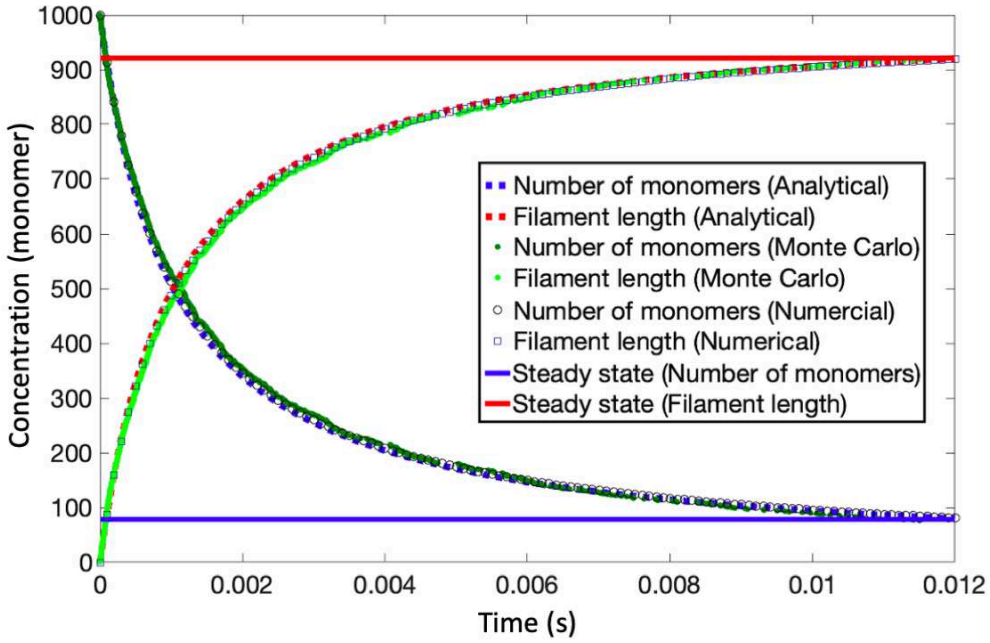

Figure 5.7 Time-varying behavior and steady state of actin nanowire formation.

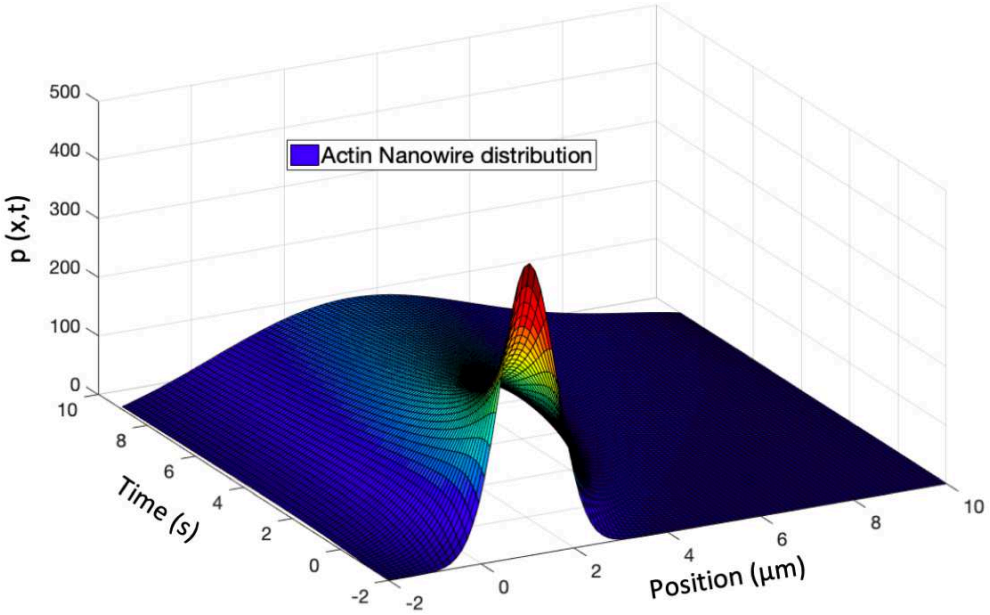

Figure 5.8 Probability density function of the actin nanowire distribution.

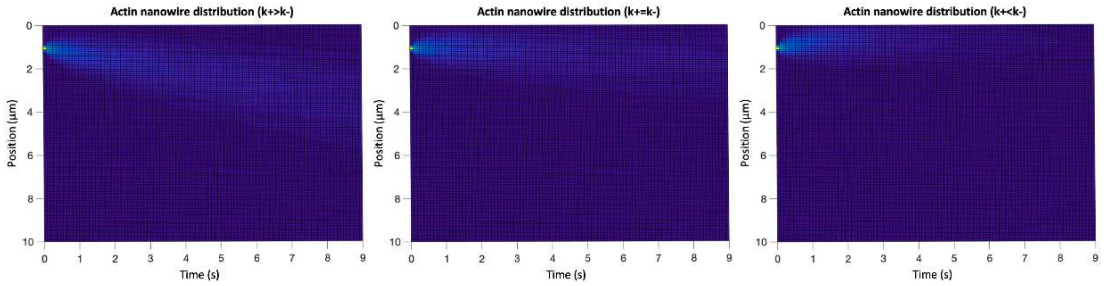

Figure 5.9 The influence of the reaction rates on the actin nanowire distribution in three scenarios, $k_+ > k_-$, $k_+ = k_-$ and $k_+ < k_-$ respectively.

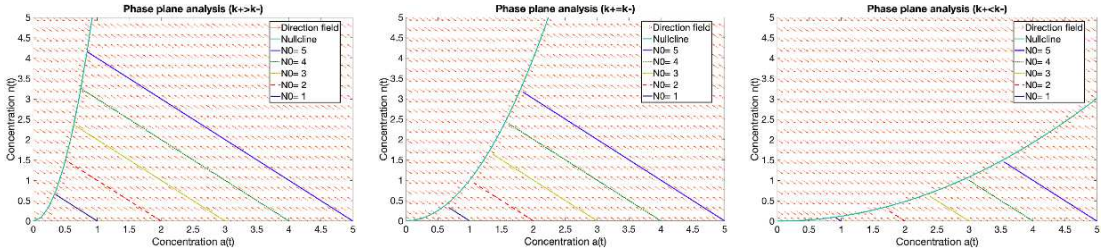

Figure 5.10 Stability analysis of the actin nanowire formation under three scenarios, $k_+ > k_-$, $k_+ = k_-$ and $k_+ < k_-$ respectively.

$x_0 = 1$ μm, where the first monomers are already anchored at the surface of the transmitter. Then, it elongates with a rate smaller than the diffusion coefficient, which explains the actin nanowire slow propagation. Most of the methods in the literature propose the use of the diffusion to propagate the information, whether by using the medium, bacteria or kinetic motors. In this study, we use the diffusion to elongate our proposed actin nanowire. Once it is attached to the receiver, the information is sent through it very rapidly by using electrons.

Actin nanowire formation is greatly influenced by the reaction rates k_+ and k_-, which themselves are influenced by enzyme concentration, viscosity of the medium and magnetic field used to guide the direction of actin assembly. Fig. 5.9 shows the influence of the reaction rates on the actin nanowire distribution in three scenarios, $k_+ > k-$, $k_+ = k_-$ and $k_+ < k_-$. We see that when $k_+ > k-$, the actin distribution is drifted from its initial position, which means that the actin nanowire starts assembling and its length doubled in 5 seconds. In the $k_+ = k_-$ scenario, we notice that the position of the actin distribution does not change with time and stays at the initial position (1 μm). This is explained by the fact that the number of actin monomers added and dissociated from the nanowire are the same, thus, the nanowire does not elongate. The last scenario shows the collapse of the actin nanowire because the number of the dissociated monomers is bigger.

The user of the actin-based nano-communication system can employ the reaction rates as a switch to enable or disable the nanowire formation, which gives more flexibility to the nanonetwork. Actin polymerization can also be inhibited by using cytochalasin enzymes [Fox and Phillips, 1981].

5.7.2 Stability Analysis of the Channel

Fig. 5.10 shows the influence of the reaction rates on the actin nanowire stability. To better analyze the stability of the nanowire, we plotted the concentrations against one another, instead of plotting them as functions of time. The phase plan graph in Fig. 5.10 plots the concentration n(t) of the actin monomers in the medium against the concentration a(t) of the actin monomers constructing the nanowire, in the three scenarios discussed above. To avoid that the phase plan becomes crowded with all possible trajectories, we plotted short arrows to indicate the motion direction, and we plotted five possible trajectories. The direction field is plotted to show the stability points of the proposed channel by using five initial concentrations of the actin monomers. We notice that whatever initial concentration we choose, the system follows the nullcline calculated in eq. 5.15, which represents the equilibrium points of the system. As revealed in the derived nullcline expression, the stability of the channel depends on the reaction rates. The equilibrium points change in each scenario, but the system always follows these points and reaches its steady state.

The stability of the channel depends on other parameters too, as explained in Fig. 5.6. The enzyme concentration, the length of the communication channel and the intensity of the magnetic field also affect the stability of the actin nanowire.

5.7.3 Channel Model Evaluation

The Probability density function of the actin nanowire distribution presented in Fig. 5.8 is dictated by a coin toss, either a molecule is added or dissociated from the nanowire. Depending on the random outcome of this probability, the actin nanowire elongates or collapses as explained by the dynamic behavior study of the proposed channel model. In order to evaluate the channel model, we compare the analytical solution of the Fokker-Planck equation calculated in 5.25 with the numerical simulations of the derived master equation in 5.10 by using Markov-Chain Monte-Carlo (MCMC) method. The comparison is shown in Fig. 5.11, where the nanowire starts distributing from its initial position ($x_0 = 1\ \mu$m) and elongates towards the receiver position ($x_l = 10\ \mu$m) with time. We notice that the calculated analytical solution of the Fokker-Planck equation and the derived master equation simulations match favorably, which validates the proposed channel model. We

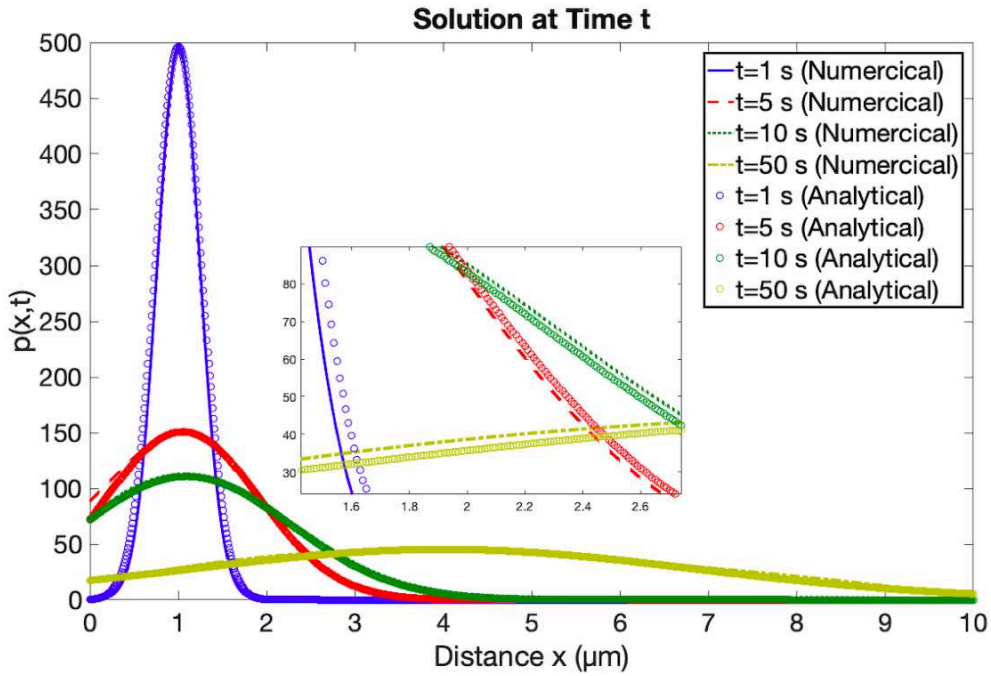

Figure 5.11 Comparison between the analytical solution of the Fokker-Planck equation and the numerical simulations of the channel's master equation.

observe that the nanowire reaches half the communication channel in 50 seconds (x= 5 μm) with the chosen parameters and initial conditions. The amplitude of $p(x,t)$ that represents the actin monomers in the medium decreases with time because monomers are added to the elongated nanowire.

5.8 Conclusion

In this paper we modeled a nano-communication wired channel based on a polymer self-assembly. We studied the dynamic behavior of the channel by deriving the chemical master equation of the polymerization reaction. We formulated the proposed channel construction in two differential equations, we solved them analytically and we validated the solution with numerical and Monte-Carlo simulations. Then, we approximated the master equation by a one-dimensional Fokker-Planck equation and we solved it analytically and numerically. Moreover, we studied the nanowire stability and we derived the expressions of its diffusion coefficient and its elongation rate.

Using the numerical evaluation of the proposed model, we show that the reaction rates of the polymer assembly influence not only its distribution, but also its stability. The study

also shows that the reaction rates can be used as a switch to enable or disable the nanowire formation by using enzymes, giving more flexibility to the polymer-based nanonetworks. In comparison with wireless molecular communication techniques proposed in the literature, the proposed wired polymer-based method promises stable and flexible nanonetworks with a much higher achievable throughput. Moreover, the proposed polymer-based nanonetworks are potentially biocompatible, which makes them a suitable candidate for designing bio-inspired nanonetworks for medical and pharmaceutical applications.

CHAPTER 6

RECEIVER DESIGN FOR WIRED NANO-COMMUNICATION

Auteurs et affiliation:

Oussama Abderrahmane Dambri: étudiant au doctorat, Département de Génie Électrique et de Génie Informatique ,Université de Sherbrooke. INTERLAB Research Laboratory.

Soumaya Cherkaoui: Professeur, Département de Génie Électrique et de Génie Informatique, Université de Sherbrooke. INTERLAB Research Laboratory.

Date de Parution: en cours de révision

Revue: *IEEE Transactions on Communications*

Titre français: Conception et évaluation d'un récepteur pour des Réseaux de nano-communication filaires

Résumé français:

Dans cet article, nous proposons un receveur bio-inspiré, qui détecte les électrons transmis à travers un nanofil, puis convertit les informations détectées en une lumière bleue en utilisant la bioluminescence. L'utilisation de la lumière permet au receveur conçu d'agir également comme un relais pour la passerelle la plus proche (photo-détecteur). Nous simulons la construction du nanofil, présentons ses caractéristiques électriques et calculons son débit maximal pour une meilleure conception du receveur. Le receveur conçu contient deux parties, une partie qui détecte les électrons transmis, que nous modélisons en utilisant un circuit équivalent, et une partie qui convertit les électrons détectés en une lumière bleue. Nous dérivons les expressions analytiques des composants du circuit équivalent, et nous calculons les photons émis pour chaque impulsion électrique détectée. Nous proposons également des techniques de modulation qui garantissent un décodage efficace des informations. Nous envoyons un message binaire et nous suivons le processus de détection d'électrons du receveur proposé jusqu'à l'émission de lumière et nous calculons le taux d'erreur binaire (BER) pour évaluer les performances du receveur conçu. Les résultats de cette étude montrent que le receveur conçu peut détecter avec précision les électrons

envoyés à travers un nanofil conducteur dans les réseaux de nano-communication filaires, et qu'il peut également servir de relais pour la passerelle la plus proche.

6.1 Design and Evaluation of a Receiver for Wired Nano-Communication Networks

6.2 Abstract

In this paper, we propose a bio-inspired receiver, which detects the electrons transmitted through a nanowire, then, it converts the detected information to blue light using bioluminescence. Using light allows the designed receiver to also act as a relay for the nearest gateway (photo-detector). We simulate the construction of the nanowire, present its electrical characteristics and calculate its maximum throughput for a better design of the receiver. The designed receiver contains two parts, a part that detects the transmitted electrons, which we model by using an equivalent circuit, and a part that converts the detected electrons to blue light. We derive the analytical expressions of the equivalent circuit's components, and we calculate the emitted photons for each electrical pulse detected. We also propose modulation techniques that guaranty an effective decoding of the information. We send a binary message and we follow the electron detection process of the proposed receiver until light emission and we calculate the Bit Error Rate (BER) to evaluate the performance of the designed receiver. The results of this study show that the designed receiver can accurately detect the electrons sent through a conductive nanowire in wired nano-communication networks, and that it can also act as a relay for the nearest gateway.

6.3 Introduction

Nanotechnology has become a key area of research in multidisciplinary fields, and its rapid and impressive advance has led to new applications in biomedical and military industries. It turned out that nanomachines need a cooperative behavior to overcome their limited-processing capacities in order to achieve a common objective. Exploiting the potential advantages of nano-communication networks between the nanomachines drove the researchers to come up with new solutions to create systems that communicate at nanoscale. Three methods are proposed in literature, wireless electromagnetic method using the THz band [Akyildiz and Jornet, 2010b; D'Oro *et al.*, 2015; Piro *et al.*, 2015; Yao and Jornet, 2016], bio-inspired wireless molecular communication using molecules [Chang

et al., 2018; Dambri *et al.*, 2019; Dambri and Cherkaoui, 2019; Farsad *et al.*, 2016; Kim *et al.*, 2014; Koo *et al.*, 2016; Noel *et al.*, 2014; Pierobon and Akyildiz, 2010; Tepekule *et al.*, 2015b] and wired nano-communication method using polymers [Dambri *et al.*, 2019].

However, on the one hand, THz band suffers from a very high path loss, mainly caused by water molecules absorption, which complicates its use in medical applications inside the human body [D'Oro *et al.*, 2015; Piro *et al.*, 2015; Yao and Jornet, 2016]. On the other hand, molecular communication biocompatibility makes it very promising for medical applications at nanoscale, such as monitoring, diagnosis and local drug delivery [Farsad *et al.*, 2016]. Nevertheless, the achievable throughput of molecular communication systems is very limited and the delay is very high due to the random distribution of molecules in the medium [Dambri *et al.*, 2019; Kim *et al.*, 2014; Koo *et al.*, 2016; Pierobon and Akyildiz, 2010]. Moreover, molecular communication systems suffer from intersymbol interference, despite the proposed techniques in literature to reduce it [Chang *et al.*, 2018; Dambri and Cherkaoui, 2018, 2019; Noel *et al.*, 2014; Tepekule *et al.*, 2015b].

Wired nano-communication is a new proposed method that uses the self-assembly ability of some polymers inside living cells to build an electrically conductive nanowire [Dambri *et al.*, 2019]. This method has the biocompatibility of molecular communication, but also, it has a very high achievable throughput since fast electrons are the carriers of information. One of the main challenges of the wired nano-communication system is detecting the electrons at the receiver without losing its biocompatibility. The proposed receivers in the literature for molecular communication are designed to observe or absorb molecules in the medium [Bao *et al.*, 2019; Kilinc and Akan, 2013; Noel *et al.*, 2016; Qian *et al.*, 2019], and thus, they cannot be used to detect electrons for wired nano-communication.

In our recent works [Dambri and Cherkaoui, 2020a; Dambri *et al.*, 2019], we proposed the idea of a receiver for a wired nano-communication system without studying or evaluating it. In this paper, we present the detailed system model of the proposed receiver, and we evaluate its performance. The proposed receiver contains a Smooth Endoplasmic Reticulum (SER), which plays the role of Ca^{2+} storage inside living cells [Koch, 1990]. The receiver also contains a recyclable concentration of a photo-protein *Aequorin*, which can be found in the jellyfish *Aequorea Victoria* that lives in North America and the Pacific Ocean [Shimomura, 1995]. The electron detection at nanoscale is extremely difficult due to the quantum trade-off between information and uncertainty. Therefore, the designed receiver uses the transmitted electrons to stimulate SER and trigger a chemical reaction that generates a bioluminescent light by using the photo-protein Aequorin, as shown in Fig. 6.1. In order to study SER stimulation with the transmitted electrons, we simulated the con-

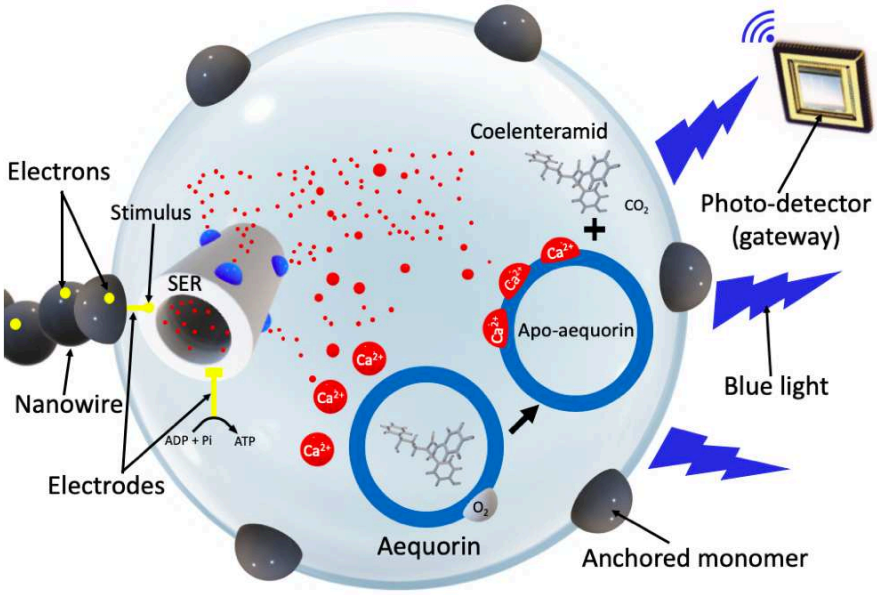

Figure 6.1 The designed receiver for wired nano-communication networks.

ductive nanowire used in wired nano-communication systems, we presented its electrical characteristics and we calculated its maximum throughput. Bioluminescence is a chemical reaction used by living organisms to generate light with enzymes and photo-proteins. Converting the transmitted electron pulses into light pulses at the receiver makes the extraction of information easier and can create a link between nanoscale and macroscale communication systems.

The rest of the paper is organized as follows. In section II, we present and explain the 2 algorithms used in our framework to simulate the nanowire's assembly in a stochastic 3D system. We also present the electrical characteristics of the nanowire and we calculate its maximum throughput and the error probability. Section III highlights an in-depth description of the designed receiver, by clarifying the SER role in electron detection, and by explaining the triggered chemical reaction that emits a blue light. In section IV, we model the designed receiver by using an equivalent circuit, where SER and its membrane represent a capacitor and the sum of Ca^{2+} channels represent a resistance linked in parallel. We derive the analytical expression of the circuit components and we calculate the emitted photons for each electron pulse detected. We also calculate the Bit Error Rate (BER) of the designed receiver. In section V, we propose modulation techniques that guaranty an effective decoding of the detected information at the designed receiver. Section VI discusses the numerical results of this study, by following the detection process of a random binary message at the receiver until its conversionto blue light. It also presents the results of BER

to evaluate the performance of the designed receiver. We conclude the paper in section VII.

6.4 Simulation Framework

GlowScript VPython is an easy and efficient way to create 3D environments for real time simulations. Our framework applies GlowScript as a browser-based implementation that runs a VPython program by using RapydScript, which is a Python-to-JavaScript compiler. In this study, we simulate the self-assembly of a polymer called "actin" to create a nanowire in real time, by using sphere molecules that diffuse randomly in a 3D cube as shown in Fig. 6.2. By using this framework, we can follow the position of the last assembled molecule in real time to study the speed of the nanowire's construction as the graph in Fig. 6.3 exhibits. In the next subsections, we present and explain the two algorithms that we used in our framework.

6.4.1 Collision Between Actin Molecules

The algorithm 6.1 is a combination of two strategies, Periodic Interference Test (PIT) and a Predicted Instant of Collision (PIC). The (PIT) consists of checking to detect if any collision has occurred between two molecules, at every frame in the simulation. It tests if the molecules are approaching each other, and whether they interfere spatially. When a collision is detected, the algorithm computes the new velocities after the shock using the momentum and energy conservation equations; and then attributes the new velocity to the moving molecules after the collision. If the simulation detects no collision in that frame, it continues to the next one. The PIC, on the other hand, pre-calculates the exact time of collisions before spatial interactions between the molecules. The difference between PIT and PIC approaches is that the later perfectly models the collisions, at the cost of some extra computation, compared to the PIT approach, which is a lazy collision detection strategy. In our algorithm 1, we used a combination of the two approaches to perfectly detect and model the collisions in real time.

6.4.2 Nanowire Formation

If a random molecule in the environment strikes the last molecule of the constructed nanowire, it will attach to it increasing the length of the nanowire. Several conditions are necessary for the molecules to stick in the nanowire, namely:

– One of the molecules having a collision is already sticking in the nanowire.

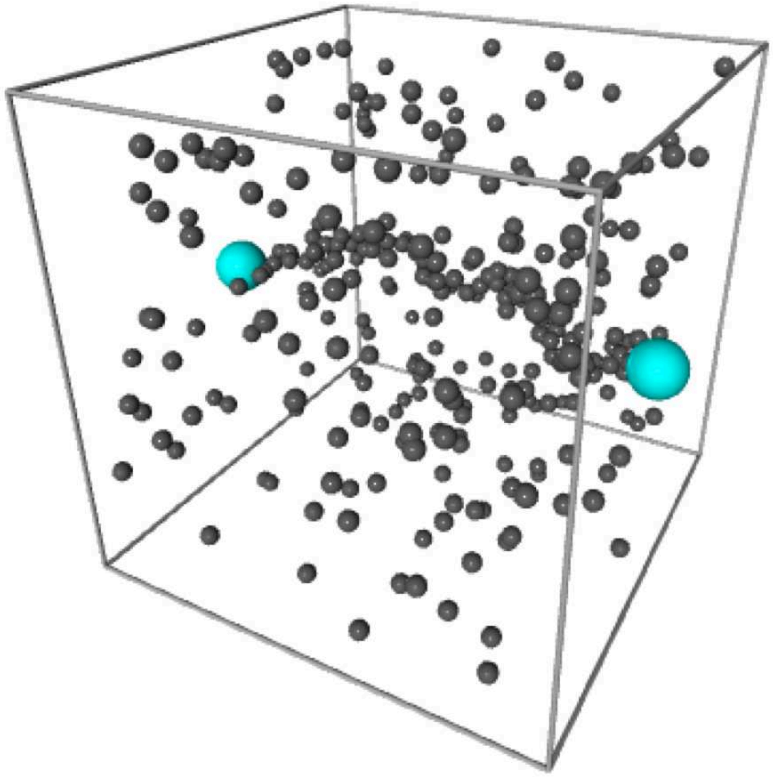

Figure 6.2 Actin-based nanowire formation represented by small black spheres, which link the transmitter to the receiver (cyan spheres).

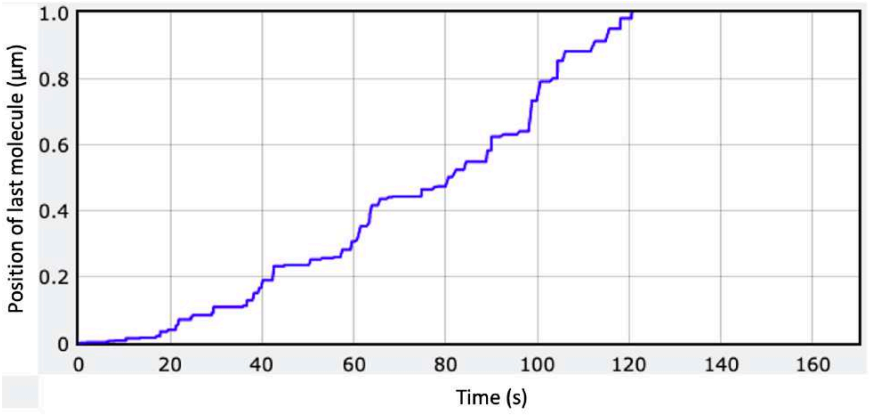

Figure 6.3 Position of the last assembled molecule as a function of time representing the speed of the nanowire formation.

Algorithm 3 Periodic Interference Test

```
1: procedure PITC( Molecule A, Molecule B ):
2:     At every frame instant t:
3:     Test if the two molecules are approaching each other.
4:     if YES then
5:         Test if they overlap (interfere) spatially.
6:         if YES then
7:             Collision detected.
8:             Compute New Velocities.
9:             T:= time of collision between A and B.
10:            if T < next frame instant: then
11:                Move frame to intermediate instant T.
12:                Calculate velocities after collision.
13:            end if
14:        else
15:            No collision detected.
16:        end if
17:        Goto next frame instant.
18:    else:
19:        Goto next frame instant.
20:    end if
21: end procedure
```

- The center of the striking molecule lies within a specified angle range from the center of the last attached molecule.
- The center of the next molecule being attached should be farther away from the transmitter and closer to the receiver, so that the nanowire is moving towards the receiver and not towards any random path.

To make the molecules stick, we give their momentum a zero value, and we do not update their position with time. The algorithm 6.2 also regulates the direction of the nanowire formation. The direction is controlled by the magnetic field. If the magnetic field is zero, then there is no guide for the direction, and the nanowire forms randomly. As the magnetic field increases, the nanowire gets more and more aligned to the straight line joining the transmitter and the receiver, as confirmed by the experimental results in [Kaur *et al.*, 2010].

6.4.3 Channel's Electrical Characteristics

The authors in [Hunley *et al.*, 2018] and [Tuszyński *et al.*, 2004] studied the electrical impulses and ionic waves propagating along actin filaments in both intracellular and in

Algorithm 4 Nanowire Formation

```
molecule_array = [Transmitter]
if collision.detected = True then
    if collision occurs with last(molecule_array) && last(molecule_array) != Receiver then
        M ← molecule hitting the wire
        if Magnetic Field = 0 then
            Randomly attach M to last(molecule_array)
            molecule_array.append(M)
        end if
        if Magnetic Field != 0 then
            if M.center.X > max(last(molecule_array) .position) then
                Z = function(magnetic field)
                if M.center.Z < max(Z) then
                    M.momentum = 0 % Stick the two molecules together
                    molecule_array.append(M)
                end if
            end if
        end if
    end if
end if
```

vitro conditions, by modeling the actin filament as an RLC equivalent circuit. The effective resistance, inductance and capacitance for a $1\mu m$ actin filament are [Tuszyński *et al.*, 2004]:

$$C_{eq} = 0.02 \times 10^{-12} \text{ F}$$

$$L_{eq} = 340 \times 10^{-12} \text{ H}$$

$$R_{eq} = 1.2 \times 10^{9} \Omega$$

The Fig. 6.4 represents actin nanowire's electrical characteristics simulated in our recent work [Dambri and Cherkaoui, 2020b], in terms of attenuation, phase and delay as a function of the frequency and the distance between the transmitter and the receiver. We can see that the attenuation of actin filaments is very high because of its resistance. The experimental study in [Hunley *et al.*, 2018] showed that despite the actin filaments attenuation, the velocity of the charges passing through it can reach $30{,}000\mu m/s$ and then slows down rapidly in the first 60 μs. Moreover, the authors in [Patolsky *et al.*, 2004] proved experimentally that adding gold nanoparticles to the actin monomers drastically decreases its attenuation.

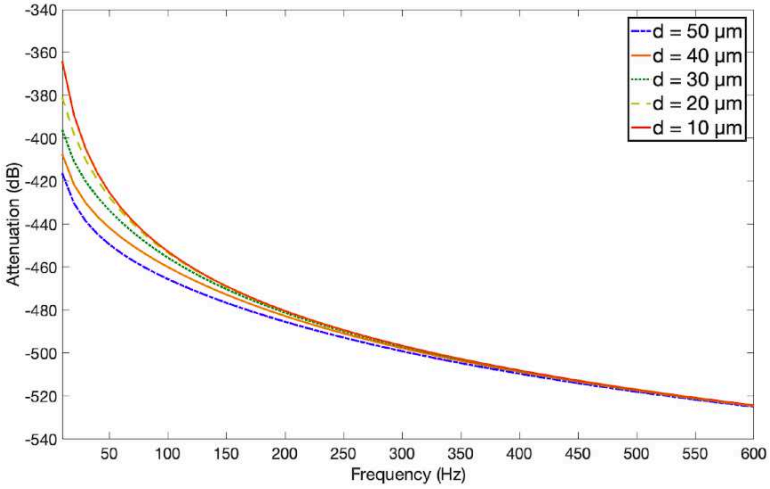

Figure 6.4 The electrical characteristics of actin nanowires in terms of attenuation as a function of the frequency and the channel distance.

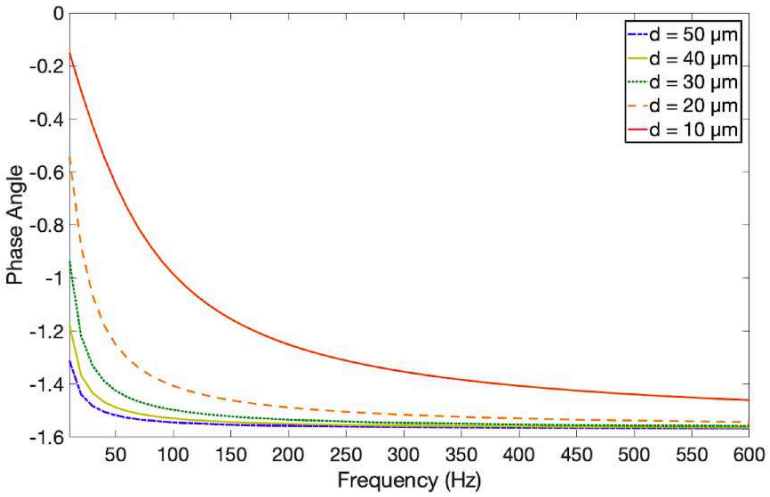

Figure 6.5 The electrical characteristics of actin nanowires in terms of phase as a function of the frequency and the channel distance.

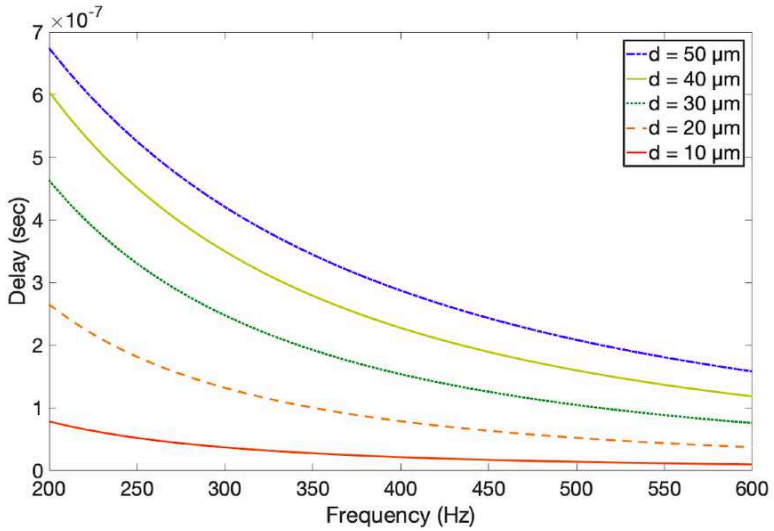

Figure 6.6 The electrical characteristics of actin nanowires in terms of delay as a function of the frequency and the channel distance.

6.4.4 Channel's Maximum Throughput

The charge capacity of each actin monomer is $\sim 4e$ [Tuszyński *et al.*, 2004], and by assuming 370 monomers/μs of an actin filament, we can deduce that the charge capacity of an actin filament 1 μm long is approximately $1480e$. By assuming that 1 e represents 1 bit of information, the maximum throughput is calculated by multiplying the total charge capacity of 1 μs actin nanowire by the speed of the charges propagation through it and we write [Dambri and Cherkaoui, 2020b]:

$$T_M(t) = v(t) \times \psi_{tot}. \tag{6.1}$$

where $T_M(t)$ represents the nanowire achievable throughput, $v(t)$ is the charge's propagation speed calculated in [Hunley *et al.*, 2018] and ψ_{tot} is the total charge capacity of 1 μs actin nanowire. Fig. 6.5 shows the maximum throughput approximation of the proposed nanowire. The decrease of the achievable throughput over time is due to the high attenuation of the actin filaments. However, despite this decrease, and to the best of our knowledge, the throughout is still very high compared to molecular communication results proposed in the literature so far.

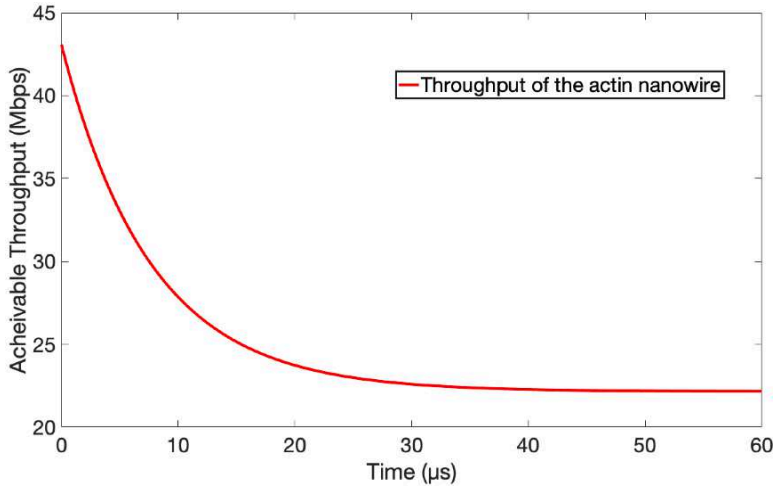

Figure 6.7 Maximum throughput approximation of the actin nanowire.

6.4.5 Error Probability

The error probability of the proposed polymer-based channel for wired nano-communication systems can be written as:

$$P_e = p_0 P_{\epsilon 0} + p_1 P_{\epsilon 1}, \tag{6.2}$$

Where $p_0 = p_1 = 0.5$ are the a priori probabilities, $P_{\epsilon 0}$ is the probability of error for a bit '0' and $P_{\epsilon 1}$ is the probability of error for a bit '1'. The constant assembly and disassembly of actin monomers to construct the actin nanowire generates a noise, which we modeled as a normal distribution. The error is more probable in bit '0' than in bit '1', because the assembly of the nanowire is more frequent than the disassembly. So, the distribution of bit '1' is skewed left compared to the distribution of bit '0', which remains Gaussian and we write [Dambri *et al.*, 2019]:

$$P_{\epsilon 0} = \frac{1}{\sqrt{2\pi}} \exp\left(\frac{-x^2}{2}\right), \tag{6.3}$$

$$P_{\epsilon 1} = \frac{1}{\sqrt{2\pi}} \exp\left(\frac{-(x-A)^2}{2}\right) \operatorname{erfc}\left(\frac{x-A}{\sqrt{2}}\right), \tag{6.4}$$

Where A is the skewness coefficient of the distribution. By substituting (6.3) and (6.4) in (6.2), we write the probability as:

$$P_e = \frac{1}{2\sqrt{2\pi}}\left[\exp\left(\frac{-(x-A)^2}{2}\right)\operatorname{erfc}\left(\frac{x-A}{\sqrt{2}}\right) + \exp\left(\frac{-x^2}{2}\right)\right]. \tag{6.5}$$

Since the distribution is negatively skewed, A is also negative. For a skew normal distribution for which the scale factor is 1, the variance is given by $1 - \frac{2\delta^2}{\pi}$, where $\delta = \frac{A}{\sqrt{1+A^2}}$.

6.5 Receiver Design

From chlorophyll pigments in plants to the neural system in human brains, biological systems always use chemical means to detect and send electrons in the medium. Inspired by muscle fiber contraction and relaxation process, we propose in this paper a receiver design for wired nano-communication networks, which uses SER to detect transmitted electrons through a nanowire. To avoid the absorption of electrons by the receiver's surface, it can be constructed with a hybrid phospholipid/alkanethiol bilayers membrane proposed in [Plant *et al.*, 1994], because of its insulating nature, in order to minimize the loss of electrons at the receiver. The nucleation of monomers that trigger the formation of the actin self-assembly can be tethered at the bio-engineered membrane of the receiver by using a polyethylene glycol (PEG) on one end and an electrode on the other end [Hoiles *et al.*, 2018]. The insertion of the monomer can be spontaneous, electrochemical or with a proteoliposome insertion as explained in [Hoiles *et al.*, 2018] with details. When the assembled nanowire reaches the receiver, it binds to one of the monomers already anchored to the receiver's membrane with electrodes, which creates a passage of electrons through the insulating membrane. As shown in Fig. 6.1, the designed receiver contains SER that stocks Ca^{2+} ions and a photo-protein that emits a blue light in the presence of Ca^{2+} ions. The emitted light is detected by a photo-detector (gateway).

6.5.1 Electrons Detection

The Ca^{2+} ion distribution is used in one of the most important biological signaling between living cells, among other functions such as hormone regulation, muscles contraction and neurons excitation [Brini *et al.*, 2013]. The concentration of Ca^{2+} ions inside the cells must be regulated all the time using a very complex system, where SER plays the role of Ca^{2+} ions storage. The smooth endoplasmic reticulum, also called "sarcoplasmic reticulum" in muscle cells, is a tubular structure organelle found in most living cells. The capacity of SER at stocking Ca^{2+} ions is huge because of a buffer called "calsequestrin" that can bind to

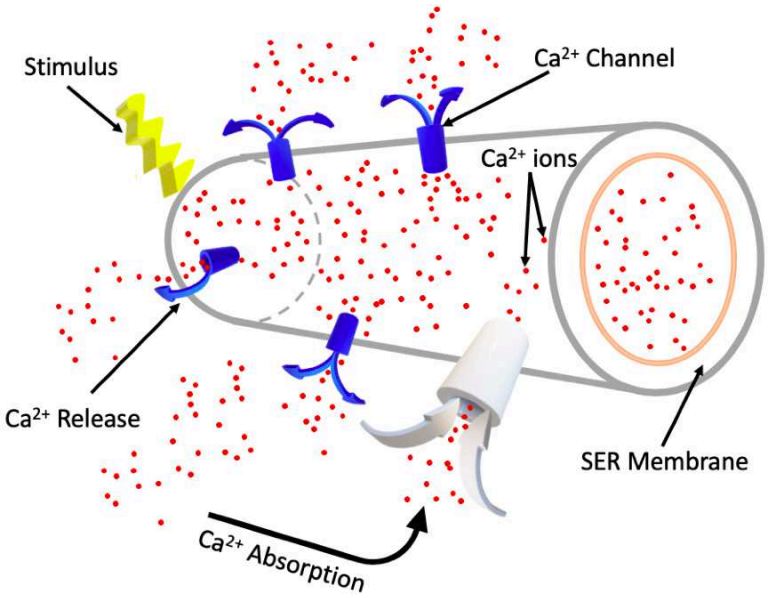

Figure 6.8 Ca^{2+} ions release by a Smooth Endoplasmic Reticulum (SER).

around 50 Ca^{2+}, which decreases the amount of free Ca^{2+} inside SER, and therefore, more calcium can be stored [MD, 2010]. When SER is stimulated with an electrical stimulus, the calcium channels open and Ca^{2+} ions get released so fast inside the cells as shown in Fig. 6.6. The Ca^{2+} concentration is so small inside the cells that a tiny increase in their concentration is detected.

The SER inside the designed receiver is linked to the nanowire with an electrode so that the transmitted electrons can stimulate the SER, which increases its membrane voltage and open calcium channels. The number of opened calcium channels, and thus, the released concentration of Ca^{2+} is proportional to the intensity of the electrical current stimulating the SER. A small electrical current in the order of picoampere (pA) is sufficient to stimulate SER and release a micromole (μM) of Ca^{2+}[Du *et al.*, 2009]. When the electrical current stops, calcium channels close and the Ca^{2+} ions will be absorbed and stocked again inside the SER. The short-time presence of Ca^{2+} ions inside the receiver triggers the bioluminescent chemical reaction, which emits a blue light.

6.5.2 Light Emission

Photo-proteins are priceless biochemical tools for a variety of fields including drug discovery, protein dynamic studies and gene expression analysis. *Aequorin* is a very important photo-protein for biological studies because it helps researchers measure and study the Ca^{2+} distribution in vivo. Upon binding to Ca^{2+} ions, the oxidation of *Aequorin* molecule

is triggered, resulting in the emission of a bioluminescent blue light (470 nm). There are other photo-proteins in nature with different wavelengths emissions such as *Luciferin* (530 nm) and some chromophores (630 nm). However, unlike other bioluminescent reactions that involve the oxidation of an organic substrate such as *Luciferin* and chromophores, adding molecular oxygen is not required in Ca^{2+}-dependent light emissions, because *Aequorin* protein has oxygen bound to it [Weeks *et al.*, 2013]. Other advantages of using *Aequorin* are that it does not involve any diffusible organic factor, no direct participation of enzymes and that it can be recycled after use [Shimomura and Johnson, n. d.]. *Aequorin* is extracted from the jellyfish *Aequorea Victoria* that lives in North America and the Pacific Ocean [Shimomura, 1995], and then purified in distilled water. This photo-protein is very sensitive to changes in the concentration of free Ca^{2+}, which explains its extensive use as an indicator of Ca^{2+} ions in biological studies. In the presence of a very low concentration of Ca^{2+}, the light intensity emitted by *Aequorin* will be independent from Ca^{2+} concentration, the bioluminescent reaction becomes Ca^{2+}-dependent only when the concentration exceeds 10^{-7} M.

The designed receiver uses the short-time presence of the released Ca^{2+} ions to trigger the oxidation of Aequorin, which emits a photon for each 3 Ca^{2+} ions bound, as shown in Fig. 6.7. This mechanism of emitting-light can trigger the release of over 70 kcal of energy as a visible radiation through a single transition [Shimomura and Johnson, n. d.]. In the next section, we model the electron detector as an RC circuit, and we calculate the radiant energy emitted from the bioluminescent reaction at each symbol interval.

6.6 Receiver Model

Cell membranes are biological structures that surround cells and separate their interior from the external environment for the protection and control of ion exchanges. The mem-

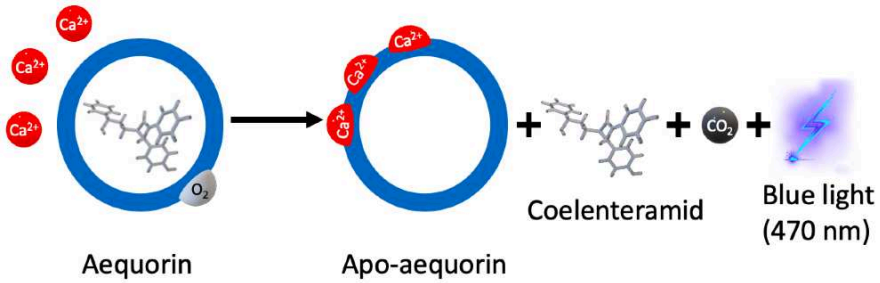

Figure 6.9 Aequorin bioluminescent reaction that generates blue light in the presence of Ca^{2+} ions.

brane is constructed with phospholipid molecules, where the lipid end is hydrophobic and the phosphate end is hydrophilic. When lipid ends get together to form a double-layered sheet and close the sphere, they create a spherical surface that perfectly separates two volumes of liquid. However, a pure phospholipid bilayer is an excellent insulator which does not allow any ion exchange, thus, other pores penetrating the membrane are necessary, allowing the ions to circulate inside and outside the cell. These pores are called "ion channels" and by controlling their opening and closing, the cell controls the ions flow. Cell membranes have specific channels for each ion type, and closing them creates a difference between the ion's concentration inside and outside the cell, which set up a specific potential for each ion type.

Let's consider V_i the reversal potential of ion species i, which is the value of the membrane potential for which the flux of ion species i is zero, and let's consider R_i the channel resistance, which is simply the inverse of channel's conductance. According to Ohm's law, the ions flow across the channel is proportional to the reversal potential, and the proportionality factor is the channel conductance g_i and we can write:

$$I_i = \frac{V_i}{R_i} = g_i V_i, \tag{6.6}$$

where I_i is the current of ion species i that flows across the membrane. The current flows until reaches an equilibrium called the resting potential V_0, which can be calculated as:

$$V_0 = \frac{\sum_i g_i V_i}{\sum_i g_i}, \tag{6.7}$$

In our case, the membrane has only specific channels for Ca^{2+} ions, therefore, g_i becomes g_{Ca} and V_i becomes V_{Ca}. The reversal potential V_{Ca} is calculated by using Nernst equation as:

$$V_{Ca} = \frac{kT}{ze} \ln \frac{P_{out}}{P_{in}}, \tag{6.8}$$

where k is the Boltzmann constant, e is the electron charge, T is the temperature in Kelvin, z is the valence of the Ca^{2+} ion, P_{out} and P_{in} are the probabilities of finding a Ca^{2+} ion outside or inside the SER respectively. When the membrane is at rest, V_{Ca} equals V_0, however, when an external potential is applied, V_{Ca} increases which opens the Ca^{2+} channels and discharges SER from Ca^{2+} ions. When the excitation is passed, special pores called pumps charges SER again with Ca^{2+} ions. The charge and discharge of SER

can be modeled as an equivalent capacitance and the inverse of the channel conductance can be modeled as an equivalent resistance in series with a voltage source. Therefore, the SER and its membrane can be modeled as an equivalent RC circuit as shown in Fig. 6.8.

6.6.1 The Capacitance

The SER membrane separates two conductive liquids that contain free ions, so we have two conductors separated by an insulator. The potential difference across the membrane that separates a charge of a Ca^{2+} ion Q_{Ca} defines a capacitance C_{Ca} that can be written as:

$$C_{Ca} = \frac{Q_{Ca}}{\mid \Delta V_{Ca} \mid}, \tag{6.9}$$

Before calculating the potential difference ΔV_{Ca} by using the Gauss's law, we define the permittivity ε of the membrane as $\varepsilon = \varepsilon_0 \varepsilon_r$, where ε_r is the relative permittivity. SER in muscle cells is composed of tubule networks called cisternae, which they have a diameter $r_{SER} = 50nm$. The SER tubules extend throughout muscle fiber filaments, so we assume that the length of SER tubules used in our designed receiver is $l = 1\mu m$. By assuming that the enclosed charge within SER's volume is Q_{Ca}, then from Gauss's law we can write the electric field at a distance r as:

$$\vec{E}_{Ca} = \frac{Q_{Ca}}{\varepsilon}\left(\frac{1}{2\pi l r}\right)\hat{r}. \tag{6.10}$$

where $\hat{r}$ is the radial vector from the Ca^{2+} charge at the origin of SER tubules to the surface of the membrane. The potential difference between the inside and the outside of SER membrane is therefore written as:

$$\Delta V_{Ca} = -\int_{r_{SER}}^{r_{SER}+\delta} E_{Ca}.dr = -\frac{Q_{Ca}}{2\pi l r}\ln\left(1 + \frac{\delta}{r_{SER}}\right), \tag{6.11}$$

where δ is the thickness of the membrane. By substituting eq. 6.11 in eq. 6.9 we find:

$$C_{Ca} = \frac{2\pi l r}{\ln\left(1 + \frac{\delta}{r_{SER}}\right)}. \tag{6.12}$$

The membrane of SER does not need a high voltage to separate charges because it is only two molecules thick ($\delta = 6\times10^{-9}m$), thus, we expect the membrane capacitance to be quite high per unit area. With the parameters given above, we estimate that the capacitance is

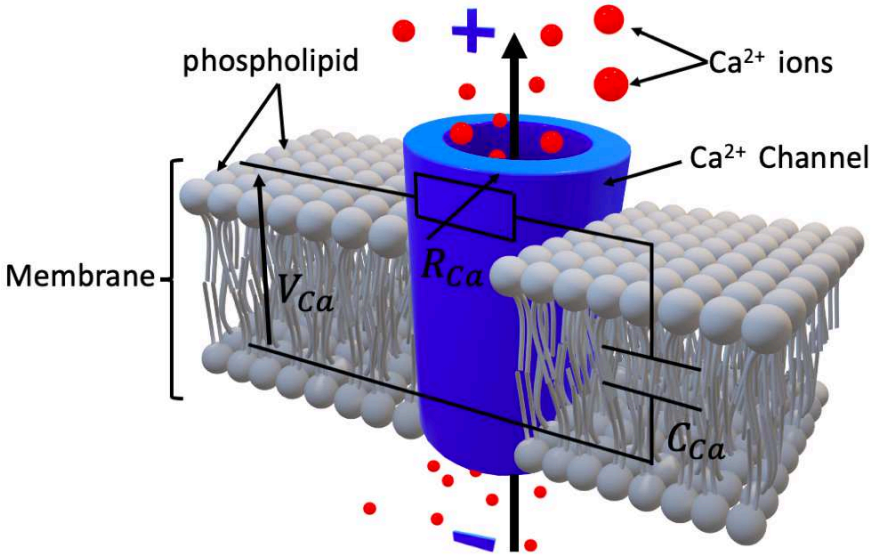

Figure 6.10 The proposed equivalent RC circuit of SER's membrane.

$C_{Ca} \simeq 5 \times 10^{-6} pF/\mu m^2$. Unlike the conductance, the capacitance of biological membranes is not influenced by the complexities of biological systems, which makes it constant.

6.6.2 The Resistance

The pure phospholipid bilayer constructing the membrane is an excellent electrical insulator with a very low conductance, but the mosaic proteins that span the surface of the membrane act as channels for ions and increase the conductance. The Ca^{2+} current flowing through SER membrane depends on the number of open channels by the applied external voltage. Depending on the type and the age of SER, the number of channels varies between 3.8 and 24.3 per μm^2 area [Orchard and Brette, n. d.]. By taking into account the infinitesimal area of channels, we consider the SER membrane as an infinite charged linear line and by using Gauss's law we can write the Ca^{2+} current I_{Ca} of one channel as:

$$I_{Ca} = \sigma \int E_{Ca}.da = \sigma \frac{\lambda l}{\varepsilon}, \tag{6.13}$$

where σ is the conductivity of one Ca^{2+} channel and $\lambda = Q_{Ca}/l$. From eq. 6.6 we can calculate the resistance of Ca^{2+} channels R_{Ca}:

$$R_{Ca} = \frac{V_{Ca}}{I_{Ca}}, \tag{6.14}$$

and by substituting eq. 6.11 and eq. 6.13 in eq. 6.14 we find:

$$R_{Ca} = \frac{\ln\left(1 + \frac{\delta}{r_{SER}}\right)}{2\pi n \sigma l}. \tag{6.15}$$

where n is the number of Ca^{2+} channels. R_{Ca} is the sum of n variable resistances linked in parallel in our equivalent circuit. The conductivity of a Ca^{2+} channel is estimated to be $\sigma = 0.5pS$ [Krishtal *et al.*, 1981], and thus, the mean value of the variable resistance in eq. 6.14 can be approximated to $R_{Ca} \simeq 6.11M\Omega$. The membrane resistance is highly variable because it is so thin that a very small change in the voltage can create a strong electric field within it.

6.6.3 Radiant Energy

The presence of Ca^{2+} ions near the photo-protein Aequorin triggers a bioluminescent reaction that emits a blue light. We assume that Ca^{2+} ions and *Aequorin* molecules have homogenous distributions inside the receiver and that for each 3 Ca^{2+} ions released outside SER, there is an *Aequorin* molecule that binds to them and emits one photon. Radiant energy is electromagnetic energy carried by a stream of photons, thus, the sum of photons emitted by the bioluminescent reaction represents the radiant energy of the designed receiver. With the assumptions we made above, we calculate the radiant energy of the designed receiver for each symbol interval as follows:

$$Q_e = \frac{1}{3}\frac{hc}{\lambda}\int_0^T p.c(t)dt, \tag{6.16}$$

where h is the Planck constant, c is the speed of light, λ is the photon wavelength. T is the symbol time, and p is the probability for each *Aequorin* molecule to emit a photon. In this paper, the concentration of the released Ca^{2+} ions for each symbol interval $c(t)$ is obtained numerically by using Simulink in MATLAB, which represents the output of the capacitor in the proposed equivalent circuit. An analytical expression for the released Ca^{2+} ion concentration will be derived in our future work.

6.7 Modulation Techniques

The process of encoding information by varying one or more properties of the carrier signal is called modulation. A variety of modulation techniques have been proposed for molecular communications networks by changing the concentration of molecules, molecules type or the time of the molecules release [Farsad *et al.*, 2016].

The first proposed method is the Concentration Shift Keying (CSK) where a bit is decoded at the receiver as "1" if the molecules concentration reaches a predefined threshold at a symbol interval, otherwise it is a "0" [Kuran *et al.*, 2012]. Molecular Shift Keying (MoSK) is another modulation method proposed by the same authors that uses 2^n molecule types to transmit n bits of information [Kuran *et al.*, 2012]. In [Garralda *et al.*, 2011], the authors proposed Pulse Position Modulation (PPM) that encodes the information by changing the time of molecules release. They divided the symbol interval into two equal halves, and the receiver decodes the bit as "1" if the pulse is in the first half, and as "0" if the pulse is in the second half. However, the modulation techniques proposed for molecular communication cannot be used for wired nano-communication networks, which they use electrons as carriers of information instead of molecules. Therefore in this paper, we propose a new modulation technique for wired nano-communication networks that encodes the information by changing the intensity of the bioluminescent light, the time between two consecutive light emissions or a combination between the intensity and the time changes. We call these methods Bioluminescence Intensity Shift Keying (BISK), Bioluminescence Time Shif Keying (BTSK) and Bioluminescence Asynchronous Shift Keying (BASK) consecutively.

6.7.1 Bioluminescence Intensity Shift Keying (BISK)

The total emitted light capacity of the designed receiver is proportional to the released Ca^{2+} concentration and the amount of recycled *Aequorin* for each symbol interval, which is proportional to the pulsed electrical intensity transmitted through the nanowire. Therefore, we can modulate the transmitted information by varying the intensity of the bioluminescent light emitted at the receiver. The change in the intensity is detected at the gateway, where an appropriate threshold is used to extract the information sent through the nanowire. A bit is decoded as "1" if the blue light intensity Q_e in eq. 16 exceeds a threshold ξ, and as "0" otherwise.

The proposed BISK modulation technique has the advantage of reducing the Inter-Symbol Interference (ISI), which is caused by the remaining molecules from a previous symbol. Even if some Ca^{2+} ions remain in the medium causing the emission of some photons, the intensity of light is still low, and we just need a photo-detector with high resolution at the gateway to eliminate the influence of ISI on the receiver.

6.7.2 Bioluminescence Time Shift Keying (BTSK)

As in PPM modulation technique proposed in [Garralda *et al.*, 2011], we can divide our symbol interval into two equal halves. The bit is decoded as "1" if the bioluminescent light is detected in the first half, and as "0" if it is detected in the second half. This method can be a little bit slower than BISK, because detecting small changes in the light intensity is much faster than waiting a hole symbol to decode one bit. However, BTSK can be more efficient in terms of bit error rate, especially when the majority of bits have the same value "1" or "0".

6.7.3 Bioluminescence Asynchronous Shift Keying (BASK)

Another technique that we propose is a hybrid modulation scheme based on a combination between BISK and BTSK. This modulation technique is asynchronous, and it can achieve a higher information rate than the intensity-based and time-based approaches separately. By using $2^k - 1$ threshold levels, BASK can use k bits with 2^k different values to represent one symbol, which increases the number of bits per symbol and thus increases the information rate. Then $k = 2$ when we encode one bit in the intensity chance and another bit in the time change. Therefore, by using the classical modulation naming convention based on the number of bits per symbol, BASK modulation technique can be called Quadruple BASK (QBASK) when $k = 2$.

In this paper we focus on Bioluminescence Intensity Shift Keying (BISK) modulation technique. The other two proposed modulation techniques will be covered in our future work.

6.7.4 Bits Decoding

Since the emission of a bioluminescent light depends on photo-proteins reacting with the Ca^{2+} ions released inside the receiver which exhibit Brownian motion, a single photon has a certain probability P_{em} of being emitted and detected at the gateway. This probability $p = P_{em}(r, t_b)$ defined in eq. 6.16 depends on the number of the recycled photo-protein per symbol interval r and the bit duration t_b. Because of the huge number of Ca^{2+} ions released by SER in each bit duration, we can safely assume that each recycled photo-protein can react with three Ca^{2+} ions at the same time. Thus, the reaction explained in Fig. 6.7 is considered as a single event instead of three separate events, whether the photo-protein is activated to emit a photon or not. We also assume that both Ca^{2+} ions and photo-proteins are uniformly distributed inside the receiver and that the bioluminescent reaction happens instantaneously. Based on the assumptions discussed above, if c ions are

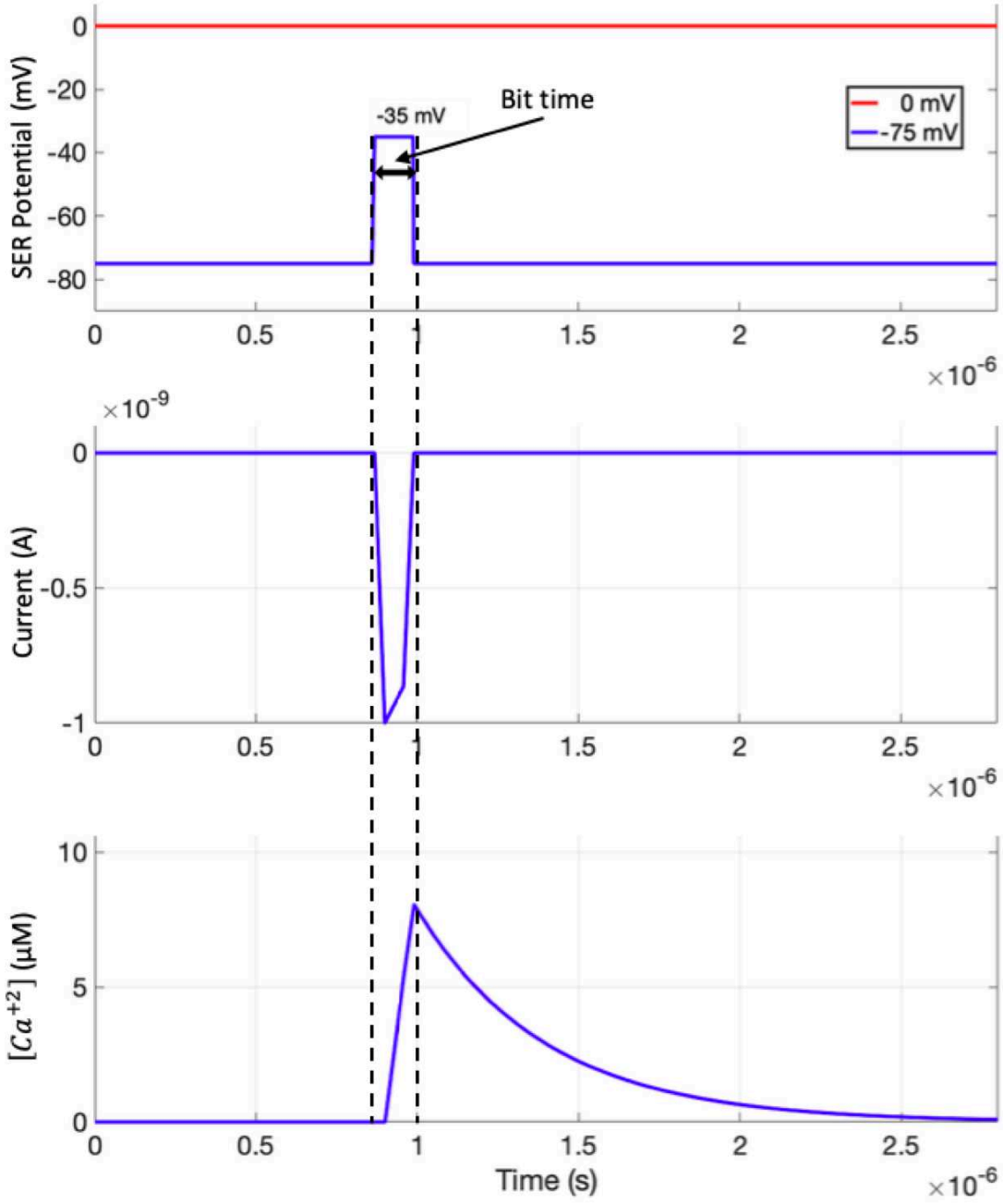

Figure 6.11 Bioluminescence Intensity Shift Keying (BISK) modulation technique.

released in a symbol duration, the number of photons emitted by reacting with these c ions is a random variable following a binomial distribution:

$$C \sim Binomial(c, P_{em}(r, t_b)) \tag{6.17}$$

The Binomial distribution can be approximated to a normal distribution by Central Theorem Limit (CLT) [Wilkinson, 2011]. When cp is large enough and p is not closer to zero or one, the distribution of the photons emission variable C can be written as:

$$C_n \sim \mathcal{N}(cp, cp(1-p)) \tag{6.18}$$

We assume that the noise inside the designed receiver is Additive Gaussian White Noise (AWGN). Therefore, the noise is also a random variable that follows a normal distribution:

$$N \sim \mathcal{N}(0, \sigma^2) \tag{6.19}$$

and thus, the probability of detecting the bioluminescent light emitted at the receiver can be found by adding the two normal distributions. The probability of detecting a previous bit is neglected in this paper by assuming that the photo-detector used at the gateway has a high resolution.

By using the proposed BISK modulation technique, the gateway decodes the detected bioluminescent light by comparing the sum of the two normal distributions with a predefined threshold value ξ. If the intended bit is "0", then the probability of an incorrect decoding for the BISK modulation technique are calculated as follows:

$$P_r = \frac{1}{3}\frac{hc}{\lambda} P(C_n + N \geqslant \xi) \tag{6.20}$$

and if the intended bit is "1":

$$P_r = \frac{1}{3}\frac{hc}{\lambda} P(C_n + N < \xi) \tag{6.21}$$

6.8 Performance Evaluation and Numerical Results

To evaluate the performance of the designed receiver, we used Simulink in MATLAB to simulate the proposed equivalent circuit. The parameters we used in this study are

mentioned in the section above. The output at the capacitance represents the released Ca^{2+} ion concentration by SER for each bit interval. As shown in Fig. 6.9, the current sent through the nanowire excites SER's membrane and increases its resting potential (-75 mV) calculated in eq. 6.7 by 35 mV, which allows the opening of Ca^{2+} channels. The output of the capacitance increases rapidly to reach more than 7 μM of Ca^{2+} ions, then when the excitation stops, SER starts absorbing the released Ca^{2+} ions and the output decreases slowly until it vanishes from the medium.

6.8.1 Number of Ca^{2+} Channels

In this study, we used the minimum possible channels number per μm^2 area in SER membrane, which is $n = 4$ channels. These 4 channels represent 4 resistances linked in parallel in our proposed equivalent circuit. We simulated 4 cases where only one channel is opened, two, three and four channels opened together and we plotted the current necessary for each case along with the output of the equivalent circuit as a function with time.

In Fig. 6.10, we can see that the number of open channels is proportional to the intensity of the transmitted current through the nanowire. We can also notice that only an intensity of 4 pA is needed to open the maximum number of channels we used in this study. This is due to the fact that the membrane's thickness is so small (6 nm) that a tiny excitation can change the voltage at the channels and open them. The sensitivity of SER's membrane to the electric current is one of the reasons why we use it to detect electrons in our designed receiver for a wired nano-communication.

Fig. 6.11 shows the output results of the proposed equivalent circuit in the 4 studied cases. We can notice that with 4 opened channels, SER can release more than 20 μM of Ca^{2+} ions. We can also notice that in the case where 4 channels are open, the signal decreased rapidly (1.5 μs) compared to the case where only one channel is open (3 μs). With 4 opened channels, the SER needs half the time that one channel needs to absorb the released Ca^{2+} ions after the excitation is stopped, which deceases the intersymbol interference between previous and next bits. The released Ca^{2+} concentration by SER is proportional to the intensity of the current sent through the nanowire, which is used to demodulate the transmitted signal.

6.8.2 Radiant Energy

We used the simulated output of the equivalent circuit which represents the concentration of the released Ca^{2+} ions for each bit interval $c(t)$ to calculate the bioluminescent radiant energy by using eq. 6.16. We used different voltage intensities at the input to show

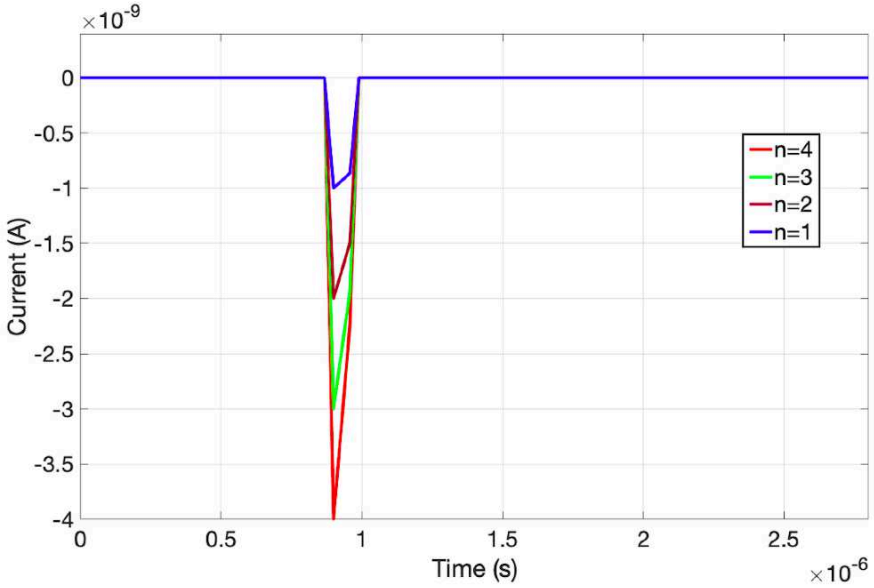

Figure 6.12 The current necessary to open the Ca2+ channels.

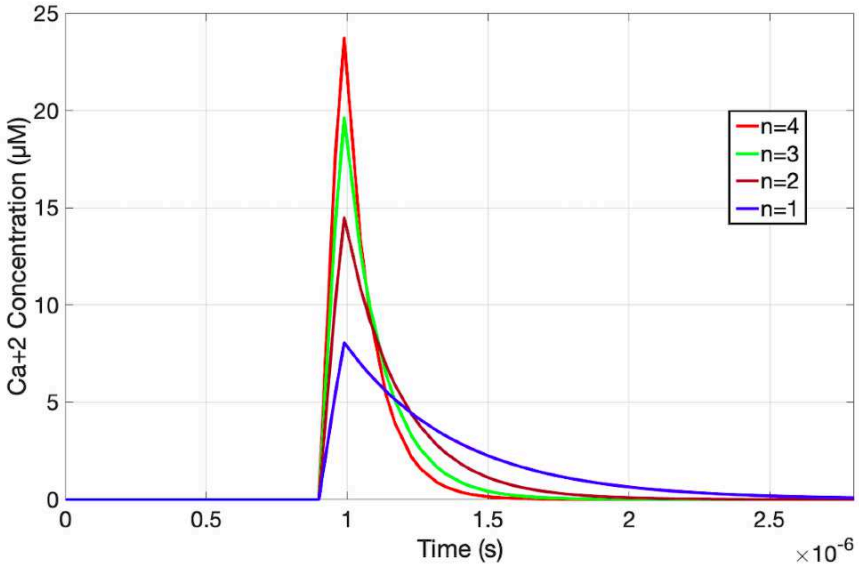

Figure 6.13 The released Ca2+ ion concentration for each number of open channels.

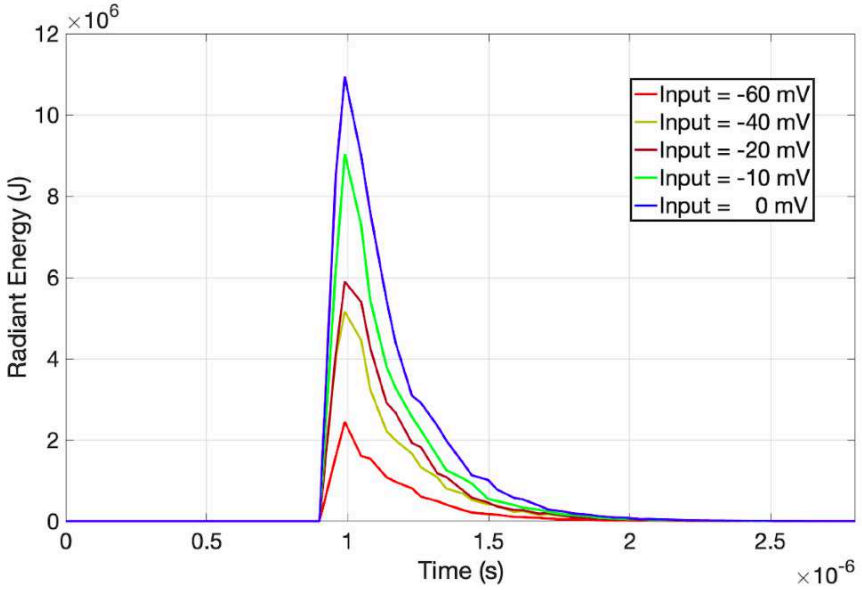

Figure 6.14 Radiant energy emitted by the bioluminescent reaction for different inputs.

the proportionality between the transmitted current through the nanowire and the light intensity emitted by the receiver. Fig. 6.12 shows that the intensity of the blue light emitted by the receiver can reach more than 10 MJ, which is enough to be detected by the gateway. It also shows that the intensity of light decreases rapidly when the medium is emptied of Ca^{2+} ions, because without the presence of Ca^{2+} ions, the bioluminescent light cannot be emitted, which decreases the intersymbol interference.

Fig. 6.13 summarizes the performance of the designed receiver by following the electrons detection and the light emission processes. The figure shows a random binary message that is detected by SER, where the bits "1" open the channels and release Ca^{2+} ions, which they combine with *Aequorin* and emit a blue light. Bit "0" keep the channels closed, SER absorbs the Ca^{2+} ions from the medium and the light emission stops. The results of this study show that light emission allows the designed receiver to play the role of a relay between the nanomachines and the gateway. This ability can be used as a link between the nanoscale and macroscale in the in-body technologies for medical applications.

6.8.3 Bit Error Rate

In order to evaluate the performance of the designed receiver, we calculate the Bit Error Rate (BER), which is the bit errors number divided by the total transmitted bits during the studied time interval. Fig. 6.14 shows the results of the calculated BER as function

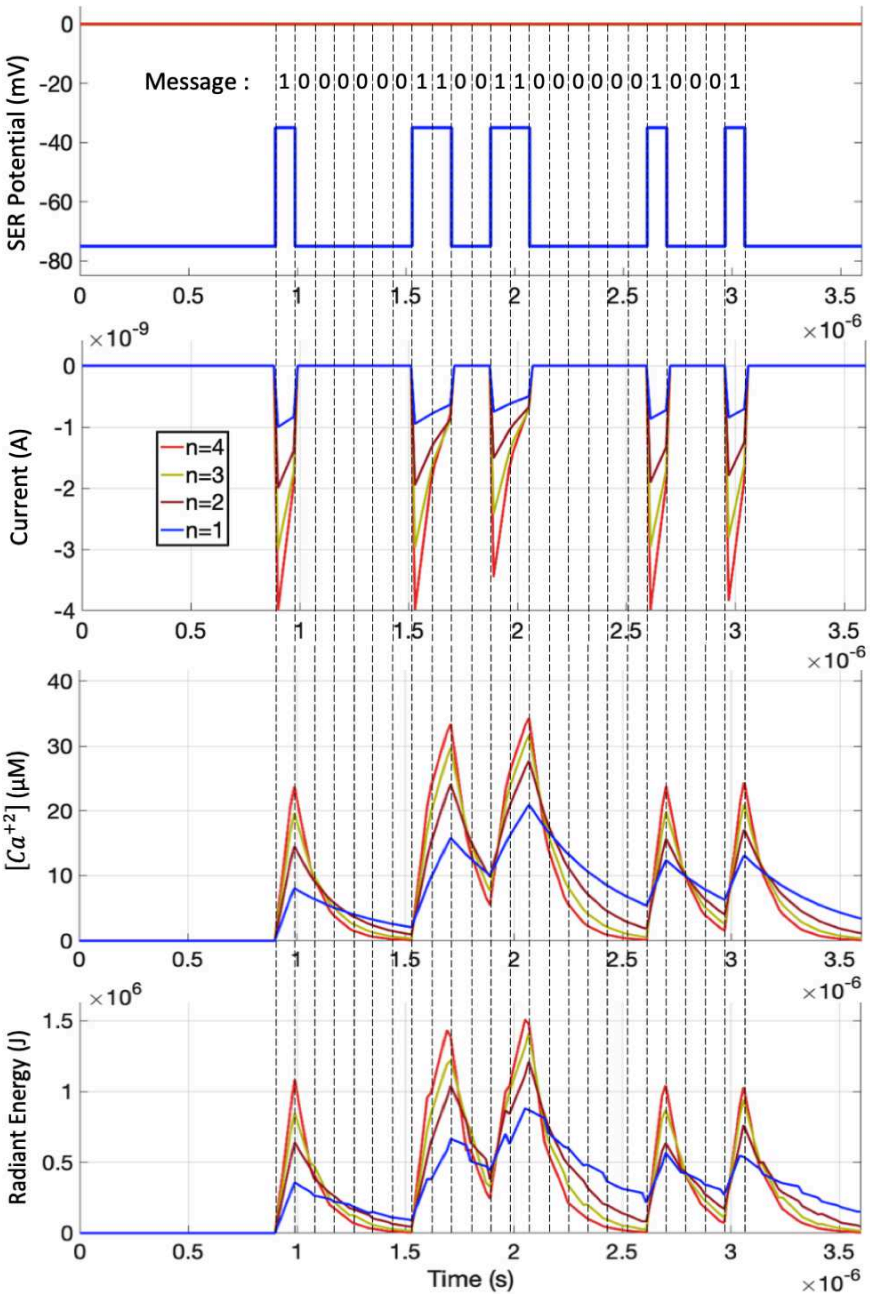

Figure 6.15 The response of the designed receiver to a random binary message.

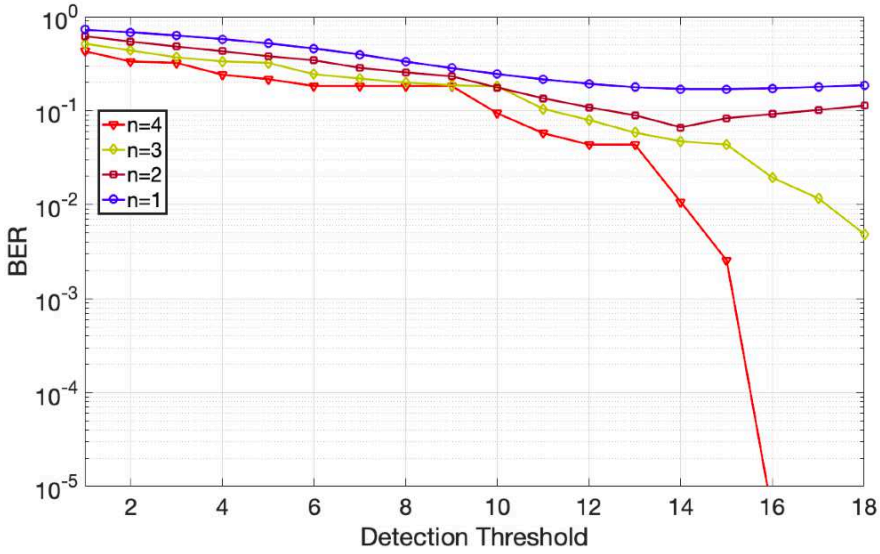

Figure 6.16 Bit error rate of the designed receiver as a function of the detection threshold.

of the detection threshold for the 4 studied cases. We notice that the case with 4 open channels has the best results with BER of 10^{-5} for a threshold 16, because 4 channels absorb the released Ca^{2+} ions faster, which deceases the intersymbol interference as we explained above. The fewer opened channels at the membrane of SER the more bit errors will be received, where 3 opened channels can reach BER of 10^{-2} for a threshold 17. The worst case is where only one channel is opened with 0.8, which is explained by the fact that one single channel will not be able to release and absorb Ca^{2+} ions rapidly, which increases intersymbol interferences, and thus, increases the BER.

6.9 Conclusion

Using the ability of certain polymers to self-assemble in order to build conductive nanowires between nanomachines is a new method proposed for establishing wired nano-communication systems. Despite the very high achievable throughput of wired nano-communication systems due to the use of electrons as information carriers, the detection of electrons on the nanometric scale is very challenging. This paper proposes a bio-inspired receiver design that uses Smooth Endoplasmic Reticulum (SER) to detect the transmitted electrons by measuring the released Ca^{2+} ions concentration with the photo-protein *Aequorin* that emits a blue light in the presence of Ca^{2+} ions. To better design the receiver, we simulate the construction of the nanowire, present its electrical characteristics and calculate its maximum throughput. We modeled the dynamic of SER with an equivalent circuit,

and we derived the analytical expression of their components. We calculated the radiant energy emitted in each symbol interval, and we simulated the detection and light emission processes of a random binary message. We also proposed modulation techniques that guaranty an effective decoding of the information and we calculated the BER of the designed receiver to evaluate its performance. The results of this study showed that the designed receiver is efficient for wired nano-communication networks and that it can also play the role of a relay for the nearest gateway.

CHAPTER 7

WIRED AD HOC NANONETWORK

Auteurs et affiliation:

Oussama Abderrahmane Dambri: étudiant au doctorat, Département de Génie Électrique et de Génie Informatique ,Université de Sherbrooke. INTERLAB Research Laboratory.

Soumaya Cherkaoui: Professeur, Département de Génie Électrique et de Génie Informatique, Université de Sherbrooke. INTERLAB Research Laboratory.

Date de Parution: Juin 2020

Revue: *IEEE International Conference on Communications (ICC)*

Titre français: Vers un nanoréseau ad hoc filaire

Résumé français:

Les nanomachines promettent de nouvelles applications médicales, notamment l'administration de médicaments et la détection de réactions chimiques en temps réel à l'intérieur du corps humain. Ces tâches complexes nécessitent une coopération entre les nanomachines utilisant un réseau de communication. Des réseaux ad hoc sans fil, utilisant une communication moléculaire ou électromagnétique, ont été proposés dans la littérature pour créer des nanoréseaux flexibles entre nanomachines. Dans cet article, nous proposons une conception de modèle Wired Ad hoc NanoNETwork (WANNET) utilisant la nano-communication basée sur l'actine. Dans le modèle proposé, l'auto-assemblage et le désassemblage des filaments d'actine sont utilisés pour créer des nanofils flexibles entre les nanomachines, et les électrons sont utilisés comme vecteurs d'information. Nous donnons un aperçu général de la couche application, de la couche de contrôle d'accès moyen et d'une couche physique du modèle. Nous détaillons également le modèle analytique de la couche physique à l'aide de circuits équivalents en nanofils d'actine et nous présentons une estimation des valeurs des composants du circuit. Les résultats numériques du modèle dérivé sont fournis en termes d'atténuation, de phase et de retard en fonction de la fréquence et des distances entre nanomachines. Le débit maximal du nanofil à base d'actine est également fourni, et une comparaison entre le débit maximal du WANNET proposé et d'autres approches proposées est présentée. Les résultats obtenus prouvent que le nanoréseau ad hoc filaire proposé peut donner un débit réalisable très élevé avec un delai plus petit.

7.1 Toward a Wired Ad Hoc Nanonetwork

7.2 Abstract

Nanomachines promise to enable new medical applications, including drug delivery and real time chemical reactions' detection inside the human body. Such complex tasks need cooperation between nanomachines using a communication network. Wireless Ad hoc networks, using molecular or electromagnetic-based communication have been proposed in the literature to create flexible nanonetworks between nanomachines. In this paper, we propose a Wired Ad hoc NanoNETwork (WANNET) model design using actin-based nano-communication. In the proposed model, actin filaments self-assembly and disassembly is used to create flexible nanowires between nanomachines, and electrons are used as carriers of information. We give a general overview of the application layer, Medium Access Control (MAC) layer and a physical layer of the model. We also detail the analytical model of the physical layer using actin nanowire equivalent circuits, and we present an estimation of the circuit component's values. Numerical results of the derived model are provided in terms of attenuation, phase and delay as a function of the frequency and distances between nanomachines. The maximum throughput of the actin-based nanowire is also provided, and a comparison between the maximum throughput of the proposed WANNET, vs other proposed approaches is presented. The obtained results prove that the proposed wired ad hoc nanonetwork can give a very high achievable throughput with a smaller delay compared to other proposed wireless molecular communication networks.

7.3 Introduction

In recent decades, nanotechnology's progress with the newly emerged nanomachines gave means to promising applications in medical and pharmaceutical fields, such as monitoring and drug delivery [Jahangirian *et al.*, 2017]. The limited capacity of the nanomachines and the complexity of the medical applications paved the way to a big interest in nanonetworks design, which helps overcome the nanomachines energy and the processing capacity limitations. Nanonetworks is a paradigm that adapts classical communication paradigms to meet the requirement of the nanosystems [Akyildiz and Jornet, 2010b]. Several studies proposed adaptations to the classical wireless and mobile ad hoc networks to be used in nanosystems using either electromagnetic or molecular communications [Atakan and Akan, 2010; Guney *et al.*, 2012; Kuscu and Akan, 2014].

A downscaled version of the traditional wireless ad hoc is proposed in [Atakan and Akan, 2010] using carbon nanotube-based communication. The authors investigated the hardware components needed for such networks at nanoscale, presented the networking issues and discussed the advantages of applying ad hoc nanosystems. However, the electromagnetic waves used in carbon nanotube-based communication oscillate at terahertz frequencies, and the design of transceivers that can capture the band peculiarities is one of its main challenges. The safety to use terahertz frequencies inside the human body for medical applications is another problem of electromagnetic communication at nanoscale, which needs further research. Molecular communication is a bioinspired paradigm that uses molecules as information carriers instead of electromagnetic waves. Molecular communication is used by nature and can be leveraged safely inside the human body. In [Guney *et al.*, 2012], the authors proposed a mobile ad hoc nanonetwork with collision-based molecular communication. This Mobile Ad hoc Molecular NETwork (MAMNET) employs infectious disease spreading principles using the electrochemical collision between mobile nanomachines to transfer information. Another MAMNET system is proposed in [Kuscu and Akan, 2014], by using Förster Resonance Energy Transfer (FRET-MAMNET), which is a nonradiative excited state energy transfer phenomenon, to send information from a donor to a nearby acceptor using fluorophores. However, the achievable throughput of both proposed methods drastically decreases with the increase in the distance between nanomachines.

In our recent work [Dambri *et al.*, 2019], we proposed self-assembled actin-based nano-communication, which uses actin filaments as a conductive nanowire to transmit electrical information and uses magnetic field for the actin direction. Actin is a bi-globular protein that exists in all human cells, and its ability to self-assemble and disassemble allows to create a flexible wired nanonetwork between mobile nanomachines. We also analyzed the stability of the nanowire with stochastic simulations, using our developed framework and we calculated the error probability.

In this paper, we take a first step toward designing a wired ad hoc nanonetwork by using the actin-based nano-communication method proposed in our recent work [Dambri *et al.*, 2019]. In the proposed model, the actin filaments self-assembly create conductive nanowires between nanomachines, and uses electrons as carriers of information. We demonstrate that once a link is established between an emitter and a receiver, the achievable throughput of the proposed Wired Ad hoc NanoNETwork (WANNET) is independent of the distance between nanomachines. The natural assembly and disassembly of actin filaments can be controlled via enzymes without the need of any infrastructure to create a flexible nanowire, which allows us, for the first time in the literature, to design wired ad

hoc networks at the nanoscale. In contrast to the previous work, the proposed system in this paper does not use magnetic field to direct actin filaments, its direction is left random so that the ad hoc system will be flexible and without any infrastructure. A proposed nanomachine is designed to trigger the formation of an actin nanowire when detecting a desired substance, which links the nanomachine with one of the surrounding neighbors. The transmitter can use the piezoelectric property of some proteins and DNA to transfer mechanical energy into electricity and send it through the constructed actin nanowire to the receiver. The receiver then triggers the formation of another actin nanowire and repeats the transmission cycle. In this paper, We also propose the OSI model-based communication layers between two nanomachines of the WANNET, and we briefly explain the role of each layer. Moreover, we derive an analytical model of the physical layer represented by the actin filaments, and we use this model to obtain the numerical analysis in order to evaluate the physical layer's performance.

The rest of the paper is organized as follows. In section II, we derive the analytical model of the physical layer represented by the actin filaments, by considering the actin monomers as an equivalent RLC circuit, and we calculate its maximum throughput. In section III, we explain the proposed wired ad hoc system and we detail the other two layers namely, application layer and MAC layer. We provide numerical results in section IV, by using the derived model, and we evaluate the performance of the physical layer in terms of attenuation, phase and delay as a function of the frequency and distances between nanomachines. We also provide an approximation of the maximum throughput of the proposed WANNET, and we compare it with the maximum throughput of FRET-MAMNET proposed in literature [Kuscu and Akan, 2014]. Finally, section V concludes the paper and presents future work.

7.4 Physical Layer Model

The physical layer, which is the main subject of this paper, uses the assembled actin nanowire. Actin is a bi-globular protein with self-assembly ability, which is controlled by specific enzymes. We assume that the distance between nanomachines does not exceed few tens of micrometers and that the radius of the nanomachines is not too small compared to the distance between them. These assumptions increase the probabilty of finding a neighbor nanomachine by the assembled nanowire, because the actin self-assembly direction is random. Moreover, actin has electrical properties that allow it to play the role of a conductive nanowire [Patolsky *et al.*, 2004]. Several experimental studies show that actin filaments can be used as electrical conductive wires [Kaur *et al.*, 2012, 2010].

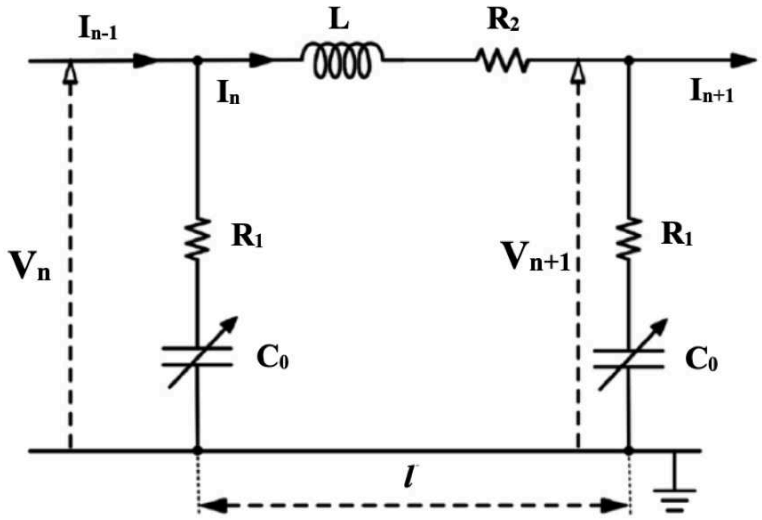

Figure 7.1 Effective circuits diagram for the n^{th} monomer of an actin filament.

The objective of modeling the ad hoc system's physical layer is to study the attenuation, phase and the delay as functions of the frequency and the channel distance. The actin monomers are modeled in the literature as an equivalent circuit based on the analogy of transmission lines with resistive, inductive and capacitive components [Tuszyński *et al.*, 2004], [Hunley *et al.*, 2018]. Each infinitesimal element of a transmission line length can be represented as a resistive and inductive components linked in series, and a capacitance with another resistive components linked in parallel. Due to the constant current in all components, transmission lines are usually modeled as infinite RLC equivalent circuits linked in series. In our proposed physical layer model, the infinitesimal elements of the actin filament are the actin monomers, and each monomer is modeled as a series RLC equivalent circuit as shown in Fig. 7.1.

7.4.1 Circuit's Components

Before explaining each of the component's physical significance, we identify the Bjerrum length λ_B as the distance where the electrostatic attractions of the actin filaments charges are stronger than the thermal fluctuations. The value of a Bjerrum length is found to be $\lambda_B = 7.13 \times 10^{-10}$ m for a temperature of 293 K [Tuszyński *et al.*, 2004]. The negative charge of proteins constructing the actin filament and the positive countrions around the

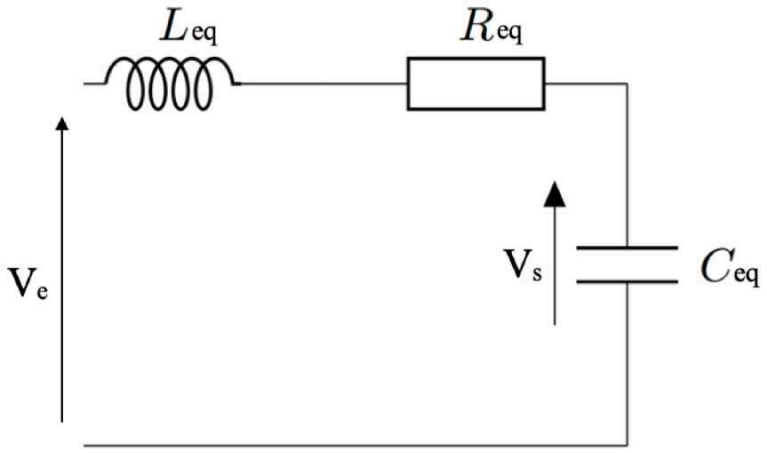

Figure 7.2 Effective circuits diagram for the total actin filament.

filament create a ~ 1 Bjerrum radius depletion area. The depletion area is modeled as a capacitance in the equivalent circuit shown in Fig. 7.1, and it can be calculated as:

$$C_0 = \frac{2\pi\varepsilon l}{ln\left(\frac{r_{actin}+\lambda_B}{r_{actin}}\right)}. \tag{7.1}$$

where ε is the permittivity, r_{actin} is the radius of actin filaments and l is the length of an actin monomer and can be approximated to $l\simeq$ 5.4 nm. The estimated capacitance per monomer can be approximated to $C_0 \simeq 96 \times 10^{-6}$ pF.

The movement of the charges in the helical shape of actin filaments induces a magnetic field, which is modeled as an inductance. The effective inductance for the actin filament in a solution can be calculated as:

$$L = \frac{\mu H^2 A}{l} \tag{7.2}$$

where μ is the magnetic permeability, A is the cross-sectional area $A = \pi(r_{actin} + \lambda_B)^2$ and H is the number of the helical turns in the actin filament. The estimated inductance per monomer is $L \simeq 1.7$ pH.

The authors in [Tuszyński *et al.*, 2004] calculated the resistance of actin monomers based on conductivities of ions in a salt solution as:

$$R = \frac{\rho ln((r_{actin} + \lambda_B)/r_{actin})}{2\pi l}. \tag{7.3}$$

where ρ is the resistivity. The estimated resistance per monomer is $R \simeq 6.11$ MΩ.

To study the electrical characteristics of an entire filament that contains n monomers, and by assuming that the values of all the components for each monomer are equal, we sum the n circuits in an equivalent circuit, that is shown in Fig. 7.2. In [Tuszyński *et al.*, 2004], the authors estimated an average of 370 monomers per μm. By summing 370 RLC circuits linked in series we got an effective resistance, inductance and capacitance for a 1 μm of the actin filaments as follows:

$$C_{eq} = 0.02 \times 10^{-12} \text{ F}$$

$$L_{eq} = 340 \times 10^{-12} \text{ H}$$

$$R_{eq} = 1.2 \times 10^{9} \Omega$$

7.4.2 Circuit Analysis

From the equivalent RLC circuit presented in Fig. 7.2, we derive the transfer function as follows:

$$\begin{aligned} T = \frac{V_s}{V_e} &= \frac{\frac{1}{sC_{eq}}}{sL_{eq} + R_{eq} + \frac{1}{sC_{eq}}} \\ &= \frac{1}{L_{eq}C_{eq}} \cdot \frac{1}{s^2 + s\frac{R_{eq}}{L_{eq}} + \frac{1}{L_{eq}C_{eq}}}, \end{aligned} \tag{7.4}$$

Where s represents the frequency. To lighten the expression, we write C_{eq}, L_{eq} and R_{eq} as C, L and R respectively. The denominator in 7.4 gives two solutions:

$$p_{1,2} = -\frac{R}{2L} \pm \sqrt{\left(\frac{R}{2L}\right)^2 - \frac{1}{LC}}, \tag{7.5}$$

Equation 7.5 includes 7.3 different cases depending on the comparison between the two expressions $(R/2L)^2$ and $1/(LC)$. In our study, due to the very high actin filament resistance, we are in the case where $(R/2L)^2$ is bigger than $1/(LC)$. The attenuation $A(s)$ is then calculated in dB as:

$$A(s)|_{dB} = 20log\frac{1}{LC} - 20log\sqrt{s^2 + p_1^2} - 20log\sqrt{s^2 + p_2^2}. \tag{7.6}$$

The phase $\varphi(s)$ of the derived transfer function is calculated:

$$\varphi(s) = tan^{-1}\left(\frac{1}{LC} \cdot \frac{1}{(s-p_1)(s-p_2)} \right). \tag{7.7}$$

The delay $\tau(s)$ can be obtained by calculating the derivative of the phase as:

$$\tau(s) = -\frac{d\varphi(s)}{ds}. \tag{7.8}$$

7.4.3 Maximum Throughput

The electrons are the carriers of information in our proposed actin-based nano-communication method. In order to calculate the maximum throughput that the proposed nanwire can provide, we need to approximate the charge capacity of the actine filaments and the speed at which the charges move through it. The charge capacity of each actin monomer is $\sim 4e$ [Tuszyński *et al.*, 2004], and by assuming 370 monomer/μm of an actin filament, we can deduce that the charge capacity of an actin filament with 1μm long is approximately 1480 e. The velocity expression of charges propagation along actin filaments in units of ms^{-1} can be written as [Hunley *et al.*, 2018]:

$$v(t) = \frac{\beta}{\alpha}\left(1 + \frac{1}{24}\frac{d\eta(\tau)}{d\tau}\bigg|_{\tau=t/(24\alpha)}\right), \tag{7.9}$$

where

$$\begin{aligned} \frac{d\eta}{\tau} &= 4\Omega^2 \frac{\exp\left(-\frac{4\tau\mu_2}{3}\right)}{1+\frac{4\mu_1\Omega^2}{5\mu_2}\left(1-\exp\left(-\frac{4\tau\mu_2}{3}\right)\right)}, \\ \alpha &= \frac{R}{L} + CR > 0, \qquad\qquad \beta = 2l. \end{aligned} \tag{7.10}$$

where $\Omega = 2.3810$, which is dependent on the voltage at the input. τ is the pulse duration of the electrical signal. $\mu_1 = \frac{6R_1}{R}$, $\mu_2 = \frac{24R_2}{R}$, where R_1 and R_2 are the longitudinal and radial ionic flow resistances consecutively.

The results in [Hunley *et al.*, 2018] shows that the velocity of charges propagation along the actin filament starts with 0.03 ms^{-1} and quickly decreases because of the filament's high resistance until it stops in t=60μs. The maximum throughput $T_M(t)$ of the proposed actin-based nano-communication physical layer is the speed of charges propagation multiplied

by the total charge capacity of 1μm long filament, where one electron represents 1 bit of information and we can write:

$$T_M(t) = v(t) \times \psi_{tot}. \tag{7.11}$$

where $v(t)$ is the velocity of charges propagation in 7.4, and ψ_{tot} is the total charge capacity of a 1μm long actin filament.

7.5 A Wired Ad Hoc Nanonetwork

An ad hoc network consists of nodes that connect with each other wirelessly, without the need of a mediating infrastructure. Each node can establish a link with its neighbor and communicate with it directly, playing a role to forward data for other nodes [Barbeau and Kranakis, 2007]. In the literature, ad hoc nanonetworks are proposed by using electromagnetic waves [Atakan and Akan, 2010] or molecules [Guney *et al.*, 2012], [Kuscu and Akan, 2014] as a link between nanomachines. However, the proposed nanonetworks based on electromagnetic links still do not addresses some of the challenges related to the peculiarities of the Terahertz band [Akyildiz and Jornet, 2010b], and those based on molecules have a weak achievable throughput and a high delay [Dambri *et al.*, 2019; Dambri and Cherkaoui, 2018, 2019].

In this paper, we propose a new method to establish wired links between N nanomachines by using the actin-based method proposed in our recent work [Dambri *et al.*, 2019]. The ability of actin proteins to assemble, create conductive filaments, and then disassemble, allows to use these actin proteins as links between static or mobile nanomachines in a wired ad hoc nanonetwork. Fig. 7.3 illustrates the proposed WANNET. In the figure, there are 13 nanomachines close to each other. The actin monomers assembly can be triggered when the n^{th} nanomachine receives the desired substance presented as a green sphere by using the chemical cascade in the cells to secrete the assembly enzymes.This in turn, creates a nanowire that connects with a neighbor randomly. After establishing a link, the sender uses the piezoelectric property of some proteins and DNA to send the information using electrons [Guerin *et al.*, 2019]. The received electrons can trigger the creation of a nanowire in the $(n+1)^{th}$ nanomachine that connects with another neighbor randomly by using the same chemical cascade and so on. The cycle of triggering the nanowire creation to send electrons that in turn, triggers another nanowire creation, can help spreading information in all the nanonetwork, until a gateway is reached.

7.5.1 Nanomachines

The nanomachines in our proposed system are bioengineered cells with DNA and ribosomes, which are already designed and presented in literature as in [Loe, 2010]. The DNA and ribosomes inside the nanomachines enable them to construct proteins and secrete the enzymes that control the actin nanowire formation. As explained earlier, the assumptions about the distance between nanomachines and their radius is due to the fact that the actin self-assembly direction is random. Therefore, small distances between nanomachines and a bigger radius increase the possibility of the random nanowire to find a neighbor. When a nanomachine detects a desired substance to be analyzed, processes take place allowing neighboring nanomachines to communicate information using the constructed nanowire. The nanowire link enables spreading information in all the nanonetwork until reaching the closest gateway. The proposed WANNET could, ultimately, be used inside the human body for monitoring, disease diagnosis and for real time chemical reactions detection. As illustrated in Fig. 7.4, the communication processes between nanomachines in the proposed WANNET are performed by three layers: the physical layer, which we modeled in the previous section, the application layer and the MAC layer.

7.5.2 Application Layer

The application layer of the proposed WANNET performs the information encoding. One way to encode the information is that specific receptors at the nanomachine membrane detect the desired substance to be analyzed and send a message to the DNA. DNA encodes the information about the detected substance by using the piezoelectric property of some proteins [Guerin *et al.*, 2019]. These proteins transform mechanical energy into electricity, which is transmitted by using the actin nanowire. The information can be modulated using the dynamic pattern frequency spectrum of the used piezoelectric proteins.

7.5.3 Medium Access Control Layer (MAC)

The MAC layer provides a control over the input of the physical layer by encapsulating the encoded information into frames. It also triggers the secretion of the enzymes that control the actin nanowire formation. In order to identify transmission errors, the MAC layer can also add some frame check sequences. A detailed protocol for the MAC layer will be proposed in future work.

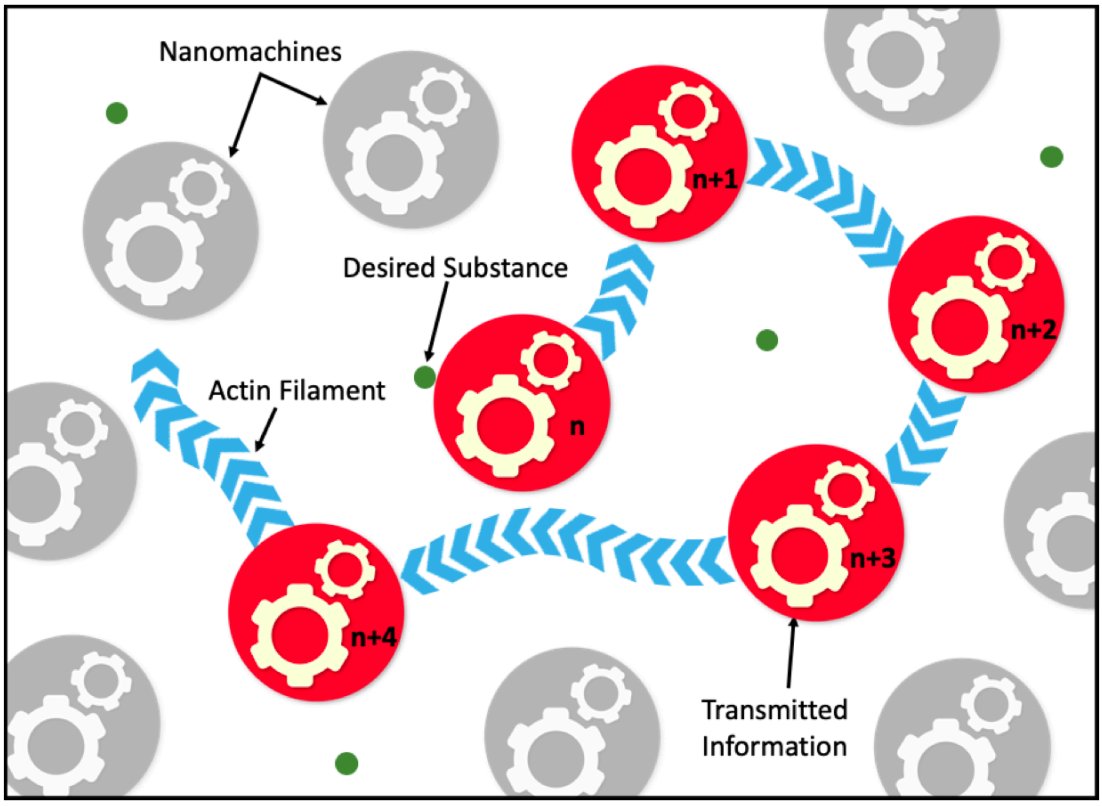

Figure 7.3 Information spreading in the proposed wired ad hoc nanonetwork.

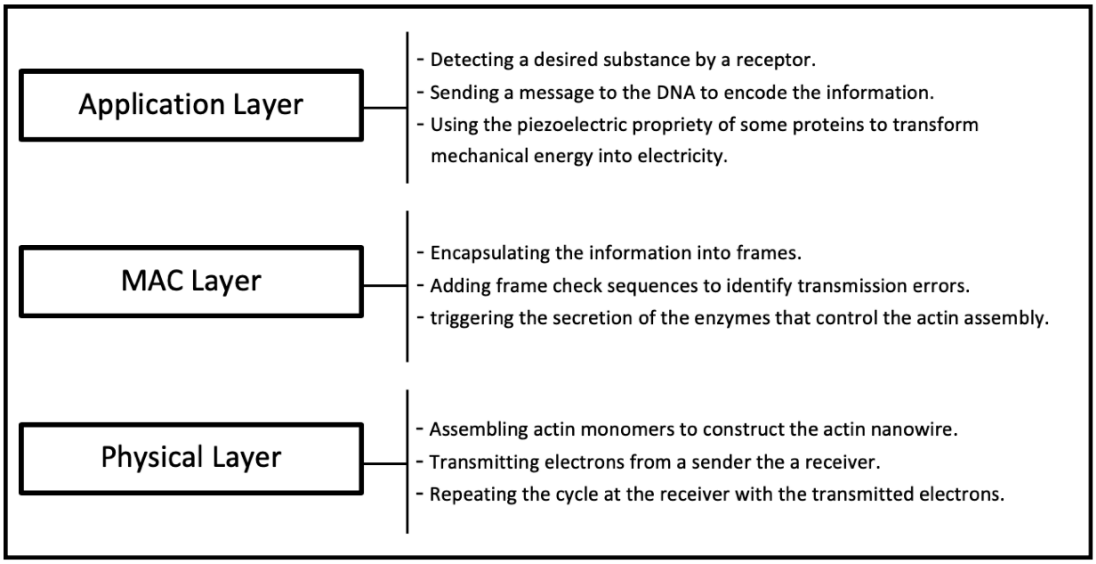

Figure 7.4 An OSI Model for the communication layers between two nanomachines.

7.6 Numerical Results

In this section, we present the numerical results of the system's physical layer in terms of attenuation, phase and delay as a function of the frequency and distances between nanomachines, as well as the maximum throughput. We considered frequency ranges [0 Hz-700 Hz] and [0 Hz-900 Hz] to ease the comparison with the studies that use the same range for molecular communications. Moreover, higher frequencies increase the attenuation of the actin filament, therefore, we expect that the chosen frequency range can give better results than higher frequency ranges. We use MATLAB to obtain the numerical results, and we use the parameters explained above to simulate the electrical characteristics of the system's physical layer.

7.6.1 Attenuation

Fig. 7.5 shows the attenuation of the system model, which is calculated with Eq. 7.6 for different actin filaments lengths (d). The attenuation starts with -364 dB for 0 Hz and d=10μm, and increases with the increase in frequency until it reaches -525 dB for 700 Hz. The high attenuation of the actin filament is due to its very high resistance calculated in Eq. 7.3. The connection of n circuits representing n monomers to get the actin filament effective circuit, makes the connected capacitances in parallel, and the impedances in series. The increase in attenuation with the frequency increase can be explained by the fact that impedances in series favor low frequencies. Moreover, capacitances in parallel favor the passing of high frequencies and take them away from the output, which makes them play the same role as the series impedances. We can also notice that the attenuation increases with the filament's length increase, for frequencies lower than 400 Hz. The explanation of this increase is that the more the length of actin filaments, the more monomers are needed, which increases the number of impedances in series.

7.6.2 Phase

Fig. 7.6 presents the phase of the system model as a function of the frequency, which is calculated with Eq. 7.7 for different actin filaments lengths. The phase starts with -0.16 degree for 0 Hz and d=10μm. The increase in frequency widen the phase to reach -1.42 degree for 700 Hz. The phase increase is due to the increase in signal attenuation; the more the signal is attenuated the more the phase between the input and the output is increased. The phase also increases with the increase in actin filament's length. The explanation of this increase is that bigger distances crossed by the signal, increase its attenuation as we saw in Fig. 7.5, and the increase in the signal attenuation also increases its phase.

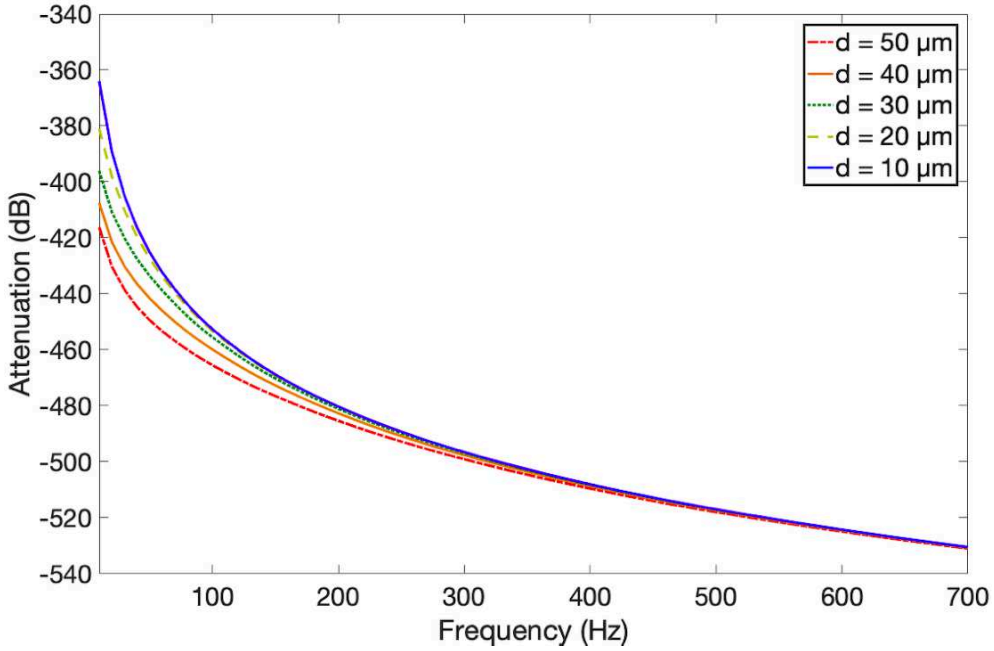

Figure 7.5 Attenuation for the actin filament model.

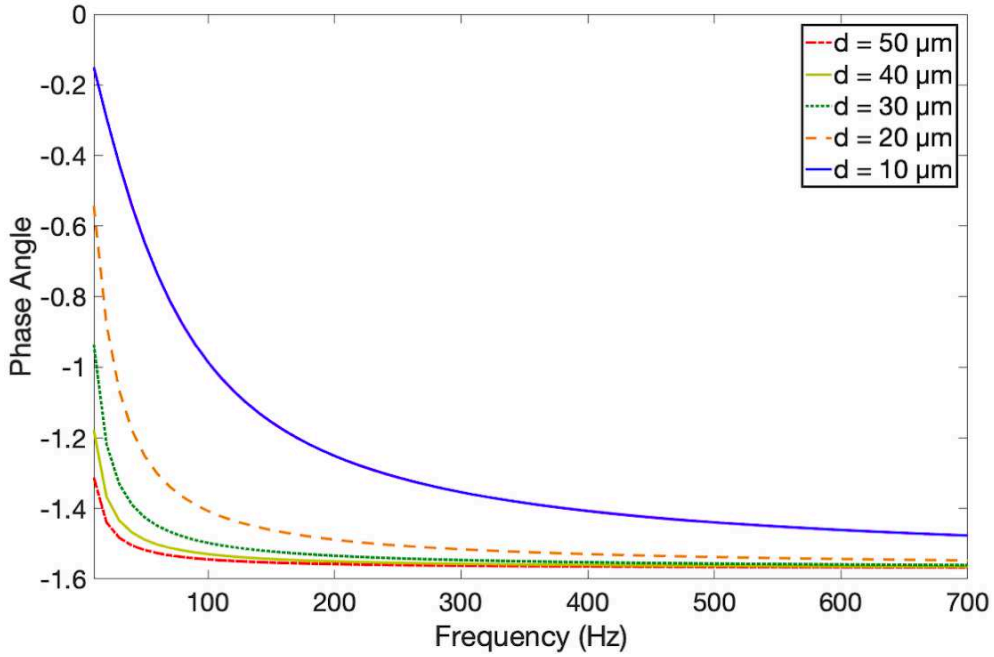

Figure 7.6 Phase for the actin filament model.

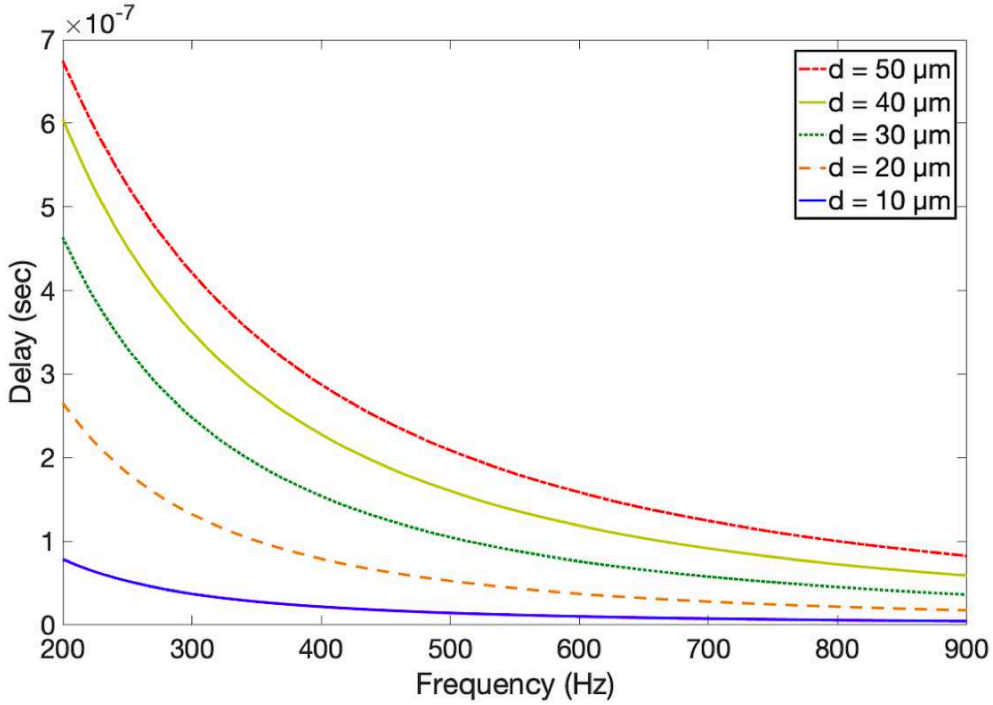

Figure 7.7 Delay for the actin filament model.

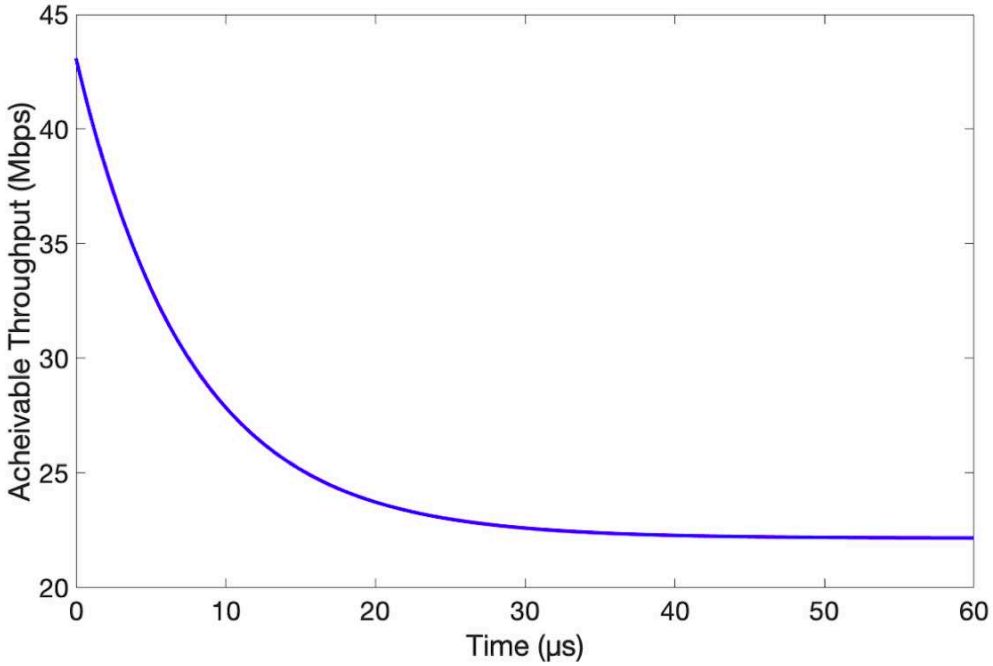

Figure 7.8 Maximum throughput approximation for the actin nanowire.

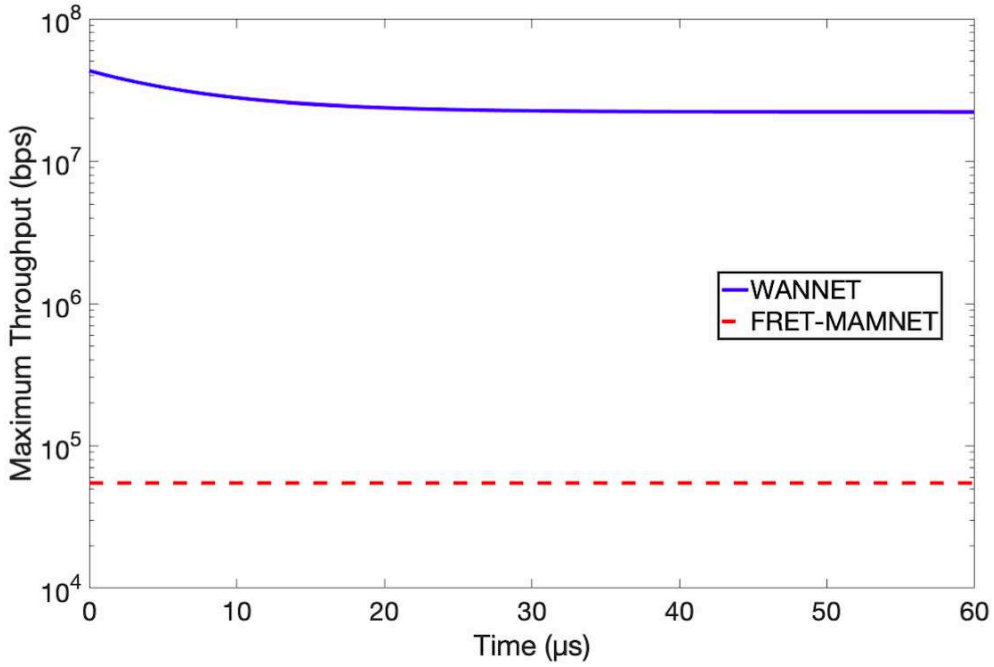

Figure 7.9 Maximum Throughput comparison between the proposed WANNET and FRET-MAMNET.

7.6.3 Delay

Fig. 7.7 presents the delay of the system model as a function of the frequency, which is calculated with Eq. 7.8 for different actin filaments lengths. The delay starts with 8 μs for 0 Hz and d=10μm. The increase in frequency decreases the delay to reach 1 μs for 900 Hz. It is obvious that when frequency increases, the speed of the signal also increases, which decreases the delay. We can also notice that the delay increases with longer actin filaments. The explanation of this increase is that in longer filaments, the signal takes more time to reach the destination, which increases the delay to reach 68 μs with d=50μm.

7.6.4 Maximum Throughput

In Fig. 7.8, we present the numerical results of the proposed physical layer's maximum throughput, which is calculated with Eq. 7.11. Charge capacity of 1 μm actin filament is 1480 e, and the speed of the charge propagation is 30,000 μm/s [Hunley *et al.*, 2018]. If we assume that one electron represents 1 bit, then the maximum throughput of 1 μm actin filament is 44,4 Mbps as shown in Fig. 7.8. However, we can notice that the maximum throughput decreases rapidly with time, to reach 23 Mbps in 30 μs. The explanation of this decrease is that the speed of the charge propagation decreases with time due to the

very high resistance of the actin filament as proven experimentally in [Hunley *et al.*, 2018]. Despite this decrease, the throughput still very high and can be used by nanomachines to propagate the information through the proposed WANNET. The best throughput results of the proposed FRET-MAMNET in [Kuscu and Akan, 2014] did not exceed 5.5 Kbps. Because of the huge difference between the results in [Kuscu and Akan, 2014] and the results of our proposed model, we need to plot them logarithmically so that the comparison becomes clear as shown in Fig. 7.9.

7.7 Conclusion and Future Work

The decentralized nature of ad hoc nanonetworks makes them suitable for a variety of medical and pharmaceutical applications. However, wireless ad hoc nanoetworks proposed in literature either suffer from scattering loss, and molecular absorption or they provide weak throughput with high delay. In this paper, we presented a first step toward designing a Wired Ad hoc NanoNETwork (WANNET) by using actin-based nano-communication. We proposed the OSI model-based communication layers between two nanomachines of the WANNET, and briefly explained the role of each layer. We also derived an analytical model of the physical layer by considering the actin filament as an equivalent RLC circuit. Moreover, we evaluated the performance of the physical layer in terms of attenuation, phase and delay as functions of the frequency and distances between nanomachines. Despite of the fact that the attenuation of the actin filament is very high because of its high resistance, it still provides a very high maximum throughput with smaller delay, compared to the methods that use molecular communication.

In future work, we will study the MAC and application layers of the proposed WANNET, and we will propose a protocol for each layer. Furthermore, we will also propose a protocol for error correction by using DNA computation.

CHAPTER 8

CONCLUSION

Bio-inspired nano-communication systems are very promising for medical applications such as diagnosis, local drug delivery and infections detection in real time. Despite the best efforts proposed in literature to improve the performance of molecular communication, there are still many open problems that need to be solved. The most important challenges to be tackled are the ISI mitigation and the increase in the achievable throughput. The principal objective of this thesis was to enhance the performance of nano-communication networks by designing and evaluating new methods. In order to reach this objective, we proposed several bio-inspired ideas that address the challenges facing nano-communication systems. In this chapter, we provide a conclusion on each proposed method and suggest some perspectives for future works.

In chapter 3, we proposed the use of photolysis reaction instead of enzymes to degrade the remaining molecules in the medium. Unlike the enzymes, the switching ability of light allows the receiver to mitigate ISI faster without decreasing the strength of the signal. We then derived a lower bound expression on the expected number of molecules to be observed at the receiver, calculated the bit error probability and used it along with interference-to-total received molecules metric to evaluate the performance of the proposed system.

Chapter 4 presented the optimization of a MIMO receiver design by focusing on three important parameters: the channel distance, the distance between the detectors constructing the receiver and the diameter of the detectors. We also formulated two optimization problems and proposed two algorithms to solve them. The study showed that a judicious choice of the optimized three parameter's combination can optimize the MIMO receiver's response by decreasing the error probability and increasing the achievable throughput.

In chapter 5, we proposed and modeled a nano-communication wired channel based on a polymer self-assembly. We studied the dynamic behavior of the channel by deriving the chemical master equation of the polymerization reaction and solved it analytically and numerically. In comparison with wireless molecular communication techniques proposed in the literature, the proposed wired polymer-based method promises stable and flexible nanonetworks with a much higher achievable throughput.

A bio-inspired receiver for wired nano-communication networks is proposed in chapter 6, which uses SER to detect the electrons sent through the nanowire, then converts them into a blue light by using photo-proteins. We also proposed new modulation techniques to guaranty an effective decoding of the information and calculated the BER of the receiver to evaluate its performance. The results showed that the designed receiver is efficient for wired nano-communication networks and that it can also play the role of a relay.

Finally, an application of the proposed wired nano-communication network is presented in chapter 7, where an adaptation of the system is used to design a wired ad hoc nanonetwork (WANNET) and proposed its OSI model. We also derived an analytical model of the physical layer by considering the polymer filament as an equivalent RLC circuit and evaluated the performance of the physical layer in terms of attenuation, phase and delay. WANNET can be very useful in infection detection in real time inside the human body.

8.1 Future Works

In this section we suggest some perspectives for future works.

- In chapter 3, the optimal time to emit a light is proportional to the distance between the transmitter and the receiver, which implies that the proposed system would favorably use a fixed transmitter and a fixed receiver. However, if the distance of the system is variable, the receiver should have a mechanism that allows it to know the position of the transmitter before emitting the light. This variable distance is an interesting problem that we will consider in future works.
- The receivers proposed in chapters 3 and 4 are passive receivers, which they only observe the molecules without any interaction with them. However, that kind of receivers do not exist in nature and thus, absorbing and reflective receivers will be considered in future works.
- We will also consider in the future an experimental study of the proposed wired nano-communication network based on self-assembled polymers, then we will provide a comparison study between analytical, simulation and experimental results.
- The MAC layer and application layer in OSI model of the proposed WANNET will be studied in future works. A protocol will be proposed for each layer along with another protocol for error correction by using DNA computation.

8.2 CONCLUSION

Les systèmes de nano-communication bio-inspirés sont très prometteurs pour des applications médicales telles que le diagnostic, l'administration locale de médicaments et la détection des infections en temps réel. Malgré les meilleurs efforts proposés dans la littérature pour améliorer les performances de la communication moléculaire, il existe encore de nombreux problèmes ouverts qui doivent être résolus. Les défis les plus importants à relever sont l'atténuation de l'ISI et l'augmentation du débit réalisable. L'objectif principal de cette thèse était d'améliorer les performances des réseaux de nano-communication en concevant et en évaluant de nouvelles méthodes. Afin d'atteindre cet objectif, nous avons proposé plusieurs idées bio-inspirées qui répondent aux défis auxquels sont confrontés les systèmes de nano-communication. Dans ce chapitre, nous fournissons une conclusion sur chaque méthode proposée et suggérons quelques perspectives pour les travaux futurs.

Au chapitre 3, nous avons proposé l'utilisation de la réaction de photolyse au lieu d'enzymes pour dégrader les molécules restantes dans le milieu. Contrairement aux enzymes, la capacité de commutation de la lumière permet au receveur d'atténuer l'ISI plus rapidement sans diminuer la force du signal. Nous avons ensuite dérivé une expression de limite inférieure sur le nombre prévu de molécules à observer au niveau du receveur, calculé la probabilité d'erreur sur les bits et nous l'avons utilisée avec une métrique d'interférence au total des molécules reçues pour évaluer les performances du système proposé.

Le chapitre 4 a présenté l'optimisation de la conception d'un receveur MIMO en se concentrant sur trois paramètres importants: la distance du canal, la distance entre les détecteurs constituant le receveur et le diamètre des détecteurs. Nous avons également formulé deux problèmes d'optimisation et proposé deux algorithmes pour les résoudre. L'étude a montré qu'un choix judicieux de la combinaison optimisée des trois paramètres peut optimiser la réponse du receveur MIMO en diminuant la probabilité d'erreur et en augmentant le débit réalisable.

Dans le chapitre 5, nous avons proposé et modélisé un canal filaire de nano-communication basé sur un auto-assemblage des polymères. Nous avons étudié le comportement dynamique du canal en dérivant l'équation maîtresse chimique de la réaction de polymérisation et l'avons résolu analytiquement et numériquement. En comparaison avec les techniques de communication moléculaire sans fil proposées dans la littérature, la méthode à base de polymère filaire proposée promet des nano-réseaux stables et flexibles avec un débit réalisable beaucoup plus élevé.

Un receveur bio-inspiré pour les réseaux de nano-communication filaires est proposé au chapitre 6, qui utilise SER pour détecter les électrons envoyés à travers le nanofil, puis les convertit en une lumière bleue en utilisant une photo-protéine. Nous avons également proposé de nouvelles techniques de modulation pour garantir un décodage efficace des informations et calculé le BER du receveur pour évaluer ses performances. Les résultats ont montré que le receveur conçu est efficace pour les réseaux de nano-communication filaires et qu'il peut également jouer le rôle de relais.

Finalement, une application du réseau de nano-communication filaire proposé est présentée au chapitre 7, où une adaptation du système est utilisée pour concevoir un nanoréseau ad hoc filaire (WANNET) et proposer son modèle OSI. Nous avons également dérivé un modèle analytique de la couche physique en considérant le filament du polymère comme un circuit RLC équivalent et évalué les performances de la couche physique en termes d'atténuation, de phase et de délai. WANNET peut être très utile dans la détection des infections en temps réel à l'intérieur du corps humain.

8.3 Travaux futurs

Dans cette section, nous suggérons quelques perspectives pour les travaux futurs.

- Au chapitre 3, le temps optimal pour émettre une lumière est proportionnel à la distance entre l'émetteur et le receveur, ce qui implique que le système proposé utiliserait favorablement un émetteur et un receveur fixes. Cependant, si la distance du système est variable, le receveur doit avoir un mécanisme qui lui permet de connaître la position de l'émetteur avant d'émettre la lumière. Cette distance variable est un problème intéressant que nous examinerons dans les travaux futurs.
- Les receveurs proposés dans les chapitres 3 et 4 sont des receveurs passifs, dont ils n'observent que les molécules sans aucune interaction avec eux. Cependant, ce type de receveurs n'existe pas dans la nature et donc, les receveurs absorbants et réfléchissants seront pris en compte dans les travaux futurs.
- Nous considérerons également dans le future de mener une étude expérimentale du réseau de nano-communication filaire proposé basé sur des polymères auto-assemblés, puis nous fournirons une étude comparative entre les résultats analytiques, de simulation et expérimentaux.
- La couche MAC et la couche application dans le modèle OSI du WANNET proposé seront étudiées dans les travaux futurs. Un protocole sera proposé pour chaque couche avec un autre protocole de correction d'erreur en utilisant la methode de calcul par ADN.

LIST OF REFERENCES

(2010). Bioengineered 3d platform to explore cell–ecm interactions and drug resistance of epithelial ovarian cancer cells. *Biomaterials*, volume 31, number 32, pp. 8494 – 8506.

Aaron, J.-J. and Aaron, S. E. (2019). Purines, pyrimidines, and nucleotides. In Worsfold, P., Poole, C., Townshend, A. and Miró, M., *Encyclopedia of Analytical Science (Third Edition)*, third edition edition. Academic Press, Oxford, pp. 432–444.

Abbasi, Q. H., Yang, K., Chopra, N., Jornet, J. M., Abuali, N. A., Qaraqe, K. A. and Alomainy, A. (2016). Nano-Communication for Biomedical Applications: A Review on the State-of-the-Art From Physical Layers to Novel Networking Concepts. *IEEE Access*, volume 4, pp. 3920–3935.

Ahmadzadeh, A., Jamali, V. and Schober, R. (2017). Stochastic Channel Modeling for Diffusive Mobile Molecular Communication Systems. *arXiv:1709.06785 [cs, math]*.

Akdeniz, B. C., Pusane, A. E. and Tugcu, T. (2018). Optimal Reception Delay in Diffusion-Based Molecular Communication. *IEEE Communications Letters*, volume 22, number 1, pp. 57–60.

Akyildiz, I. F. and Jornet, J. M. (2010a). Electromagnetic wireless nanosensor networks. *Nano Communication Networks*, volume 1, number 1, pp. 3–19.

Akyildiz, I. F. and Jornet, J. M. (2010b). The Internet of nano-things. *IEEE Wireless Communications*, volume 17, number 6, pp. 58–63.

Akyildiz, I. F., Jornet, J. M. and Han, C. (2014). Terahertz band: Next frontier for wireless communications. *Physical Communication*, volume 12, number Supplement C, pp. 16–32.

Alberts, B., Johnson, A., Lewis, J., Raff, M., Roberts, K. and Walter, P. (2002). The Self-Assembly and Dynamic Structure of Cytoskeletal Filaments. *Molecular Biology of the Cell. 4th edition*.

Alsheikh, R., Akkari, N. and Fadel, E. (2016). Grid Based Energy-Aware MAC Protocol for Wireless Nanosensor Network. In *2016 8th IFIP International Conference on New Technologies, Mobility and Security (NTMS)*. pp. 1–5.

America, L. I. o. and N/A (2014). *ANSI Z136.1 - Safe Use of Lasers*. Laser Institute of America.

Ardeshiri, G., Jamshidi, A. and Keshavarz-Haddad, A. (2017). Performance analysis of Decode and Forward Relay network in Diffusion based Molecular Communication. In *2017 Iranian Conference on Electrical Engineering (ICEE)*. pp. 1992–1997.

Arjmandi, H., Ahmadzadeh, A., Schober, R. and Kenari, M. N. (2016). Ion Channel Based Bio-Synthetic Modulator for Diffusive Molecular Communication. *IEEE Transactions on NanoBioscience*, volume 15, number 5, pp. 418–432.

Arjmandi, H., Gohari, A., Kenari, M. N. and Bateni, F. (2012). Diffusion Based Nanonetworking: A New Modulation Technique and Performance Analysis. *arXiv:1209.5511 [cs, math]*.

Arjmandi, H., Movahednasab, M., Gohari, A., Mirmohseni, M., Nasiri-Kenari, M. and Fekri, F. (2017). ISI-Avoiding Modulation for Diffusion-Based Molecular Communication. *IEEE Transactions on Molecular, Biological and Multi-Scale Communications*, volume 3, number 1, pp. 48–59.

Arsenault, M. E., Zhao, H., Purohit, P. K., Goldman, Y. E. and Bau., H. H. (2007). Confinement and manipulation of actin filaments by electric fields. *Biophysical Journal*, volume 93, number 8.

Assaf, S. S., Salehi, S., Cid-Fuentes, R. G., Solé-Pareta, J. and Alarcón, E. (2017). Influence of neighboring absorbing receivers upon the inter-symbol interference in a diffusion-based molecular communication system. *Nano Communication Networks*, volume 14, number Supplement C, pp. 40–47.

Atakan, B. (2016). *Molecular Communications and Nanonetworks: From Nature To Practical Systems*, softcover reprint of the original 1st ed. 2014 edition edition. Springer.

Atakan, B. and Akan, O. B. (2010). Carbon nanotube-based nanoscale ad hoc networks. *IEEE Communications Magazine*, volume 48, number 6, pp. 129–135.

Badr, C. (2014). *Bioluminescence Imaging: Basics and Practical Limitations*, volume 1098.

Bao, X., Lin, J. and Zhang, W. (2019). Channel modeling of molecular communication via diffusion with multiple absorbing receivers. *IEEE Wireless Communications Letters*, volume 8, number 3, pp. 809–812.

Barbeau, M. and Kranakis, E. (2007). *Principles of Ad-hoc Networking*, 1st edition. Wiley, Chichester, England ; Hoboken, NJ.

Barros, M. T. (2017). Ca2+-signaling-based molecular communication systems: Design and future research directions. *Nano Communication Networks*, volume 11, number Supplement C, pp. 103–113.

Betz, T., D. Koch, a. D. L. and Kas, J. A. (2009). Stochastic actin polymerization and steady retrograde flow determine growth cone advancement. *Biophysical Journal*, volume 96, number 12, pp. 5130–5138.

Bicen, A. O., Akyildiz, I. F., Balasubramaniam, S. and Koucheryavy, Y. (2016). Linear Channel Modeling and Error Analysis for Intra/Inter-Cellular Ca2+ Molecular Communication. *IEEE Transactions on NanoBioscience*, volume 15, number 5, pp. 488–498.

Brini, M., Calì, T., Ottolini, D. and Carafoli, E. (2013). Intracellular calcium homeostasis and signaling. *Metal ions in life sciences*, volume 12, p. 119—168.

Chahibi, Y., Akyildiz, I. F. and Balasingham, I. (2016). Propagation Modeling and Analysis of Molecular Motors in Molecular Communication. *IEEE Transactions on NanoBioscience*, volume 15, number 8, pp. 917–927.

Chang, G., Lin, L. and Yan, H. (2018). Adaptive Detection and ISI Mitigation for Mobile Molecular Communication. *IEEE transactions on nanobioscience*, volume 17, number 1, pp. 21–35.

Cho, Y. J., Yilmaz, H. B., Guo, W. and Chae, C.-B. (2017). Effective Enzyme Deployment for Degradation of Interference Molecules in Molecular Communication. *arXiv:1703.06384 [cs]*.

Chopra, N., Yang, K., Abbasi, Q. H., Qaraqe, K. A., Philpott, M. and Alomainy, A. (2016). THz Time-Domain Spectroscopy of Human Skin Tissue for In-Body Nanonetworks. *IEEE Transactions on Terahertz Science and Technology*, volume 6, number 6, pp. 803–809.

Chowdhury, A. M. S. (1998). Photodissociation of Ozone at 248 nm and Vacuum Ultraviolet Laser-Induced Fluorescence Detection of O(1d).

Chude-Okonkwo, U., Malekian, R. and Maharaj, B. (2019). Understanding Delivery Routes and Operational Environments of Nanosystems. In: Advanced Targeted Nanomedicine. *Nanomedicine and Nanotoxicology*.

Chude-Okonkwo, U. A. K., Malekian, R., Maharaj, B. T. and Vasilakos, A. V. (2017). Molecular Communication and Nanonetwork for Targeted Drug Delivery: A Survey. *IEEE Communications Surveys Tutorials*, volume 19, number 4, pp. 3046–3096.

Cobo, L. C. and Akyildiz, I. F. (2010). Bacteria-based communication in nanonetworks. *Nano Communication Networks*, volume 1, number 4, pp. 244–256.

Dambri, O. A., Abouaomar, A. and Cherkaoui, S. (2019). Design optimization of a mimo receiver for diffusion-based molecular communication. In *2019 IEEE Wireless Communications and Networking Conference (WCNC)*. pp. 1–6.

Dambri, O. A. and Cherkaoui, S. (2018). Enhancing Signal Strength and ISI-Avoidance of Diffusion-based Molecular Communication. In *2018 14th International Wireless Communications Mobile Computing Conference (IWCMC)*. pp. 1–6.

Dambri, O. A. and Cherkaoui, S. (2019). Performance enhancement of diffusion-based molecular communication. *IEEE Transactions on NanoBioscience*, volume 19, number 1.

Dambri, O. A. and Cherkaoui, S. (2020a). A physical channel model for wired nanocommunication networks. *arXiv:2005.12328 [cs.ET]*.

Dambri, O. A. and Cherkaoui, S. (2020b). Toward a wired ad hoc nanonetwork. *to appear in Proc. IEEE ICC 2020, Jun 7-12*.

Dambri, O. A., Cherkaoui, S. and Chakraborty, B. (2019). Design and Evaluation of Self-Assembled Actin-Based Nano-Communication. In *2019 15th International Wireless Communications Mobile Computing Conference (IWCMC)*. pp. 208–213.

Damrath, M., Korte, S. and Hoeher, P. A. (2017). Equivalent Discrete-Time Channel Modeling for Molecular Communication With Emphasize on an Absorbing Receiver. *IEEE Transactions on NanoBioscience*, volume 16, number 1, pp. 60–68.

Deng, Y., Noel, A., Guo, W., Nallanathan, A. and Elkashlan, M. (2016). 3d Stochastic Geometry Model for Large-Scale Molecular Communication Systems. In *2016 IEEE Global Communications Conference (GLOBECOM)*. pp. 1–6.

Dishoeck, E. F. v., Black, J. H. and Natuurwetenschappen, F. d. W. e. (1988). The photodissociation and chemistry of interstellar CO.

Du, P., Li, S., O'Grady, G., Cheng, L. K., Pullan, A. J. and Chen, J. D. Z. (2009). Effects of electrical stimulation on isolated rodent gastric smooth muscle cells evaluated via a joint computational simulation and experimental approach. *American Journal of Physiology-Gastrointestinal and Liver Physiology*, volume 297, number 4, pp. G672–G680.

D'Oro, S., Galluccio, L., Morabito, G. and Palazzo, S. (2015). A timing channel-based MAC protocol for energy-efficient nanonetworks. *Nano Communication Networks*, volume 2, number 6, pp. 39–50.

Einolghozati, A., Sardari, M. and Fekri, F. (2016). Networks of bacteria colonies: A new framework for reliable molecular communication networking. *Nano Communication Networks*, volume 7, pp. 17–26.

Einstein, A. (1905). Investigations On The Theory Of The Brownian Movement. *Ann. der Physik*.

Enomoto, A., Moore, M. J., Suda, T. and Oiwa, K. (2011). Design of self-organizing microtubule networks for molecular communication. *Nano Communication Networks*, volume 2, number 1, pp. 16–24.

Farsad, N., Yilmaz, H. B., Eckford, A., Chae, C. B. and Guo, W. (2016). A Comprehensive Survey of Recent Advancements in Molecular Communication. *IEEE Communications Surveys Tutorials*, volume 18, number 3, pp. 1887–1919.

Federici, J. and Moeller, L. (2010). Review of terahertz and subterahertz wireless communications. *Journal of Applied Physics*, volume 107, number 11, p. 111101.

Felicetti, L., Femminella, M., Reali, G., Nakano, T. and Vasilakos, A. V. (2014). TCP-Like Molecular Communications. *IEEE Journal on Selected Areas in Communications*, volume 32, number 12, pp. 2354–2367.

Femminella, M., Reali, G. and Vasilakos*, A. V. (2015). A Molecular Communications Model for Drug Delivery. *IEEE Transactions on NanoBioscience*, volume 14, number 8, pp. 935–945.

Feynman, R. P. (1960). There's Plenty of Room at the Bottom. *Engineering and Science*, volume 23, number 5, pp. 22–36.

Fox, J. E. B. and Phillips, D. R. (1981). Inhibition of actin polymerization in blood platelets by cytochalasins. *Nature*, volume 292, number 5824, pp. 650–652.

Garralda, N., Llatser, I., Cabellos-Aparicio, A., Alarcón, E. and Pierobon, M. (2011). Diffusion-based physical channel identification in molecular nanonetworks. *Nano Communication Networks*, volume 2, number 4, pp. 196–204.

Geim, A. K. (2009). Graphene: Status and Prospects. *Science*, volume 324, number 5934, pp. 1530–1534.

Gillespie, D. T. (1992). A rigorous derivation of the chemical master equation. *Physica A: Statistical Mechanics and its Applications*, volume 188, number 1, pp. 404–425.

Goldberg, G. S., Valiunas, V. and Brink, P. R. (2004). Selective permeability of gap junction channels. *Biochimica et Biophysica Acta (BBA) - Biomembranes*, volume 1662, number 1, pp. 96–101.

Goode, B. L., Drubin, D. G. and Barnes, G. (2000). Functional cooperation between the microtubule and actin cytoskeletons. *Current Opinion in Cell Biology*, volume 12, number 1, pp. 63–71.

Gottfried, N., Kaiser, W., Braun, M., Fuss, W. and Kompa, K. L. (1984). Ultrafast electrocyclic ring opening in previtamin D photochemistry. *Chemical Physics Letters*, volume 110, number 4, pp. 335–339.

Gross, J. D. and Caro, L. G. (1966). DNA transfer in bacterial conjugation. *Journal of Molecular Biology*, volume 16, number 2, pp. 269–IN1.

Guerin, S., O'Donnell, J., Haq, E. U., McKeown, C., Silien, C., Rhen, F. M., Soulimane, T., Tofail, S. A. and Thompson, D. (2019). Racemic Amino Acid Piezoelectric Transducer. *Physical Review Letters*, volume 122, number 4, p. 047701.

Guney, A., Atakan, B. and Akan, O. B. (2012). Mobile Ad Hoc Nanonetworks with Collision-Based Molecular Communication. *IEEE Transactions on Mobile Computing*, volume 11, number 3, pp. 353–366.

Guo, H., Johari, P., Jornet, J. M. and Sun, Z. (2016). Intra-Body Optical Channel Modeling for In Vivo Wireless Nanosensor Networks. *IEEE Transactions on NanoBioscience*, volume 15, number 1, pp. 41–52.

Han, C. and Akyildiz, I. F. (2017). Three-Dimensional End-to-End Modeling and Analysis for Graphene-Enabled Terahertz Band Communications. *IEEE Transactions on Vehicular Technology*, volume 66, number 7, pp. 5626–5634.

Han, C., Tong, W. and Yao, X.-W. (2017). MA-ADM: A memory-assisted angular-division-multiplexing MAC protocol in Terahertz communication networks. *Nano Communication Networks*, volume 13, pp. 51–59.

Handy, B. E., Maciejewski, M. and Baiker, A. (1992). Vanadia, vanadia-titania, and vanadia-titania-silica gels: Structural genesis and catalytic behavior in the reduction of nitric oxide with ammonia. *Journal of Catalysis*, volume 134, number 1, pp. 75–86.

He, D., Guan, K. and Fricke, A. (2017). Stochastic Channel Modeling for Kiosk Applications in the Terahertz Band. *IEEE Transactions on Terahertz Science and Technology*, volume 7, number 5, pp. 502–513.

Hesam, S., Nazemi, A. R. and Haghbin, A. (2012). Analytical solution for the fokker–planck equation by differential transform method. *Scientia Iranica*, volume 19, number 4, pp. 1140–1145.

Hiyama, S., Gojo, R., Shima, T., Takeuchi, S. and Sutoh, K. (2009). Biomolecular-Motor-Based Nano- or Microscale Particle Translocations on DNA Microarrays. *Nano Letters*, volume 9, number 6, pp. 2407–2413.

Hoiles, W., Krishnamurthy, V. and Cornell, B. (2018). *Dynamics of Engineered Artificial Membranes and Biosensors*, 1st edition. Cambridge University Press.

Hosseininejad, S. E., Alarcón, E., Komjani, N., Abadal, S., Lemme, M. C., Haring Bolívar, P. and Cabellos-Aparicio, A. (2017). Study of hybrid and pure plasmonic terahertz antennas based on graphene guided-wave structures. *Nano Communication Networks*, volume 12, pp. 34–42.

Hunley, C., Uribe, D. and Marucho, M. (2018). A multi-scale approach to describe electrical impulses propagating along actin filaments in both intracellular and in vitro conditions. *RSC Advances*, volume 8, number 22, pp. 12017–12028.

Ingalls, B. P. (2013). *Mathematical Modeling in Systems Biology: An Introduction*, 1st edition. The MIT Press, Cambridge, Massachusetts.

Jacob, D. (2000). *Introduction to Atmospheric Chemistry*, 1st edition. Princeton University Press, Princeton, N.J.

Jadidi, M. M., Sushkov, A. B., Myers-Ward, R. L., Boyd, A. K., Daniels, K. M., Gaskill, D. K., Fuhrer, M. S., Drew, H. D. and Murphy, T. E. (2015). Tunable Terahertz Hybrid Metal–Graphene Plasmons. *Nano Letters*, volume 15, number 10, pp. 7099–7104.

Jahangirian, H., Lemraski, E. G., Webster, T. J., Rafiee-Moghaddam, R. and Abdollahi, Y. (2017). A review of drug delivery systems based on nanotechnology and green chemistry: green nanomedicine. *International Journal of Nanomedicine*, volume 12, pp. 2957–2978.

Jianling, C., Min, W., Cong, C. and Zhi, R. (2016). High-throughput low-delay MAC protocol for TeraHertz ultra-high data-rate wireless networks. *The Journal of China Universities of Posts and Telecommunications*, volume 23, number 4, pp. 17–24.

Jäpelt, R. B. and Jakobsen, J. (2013). Vitamin D in plants: a review of occurrence, analysis, and biosynthesis. *Frontiers in Plant Science*, volume 4, p. 136.

Jéquier, E. and Constant, F. (2010). Water as an essential nutrient: the physiological basis of hydration. *European Journal of Clinical Nutrition*, volume 64, number 2, pp. 115–123.

Kadloor, S., Adve, R. S. and Eckford, A. W. (2012). Molecular Communication Using Brownian Motion With Drift. *IEEE Transactions on NanoBioscience*, volume 11, number 2, pp. 89–99.

Kampen, N. G. V. (2007). *Stochastic Processes in Physics and Chemistry*, 3rd edition. North Holland.

Kaur, H., Kumar, S. and Bharadwaj, L. M. (2012). Electric Field Induces Alignment of Actin Filaments. *Procedia Engineering*, volume 44, pp. 892–895.

Kaur, H., Kumar, S., Kaur, I., Singh, K. and Bharadwaj, L. M. (2010). Low-intensity magnetic fields assisted alignment of actin filaments. *International Journal of Biological Macromolecules*, volume 47, number 3, pp. 371–374.

Khan, I., Belqasmi, F., Glitho, R., Crespi, N., Morrow, M. and Polakos, P. (2016). Wireless sensor network virtualization: A survey. *IEEE Communications Surveys Tutorials*, volume 18, number 1, pp. 553–576.

Kilinc, D. and Akan, O. B. (2013). Receiver Design for Molecular Communication. *IEEE Journal on Selected Areas in Communications*, volume 31, number 12, pp. 705–714.

Kim, N. R. and Chae, C. B. (2013). Novel Modulation Techniques using Isomers as Messenger Molecules for Nano Communication Networks via Diffusion. *IEEE Journal on Selected Areas in Communications*, volume 31, number 12, pp. 847–856.

Kim, N. R., Eckford, A. W. and Chae, C. B. (2014). Symbol Interval Optimization for Molecular Communication With Drift. *IEEE Transactions on NanoBioscience*, volume 13, number 3, pp. 223–229.

Kim, S. and Zajić, A. (2016). Statistical Modeling and Simulation of Short-Range Device-to-Device Communication Channels at Sub-THz Frequencies. *IEEE Transactions on Wireless Communications*, volume 15, number 9, pp. 6423–6433.

Kimlin, M. G. (2008). Geographic location and vitamin D synthesis. *Molecular Aspects of Medicine*, volume 29, number 6, pp. 453–461.

Koch, G. L. (1990). The endoplasmic reticulum and calcium storage. *BioEssays: News and Reviews in Molecular, Cellular and Developmental Biology*, volume 12, number 11, pp. 527–531.

Kokkoniemi, J., Lehtomäki, J., Umebayashi, K. and Juntti, M. (2015). Frequency and Time Domain Channel Models for Nanonetworks in Terahertz Band. *IEEE Transactions on Antennas and Propagation*, volume 63, number 2, pp. 678–691.

Koo, B. H., Lee, C., Yilmaz, H. B., Farsad, N., Eckford, A. and Chae, C. B. (2016). Molecular MIMO: From Theory to Prototype. *IEEE Journal on Selected Areas in Communications*, volume 34, number 3, pp. 600–614.

Kostoff, R. N., Koytcheff, R. G. and Lau, C. G. Y. (2007). Global nanotechnology research literature overview. *Technological Forecasting and Social Change*, volume 74, number 9, pp. 1733–1747.

Krishtal, O. A., Pidoplichko, V. I. and Shakhovalov, Y. A. (1981). Conductance of the calcium channel in the membrane of snail neurones. *The Journal of Physiology*, volume 310, number 1, pp. 423–434.

Krouk, E. and Semenov, S. (2011). *Modulation and Coding Techniques in Wireless Communications*, 1st edition. Wiley, Chichester, West Sussex.

Kuran, M. S., Yilmaz, H. B., Tugcu, T. and Akyildiz, I. F. (2011). 2011 ieee international conference on communications (icc), pp. 1–5.

Kuran, M. s., Yilmaz, H. B., Tugcu, T. and Akyildiz, I. F. (2012). Interference effects on modulation techniques in diffusion based nanonetworks. *Nano Communication Networks*, volume 3, number 1, pp. 65–73.

Kuscu, M. and Akan, O. B. (2014). A communication theoretical analysis of fret-based mobile ad hoc molecular nanonetworks. *IEEE Transactions on NanoBioscience*, volume 13, number 3, pp. 255–266.

Laurenzi, I. J. (2000). An analytical solution of the stochastic master equation for reversible bimolecular reaction kinetics. *The Journal of Chemical Physics*, volume 113, number 8, pp. 3315–3322.

Lawler, N. B., Ho, D., Evans, C. W., Wallace, V. P. and Iyer, K. S. (2020). Convergence of terahertz radiation and nanotechnology. *The Royal Society of Chemistry*, volume 8, pp. 10942–10955.

Lee, C. H. and Kim, P. (2012). An analytical approach to solutions of master equations for stochastic nonlinear reactions. *Journal of Mathematical Chemistry*, volume 50, number 6, pp. 1550–1569.

Liu, S.-L., May, J. R., Helgeson, L. A. and Nolen, B. J. (2013). Insertions within the actin core of actin-related protein 3 (arp3) modulate branching nucleation by arp2/3 complex. *The Journal of Biological Chemistry*, volume 288, number 1, pp. 487–497.

Liu, Y., Li, J., Tschirhart, T., Terrell, J. L., Kim, E., Tsao, C.-Y., Kelly, D. L., Bentley, W. E. and Payne, G. F. (2017). Connecting biology to electronics: Molecular communication via redox modality. *Advanced Healthcare Materials*, volume 6, number 24, p. 1700789.

Lodish, H., Berk, A., Zipursky, S. L., Matsudaira, P., Baltimore, D. and Darnell, J. (2000). *The Actin Cytoskeleton*.

MacLaughlin, J. A., Anderson, R. R. and Holick, M. F. (1982). Spectral character of sunlight modulates photosynthesis of previtamin D3 and its photoisomers in human skin. *Science*, volume 216, number 4549, pp. 1001–1003.

Mahfuz, M. U. (2016). Achievable Strength-Based Signal Detection in Quantity-Constrained PAM OOK Concentration-Encoded Molecular Communication. *IEEE Transactions on NanoBioscience*, volume 15, number 7, pp. 619–626.

Mahfuz, M. U., Makrakis, D. and Mouftah, H. T. (2011). Characterization of intersymbol interference in concentration-encoded unicast molecular communication. In *2011 24th Canadian Conference on Electrical and Computer Engineering(CCECE)*. pp. 000164–000168.

Mahfuz, M. U., Makrakis, D. and Mouftah, H. T. (2015). A comprehensive analysis of strength-based optimum signal detection in concentration-encoded molecular communication with spike transmission. *IEEE transactions on nanobioscience*, volume 14, number 1, pp. 67–83.

Marconi, G. (1902). Progress of electric space telegraphy. *Royal Institution,*.

McEvoy, J. P. and Brudvig, G. W. (2006). Water-Splitting Chemistry of Photosystem II. *Chemical Reviews*, volume 106, number 11, pp. 4455–4483.

McKenzie, A. L. (1990). Physics of thermal processes in laser-tissue interaction. *Physics in Medicine and Biology*, volume 35, number 9, pp. 1175–1209.

MD, A. M. K. (2010). *Physiology of the Heart*, fifth edition edition. Lippincott Williams and Wilkins, 576 pp.

Meer, R. K. V., Breed, M. D., Winston, M. and Espelie, K. E. (1997). *Pheromone Communication In Social Insects: Ants, Wasps, Bees, And Termites*, 1st edition. Westview Press, Boulder, Colo.

Meng, L. S., Yeh, P. C., Chen, K. C. and Akyildiz, I. F. (2012). MIMO communications based on molecular diffusion. In *2012 IEEE Global Communications Conference (GLOBECOM)*. pp. 5380–5385.

Meysman, F. J. (2018). Cable bacteria take a new breath using long-distance electricity. *Trends in Microbiology*, volume 26, number 5, pp. 411–422.

Michelusi, N. and Mitra, U. (2015). Capacity of electron-based communication over bacterial cables: The full-csi case with binary inputs. pp. 1072–1077.

Michelusi, N., Pirbadian, S., El-Naggar, M. Y. and Mitra, U. (2014). A stochastic model for electron transfer in bacterial cables. *IEEE Journal on Selected Areas in Communications*, volume 32, number 12, pp. 2402–2416.

Moore, J. D. and Endow, S. A. (1996). Kinesin proteins: A phylum of motors for microtubule-based motility. *BioEssays*, volume 18, number 3, pp. 207–219.

Moore, M. J., Suda, T. and Oiwa, K. (2009). Molecular Communication: Modeling Noise Effects on Information Rate. *IEEE Transactions on NanoBioscience*, volume 8, number 2, pp. 169–180.

Mosayebi, R., Gohari, A., Mirmohseni, M. and Kenari, M. N. (2016). Type based sign modulation for molecular communication. In *2016 Iran Workshop on Communication and Information Theory (IWCIT)*. pp. 1–6.

Nafari, M., Feng, L. and Jornet, J. M. (2017). On-Chip Wireless Optical Channel Modeling for Massive Multi-Core Computing Architectures. In *2017 IEEE Wireless Communications and Networking Conference (WCNC)*. pp. 1–6.

Nakano, T. (2017). Molecular Communication: A 10 Year Retrospective. *IEEE Transactions on Molecular, Biological and Multi-Scale Communications*, volume 3, number 2, pp. 71–78.

Nakano, T., Eckford, A. W. and Haraguchi, T. (2013). *Molecular Communication*. Cambridge University Press.

Nakano, T., Moore, M. J., Wei, F., Vasilakos, A. V. and Shuai, J. (2012). Molecular Communication and Networking: Opportunities and Challenges. *IEEE Transactions on NanoBioscience*, volume 11, number 2, pp. 135–148.

Nakano, T. and Suda, T. (2017). Molecular Communication Using Dynamic Properties of Oscillating and Propagating Patterns in Concentration of Information Molecules. *IEEE Transactions on Communications*, volume 65, number 8, pp. 3386–3398.

Nakano, T., Suda, T., Moore, M., Egashira, R., Enomoto, A. and Arima, K. (2005). Molecular communication for nanomachines using intercellular calcium signaling. *5th IEEE Conference on Nanotechnology, 2005.*, volume 2, pp. 478–481.

Noel, A., Cheung, K. C. and Schober, R. (2014). Improving Receiver Performance of Diffusive Molecular Communication With Enzymes. *IEEE Transactions on NanoBioscience*, volume 13, number 1, pp. 31–43.

Noel, A., Cheung, K. C., Schober, R., Makrakis, D. and Hafid, A. (2017). Simulating with AcCoRD: Actor-Based Communication via Reaction-Diffusion. *Nano Communication Networks*, volume 11, pp. 44–75.

Noel, A., Deng, Y., Makrakis, D. and Hafid, A. (2016). Active versus Passive: Receiver Model Transforms for Diffusive Molecular Communication. In *2016 IEEE Global Communications Conference (GLOBECOM)*. pp. 1–6.

Oldham, K. B., Myland, J. and Spanier, J. (2008). *An Atlas of Functions: with Equator, the Atlas Function Calculator*, 2nd edition. Springer, Philadelphia.

Orchard, C. and Brette, F. (????). t-tubules and sarcoplasmic reticulum function in cardiac ventricular myocytes. volume 77, number 2.

Pacheco, A. R. and Sperandio, V. (2009). Inter-kingdom signaling: chemical language between bacteria and host. *Current Opinion in Microbiology*, volume 12, number 2, pp. 192–198.

Patolsky, F., Weizmann, Y. and Willner, I. (2004). Actin-based metallic nanowires as bio-nanotransporters. *Nature Materials*, volume 3, number 10, pp. 692–695.

Pierobon, M. and Akyildiz, I. F. (2010). A physical end-to-end model for molecular communication in nanonetworks. *IEEE Journal on Selected Areas in Communications*, volume 28, number 4, pp. 602–611.

Pierobon, M. and Akyildiz, I. F. (2012). Intersymbol and co-channel interference in diffusion-based molecular communication. In *2012 IEEE International Conference on Communications (ICC)*. pp. 6126–6131.

Piro, G., Bia, P., Boggia, G., Caratelli, D., Grieco, L. A. and Mescia, L. (2016). Terahertz electromagnetic field propagation in human tissues: A study on communication capabilities. *Nano Communication Networks*, volume 10, number Supplement C, pp. 51–59.

Piro, G., Yang, K., Boggia, G., Chopra, N., Grieco, L. A. and Alomainy, A. (2015). Terahertz Communications in Human Tissues at the Nanoscale for Healthcare Applications. *IEEE Transactions on Nanotechnology*, volume 14, number 3, pp. 404–406.

Plant, A. L., Gueguetchkeri, M. and Yap, W. (1994). Supported phospholipid/alkanethiol biomimetic membranes: insulating properties. *Biophysical Journal*, volume 67, number 3, pp. 1126–1133.

Pollard, T. D. and Mooseker, M. S. (1981). Direct measurement of actin polymerization rate constants by electron microscopy of actin filaments nucleated by isolated microvillus cores. *The Journal of Cell Biology*, volume 88, number 3, pp. 654–659.

Proakis, J. and Salehi, M. (2007). *Digital Communications*.

Qian, X., Di Renzo, M. and Eckford, A. (2019). Molecular communications: Model-based and data-driven receiver design and optimization. *IEEE Access*, volume 7, pp. 53555–53565.

Roussel, M. R. (2019). Stability analysis for odes. *Morgan and Claypool Publishers*, pp. 3–12.

Scemes, E. and Giaume, C. (2006). Astrocyte calcium waves: What they are and what they do. *Glia*, volume 54, number 7, pp. 716–725.

Seo, M., Kang, J.-H., Kim, H.-S., Hyong Cho, J., Choi, J., Min Jhon, Y., Lee, S., Hun Kim, J., Lee, T., Park, Q.-H. and Kim, C. (2015). Observation of terahertz-radiation-induced ionization in a single nano island. *Scientific Reports*, volume 5, number 1, p. 10280.

Shimomura, O. (1995). A Short Story of Aequorin. *The Biological Bulletin*, volume 189, number 1, pp. 1–5.

Shimomura, O. and Johnson, F. H. (????). Properties of the bioluminescent protein aequorin. volume 8, number 10, pp. 3991–3997.

Sliney, D. H. and Trokel, S. L. (2012). *Medical Lasers and Their Safe Use*. Springer Science & Business Media.

Smye, S. W., Chamberlain, J. M., Fitzgerald, A. J. and Berry, E. (2001). The interaction between terahertz radiation and biological tissue. *Physics in Medicine and Biology*, volume 46, number 9, pp. R101–R112.

Song, H. J. and Nagatsuma, T. (2011). Present and Future of Terahertz Communications. *IEEE Transactions on Terahertz Science and Technology*, volume 1, number 1, pp. 256–263.

Speight, J. G. (2017). Chapter 2 - Organic Chemistry. In Speight, J. G., *Environmental Organic Chemistry for Engineers*. Butterworth-Heinemann, pp. 43–86.

Srinivas, K. V., Eckford, A. W. and Adve, R. S. (2012). Molecular Communication in Fluid Media: The Additive Inverse Gaussian Noise Channel. *IEEE Transactions on Information Theory*, volume 58, number 7, pp. 4678–4692.

Székely, T. and Burrage, K. (2014). Stochastic simulation in systems biology. *Computational and Structural Biotechnology Journal*, volume 12, number 20, pp. 14–25.

Tavakkoli, N., Azmi, P. and Mokari, N. (2017a). Optimal Positioning of Relay Node in Cooperative Molecular Communication Networks. *IEEE Transactions on Communications*, volume 65, number 12, pp. 5293–5304.

Tavakkoli, N., Azmi, P. and Mokari, N. (2017b). Performance Evaluation and Optimal Detection of Relay-Assisted Diffusion-Based Molecular Communication With Drift. *IEEE Transactions on NanoBioscience*, volume 16, number 1, pp. 34–42.

Tepekule, B., Pusane, A. E., Kuran, M. S. and Tugcu, T. (2015a). A Novel Pre-Equalization Method for Molecular Communication via Diffusion in Nanonetworks. *IEEE Communications Letters*, volume 19, number 8, pp. 1311–1314.

Tepekule, B., Pusane, A. E., Yilmaz, H. B., Chae, C. B. and Tugcu, T. (2015b). ISI Mitigation Techniques in Molecular Communication. *IEEE Transactions on Molecular, Biological and Multi-Scale Communications*, volume 1, number 2, pp. 202–216.

Tuszyński, J. A., Portet, S., Dixon, J. M., Luxford, C. and Cantiello, H. F. (2004). Ionic Wave Propagation along Actin Filaments. *Biophysical Journal*, volume 86, number 4, pp. 1890–1903.

Unluturk, B. D. and Akyildiz, I. F. (2017). An End-to-End Model of Plant Pheromone Channel for Long Range Molecular Communication. *IEEE Transactions on NanoBioscience*, volume 16, number 1, pp. 11–20.

Vizi, E. S., Kiss, J. P. and Lendvai, B. (2004). Nonsynaptic communication in the central nervous system. *Neurochemistry International*, volume 45, number 4, pp. 443–451.

Wadhams, G. H. and Armitage, J. P. (2004). Making sense of it all: bacterial chemotaxis. *Nature Reviews Molecular Cell Biology*, volume 5, number 12, pp. 1024–1037.

Wakeham, W. A., Salpadoru, N. H. and Caro, C. G. (1976). Diffusion coefficients for protein molecules in blood serum. *Atherosclerosis*, volume 25, number 2, pp. 225–235.

Wang, L., Liu, C., Chen, X., Zhou, J., Hu, W., Wang, X., Li, J., Tang, W., Yu, A., Wang, S.-W. and Lu, W. (2017). Toward Sensitive Room-Temperature Broadband Detection from Infrared to Terahertz with Antenna-Integrated Black Phosphorus Photoconductor. *Advanced Functional Materials*, volume 27, number 7, pp. n/a–n/a.

Wang, Z. L. (2010). Top emerging technologies for self-powered nanosystems: nanogenerators and nanopiezotronics. In *2010 3rd International Nanoelectronics Conference (INEC)*. pp. 63–64.

Weeks, I., Kricka, L. J. and Wild, D. (2013). Chapter 3.2 - signal generation and detection systems (excluding homogeneous assays). In Wild, D., *The Immunoassay Handbook (Fourth Edition)*, fourth edition edition. Elsevier, pp. 267 – 285.

Wilkinson, D. J. (2011). *Stochastic Modelling for Systems Biology*, 2nd edition. CRC Press, Boca Raton.

Yang, K., Pellegrini, A., Munoz, M. O., Brizzi, A., Alomainy, A. and Hao, Y. (2015). Numerical Analysis and Characterization of THz Propagation Channel for Body-Centric Nano-Communications. *IEEE Transactions on Terahertz Science and Technology*, volume 5, number 3, pp. 419–426.

Yao, X.-W. and Jornet, J. M. (2016). TAB-MAC: Assisted beamforming MAC protocol for Terahertz communication networks. *Nano Communication Networks*, volume 9, pp. 36–42.

Yifat, Y., Iluz, Z., Eitan, M., Friedler, I., Hanein, Y., Boag, A. and Scheuer, J. (2012). Quantifying the radiation efficiency of nano antennas. *Applied Physics Letters*, volume 100, number 11, p. 111113.

Yilmaz, H. B. and Chae, C.-B. (2014). Simulation study of molecular communication systems with an absorbing receiver: Modulation and isi mitigation techniques. *Simulation Modelling Practice and Theory*, volume 49, pp. 136–150.

Yilmaz, H. B., Cho, Y. J., Guo, W. and Chae, C. B. (2016). Interference reduction via enzyme deployment for molecular communication. *Electronics Letters*, volume 52, number 13, pp. 1094–1096.

Zakrajsek, L., Einarsson, E., Thawdar, N., Medley, M. and Jornet, J. M. (2017). Design of graphene-based plasmonic nano-antenna arrays in the presence of mutual coupling. In *2017 11th European Conference on Antennas and Propagation (EUCAP)*. pp. 1381–1385.

Zarrabi, F. B., Seyedsharbaty, M. M., Ahmed, Z., Arezoomand, A. S. and Heydari, S. (2017). Wide band yagi antenna for terahertz application with graphene control. *Optik - International Journal for Light and Electron Optics*, volume 140, pp. 866–872.

Zhang, H. P., Be'er, A., Florin, E.-L. and Swinney, H. L. (2010). Collective motion and density fluctuations in bacterial colonies. *Proceedings of the National Academy of Sciences*, volume 107, number 31, pp. 13626–13630.

Zhang, X., Chung, C.-J., Subbaraman, H., Pan, Z., Chen, C.-T. and Chen, R. T. (2016). Design of a plasmonic-organic hybrid slot waveguide integrated with a bowtie-antenna for terahertz wave detection. Volume 9756. International Society for Optics and Photonics, p. 975614.

Zhao, J., Chu, W., Guo, L., Wang, Z., Yang, J., Liu, W., Cheng, Y. and Xu, Z. (2014). Terahertz imaging with sub-wavelength resolution by femtosecond laser filament in air. *Scientific Reports*, volume 4, p. srep03880.

Zou, Z., Xu, F., Tian, Y., Jiang, X. and Hou, X. (2018). A miniaturized UV-LED photochemical vapor generator for atomic fluorescence spectrometric determination of trace selenium. *Journal of Analytical Atomic Spectrometry*, volume 33, number 7, pp. 1217–1223.